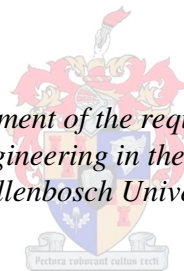


The Effect of Seismic Activity on Reinforced Concrete Frame Structures with Infill Masonry Panels

by
Wesley James Jarvis

*Thesis presented in fulfilment of the requirements for the degree of
Master of Structural Engineering in the Faculty of Engineering at
Stellenbosch University*



Supervisor: Dr. Trevor Neville Haas

April 2014

Declaration

By submitting this thesis electronically, I declare that the entirety of the work contained therein is my own, original work, that I am the sole author thereof (save to the extent explicitly otherwise stated), that reproduction and publication thereof by Stellenbosch University will not infringe any third party rights and that I have not previously in its entirety or in part submitted it for obtaining any qualification.

Date:

Copyright © 2013 Stellenbosch University
All rights reserved.

Abstract

The Effect of Seismic Activity on Reinforced Concrete Frame Structures with Infill Masonry Panels

W.J. Jarvis

Thesis: MEng (Civ)

December 2013

Certain regions within the Western Cape Province are at risk of a moderate intensity earthquake. It is therefore crucial that infrastructure in these areas be designed to resist its devastating effect. Numerous types of structural buildings exist in these seismic prone areas. The most common types are either reinforced concrete framed buildings with masonry infill or unreinforced masonry buildings. Many of these buildings predate the existence of the first loading code of 1989 which provided regulations for seismic design. The previous code was superseded in 2010 with a code dedicated to providing guidelines for seismic design of infrastructure. A concern was raised whether these buildings meet the requirements of the new code. A numerical investigation was performed on a representative reinforced concrete framed building with masonry infill to determine whether the building meets the new code's requirements. The results from the investigation show that the stresses at critical points in the columns exceed the codified requirements, thus leading to local failure. After careful review it was discovered that these local failures in the columns will most likely lead to global failure of the building.

Uittreksel

Die Effek van Seismiese Aktiwiteit op Gewapende Beton-Raam Strukture met Baksteen Invul Panele

W.J. Jarvis

Tesis: MEng (Siv)

Desember 2013

In sekere streke in die Wes-Kaap bestaan daar risiko van matige intensiteit aardbewings. Dit is dus noodsaaklik dat die infrastruktuur in hierdie gebiede ontwerp word om die vernietigende uitwerking te weerstaan. Geboue met verskillende tipes strukturele uitlegte kom in hierdie gebied voor. Die mees algemene struktuur tipe is gewapende beton-raam geboue met baksteen invul panele sowel as ongewapende baksteen geboue. Baie van hierdie geboue is gebou voor die eerste las-kode van 1989 wat regulasies vir seismiese ontwerp voorsien in gebruik geneem is. Die vorige kode is vervang in 2010 met 'n kode toegewy tot die verskaffing van riglyne vir seismiese ontwerp van infrastruktuur. Kommer het ontstaan of hierdie geboue voldoen aan die vereistes van die nuwe kode. 'n Numeriese ondersoek is uitgevoer op 'n verteenwoordigende gewapende beton geraamde gebou met baksteen panele om te bepaal of die gebou voldoen aan die nuwe kode vereistes rakende seismiese ontwerp. Die resultate van die ondersoek toon dat die spanning op kritieke punte in die kolomme die gekodifiseerde vereistes oorskry, wat tot plaaslike faling lei. Na verdere ondersoek is dit bepaal dat die plaaslike faling in die kolomme waarskynlik tot globale faling van die gebou sal lei.

Acknowledgements

I would like to extend my heartfelt thanks to my parents and my sister for all the support they have given to me over the years. I would never be where I am today without them. I would like to thank the rest of my extended family for the support they gave me during my entire university life. I would also like to thank my supervisor Dr. Trevor Haas for his guidance and effort throughout the process of writing this thesis. I would like to thank the South African Nuclear Energy Corporation and Ben Blom for providing me with the bursary that enabled me to do this thesis. I would also like to extend my thanks to my classmates who took this journey with me. Finally, I would like to thank the lecturers and staff of the Structural Engineering Department at Stellenbosch University who were always willing to help with any problem.

Dedication

I would like to dedicate this thesis to my parents, Neil and Liz Jarvis, for the numerous opportunities and support they gave throughout my life.

Contents

Declaration	i
Abstract	ii
Uittreksel	iii
Acknowledgements	iv
Dedication	v
Contents	vi
List of Figures	x
List of Tables	xiii
Nomenclature	xv
1 Introduction	1
1.1 Introduction to the Problem	1
1.2 The Effect of Earthquakes on Structures	2
1.3 Reinforced Concrete Framed Buildings in Earthquakes	4
1.4 Failure Modes of Reinforced Concrete Framed Buildings under Seismic Loading	5
1.4.1 Failure Modes without Masonry Infills	5
1.4.2 Failure Modes with a Stiffness Discontinuity	5
1.4.3 Failure Modes with Masonry Infill	7
2 Theory	10
2.1 Earthquakes in South Africa	10

2.1.1	Introduction to Earthquakes	10
2.1.2	Seismic Waves	10
2.1.3	History of Earthquakes in South Africa	11
2.2	Seismic Design Code for South Africa	14
2.2.1	Design Methodology in SABS 0160-1989	14
2.2.2	Changes in SABS 0160-1989 to SANS 10160-2010	18
2.3	Modelling	23
2.3.1	The Conversion of 3D Members into Beam Elements	23
2.3.2	The Equivalent Strut Method	23
3	Model	28
3.1	Introduction	28
3.2	Test Structure	28
3.2.1	Information on the Test Specimen	29
3.2.2	Material Properties	32
3.2.3	The Earthquake Applied to the Test Structure	34
3.2.4	The Calibration of the Numerical Model of the Test Structure	34
3.3	The Representative Structure	48
3.3.1	Information on the Building	49
3.3.2	Structural Information	49
3.3.3	Material Properties	51
3.3.4	Beam Element Stiffness	51
3.3.5	Masonry Struts	52
3.3.6	Representative Earthquakes Chosen	53
3.3.7	Three Dimensional Frame Model	54
3.3.8	Modelling of an Individual Column	56
3.3.9	Comments on the Modelling of the Representative Struc- ture	59
4	Results	60
4.1	Introduction	60
4.2	Results of the Individual Column	60
4.2.1	The Resultant Stresses of the Concrete	60
4.2.2	The Resultant Stresses in the Steel	61

4.2.3	The Summary of the Stresses in the Concrete and the Steel	71
5	Discussions	72
5.1	Introduction	72
5.1.1	The Failure Criteria	73
5.1.2	Stresses in the Columns	73
6	Conclusions	89
6.1	The Global Response of the Structure	89
6.1.1	Compression Stress in the Columns	89
6.1.2	Tensile Stress in the Columns	90
6.1.3	Shear Stress in the Columns	90
6.2	Conclusions on the Results with Regard to SANS 10160-4	90
6.3	Conclusions on the Modeling of Masonry Infill	91
6.4	Conclusions on the Results	91
6.5	Conclusions on the Results in Context of Reality	91
7	Suggestions for Future Projects	93
7.1	Introduction	93
7.1.1	Masonry in South Africa	93
7.1.2	Soil Conditions in South Africa	93
7.1.3	Retrofitting Structures	94
7.1.4	Ductility of Reinforced Concrete Framed Structures in South Africa	94
	List of References	95
A	Applied Earthquakes	99
A.1	The Seismographs of the Earthquakes Applied to the Full Structure	99
B	The Forces in the Ground Floor Columns	106
B.1	The Resultant Force Diagrams on the Columns	106
B.1.1	The Resultant Forces During the Coalinga Earthquake	107
B.1.2	The Resultant Forces During the Coyota Lake Earthquake	113
B.1.3	The Resultant Forces During the Morgan Hill Earthquake	119

B.1.4	The Resultant Forces During the Palm Springs Earthquake	125
B.1.5	The Resultant Forces During the Whittier Narrows Earthquake	131

List of Figures

1.1	Response of a Structure to Ground Motion	2
1.2	The Failure of a Column at Olive View Hospital in 1971	3
1.3	The Failure of a California State University Structure in 1994	3
1.4	Example of a Reinforced Concrete Frame	4
1.5	Plastic Hinges on a Frame Subjected to Seismic Excitation	6
1.6	The Response of a Structure with Uniform Stiffness Subjected to Seismic Excitation	6
1.7	The Response of a Structure with a Stiffness Discontinuity Sub- jected to Seismic Excitation	7
1.8	Response to Lateral Loading in an Infilled Reinforced Concrete Frame	8
1.9	Failure Modes Caused by Infill Masonry	8
2.1	Types of Seismic Waves	11
2.2	History of Earthquakes in Southern Africa from 1620 to 2005	13
2.3	Seismic Hazard Zones - 1989	15
2.4	Peak Ground Acceleration - 1989	15
2.5	Normalized Response Spectra - 1989	16
2.6	Giosciences' Seismic Hazard Zones - 2003	19
2.7	Seismic Hazard Zones - 2010	19
2.8	Response Spectra Comparison	20
2.9	The Development of a Strut in Infilled Frames	24
2.10	Proposed Modified Equivalent Strut Methods	25
2.11	Defining the Diagonal Strut	26
2.12	The Equivalent Strut Method Selected with Eccentricity	27
3.1	The Frame Used for Calibration	29
3.2	The Specimen (Dimensions in m)	30

3.3	The Reinforcement Detail (Dimensions in mm)	31
3.4	The Transverse Beams and Slab	32
3.5	The Transverse Beams and Slab Reinforcement Detail	32
3.6	The Unscaled Ground Acceleration of the Loma Prieta Earthquake Measured at the Gilroy 3 Station	34
3.7	The Structure as Modelled in Abaqus	36
3.8	The Weight of the Structure at Various Densities	37
3.9	The Acceleration at the Excitation Point	43
3.10	The Velocity at the Excitation Point	44
3.11	The Displacement at the Excitation Point	44
3.12	The Acceleration of the Roof without Damping	45
3.13	The Acceleration of the Roof	47
3.14	The Base Shear of the Test Structure	48
3.15	A 3D Representation of the Representative Structure	49
3.16	The Plan View of the Representative Structure	50
3.17	Frequency Mode 1 of Representative Structure	56
3.18	Frequency Mode 2 of Representative Structure	56
3.19	The Forces in Column C13 when the Palm Springs Earthquake is Applied	57
3.20	The 3D Model of Column C3	58
4.1	The Elements Where Stresses Were Obtained on Column C3	61
5.1	The Columns Numbers Chosen for Modelling	72
5.2	The Cross-Section of Column C1	74
5.3	The Maximum Normal Stresses in Column C1 in the Concrete	74
5.4	The Maximum Axial Stresses in Column C1 in the Reinforcement	75
5.5	The Maximum Shear Stresses in Column C1 in the Concrete	76
5.6	The Cross-Section of Column C3	77
5.7	The Maximum Compression Stresses in Column C3 in the Concrete	77
5.8	The Maximum Axial Stresses in Column C3 in the Reinforcement	78
5.9	The Maximum Shear Stresses in Column C3 in the Concrete	78
5.10	The Cross-Section of Column C6	79
5.11	The Maximum Stresses in Column C6 in the Concrete	79
5.12	The Maximum Axial Stresses in Column C6 in the Reinforcement	80
5.13	The Maximum Shear Stresses in Column C6 in the Concrete	81

5.14	The Cross-Section of Column C8	81
5.15	The Maximum Compression Stresses in Column C8 in the Concrete	82
5.16	The Maximum Axial Stresses in Column C8 in the Reinforcement	82
5.17	The Maximum Shear Stresses in Column C8 in the Concrete	83
5.18	The Cross-Section of Column C11	83
5.19	The Maximum Normal Stresses in Column C11 in the Concrete	84
5.20	The Maximum Axial Stresses in Column C1 in the Reinforcement	85
5.21	The Maximum Shear Stresses in Column C11 in the Concrete	85
5.22	The Cross-Section of Column C13	86
5.23	The Normal Compression Stresses in Column C13 in the Concrete	86
5.24	The Maximum Axial Stresses in Column C13 in the Reinforcement	87
5.25	The Maximum Shear Stresses in Column C13 in the Concrete	88

List of Tables

2.1	Noteworthy Earthquakes of the 20th Century in South Africa	12
2.2	Provincial Breakdown of South African Earthquakes	12
2.3	Provincial Breakdown of Earthquakes with a Seismic Intensity Greater than Five	14
2.4	Normalized Response Spectrum Parameters from SABS 0160	17
2.5	Behaviour Factors - 1989	17
2.6	The Behaviour Factors Specified in SANS 10160-4	22
3.1	Conversion of American Reinforcement Designation to Metric	31
3.2	The Material Properties of the Concrete at 28 Days	33
3.3	The Material Properties of the Masonry at 28 Days	33
3.4	The Properties of Grade 60 Reinforcement	33
3.5	The Weight of the Structure Given Different Concrete Densities	37
3.6	The Equivalent Elastic Modulus of the Cross-Sections	38
3.7	The Opening Factor of the Masonry Panel	39
3.8	The Properties of the Masonry Strut	40
3.9	The Equivalent Elastic Modulus of the Cross-Sections with New Concrete Elastic Modulus	41
3.10	The Frequency of the Structure at Various Elastic Moduli of Masonry	42
3.11	The Acceleration of the Roof at Various β Values	46
3.12	The Acceleration of the Roof with Final Damping Factor Values	47
3.13	The Dimensions of the Columns	51
3.14	The Concrete Properties	51
3.15	The Masonry Properties	52
3.16	The Steel Properties	52
3.17	The Effective Stiffness of the Columns for Various Floor	52
3.18	The Information on the Masonry Panels	53

3.19	The Area of Each Masonry Panel's Strut	53
3.20	The Five Representative Earthquakes Chosen	55
3.21	Area of Steel for the Modelling of the Columns	58
4.1	The Principal and Shear Stresses of Column C1	62
4.2	The Principal and Shear Stresses of Column C3	63
4.3	The Principal and Shear Stresses of Column C6	64
4.4	The Principal and Shear Stresses of Column C8	65
4.5	The Principal and Shear Stresses of Column C11	66
4.6	The Principal and Shear Stresses of Column C13	67
4.7	The Stresses in the Reinforcing Steel in Column C1	68
4.8	The Stresses in the Reinforcing Steel in Column C3	68
4.9	The Stresses in the Reinforcing Steel in Column C6	69
4.10	The Stresses in the Reinforcing Steel in Column C8	69
4.11	The Stresses in the Reinforcing Steel in Column C11	70
4.12	The Stresses in the Reinforcing Steel in Column C13	70
4.13	A Summary of the Stress in the Concrete	71
4.14	A Summary of the Stress in the Steel	71
6.1	The Summary of the Different Failures in the Columns	89

Nomenclature

Constants

$$g = 9.81 \text{ m/s}^2$$

$$\pi = 3.14159$$

Variables

a_n	Nominal Ground Acceleration	[m/s ²]
A	Area	[m ²]
A_B	Cross-Sectional Area of the Shear Wall	[m ²]
A_{Open}	Area of Openings in a Masonry Panel	[m ²]
A_{Panel}	Area of a Masonry Panel	[m ²]
C_s	Nominal Seismic Base Shear Coefficient	[]
C_T	The Building Type Coefficient	[]
d_m	The Diagonal Length of the Masonry Panel	[m]
D_n	Nominal Self-Weight Load	[kN]
E	Seismic Load	[kN]
E	Elastic Modulus	[GPa]
\bar{E}	Effective Elastic Modulus	[GPa]
f	Frequency	[Hz]
f_{cu}	Ultimate Yield Stress of Concrete	[MPa]
f_a	Stress Applied	[MPa]
f_y	Ultimate Yield Stress of Steel in Tension	[MPa]
f_{yc}	Ultimate Yield Stress of Steel in Compression	[MPa]
h	Height of the Frame	[m]
h_t	Height of the Structure	[m]

h_m	Height of the Masonry Panel	[m]
I	Moment of Inertia	[m ⁴]
K	Stiffness	[N/m]
K	Behaviour Factor	[]
L_{ni}	Imposed Vertical Load	[kN]
L_m	Length of the Masonry Panel	[m]
M	Mass	[kg]
q	Behaviour Factor	[]
r_{max}	Shear Wall Ratio	[]
R	Opening Reduction Factor	[]
T	Period of the Building	[s]
V_n	Seismic Base Shear	[kN]
w	Width of the Equivalent Masonry Strut	[m]
W_n	Nominal Sustained Vertical Load	[kN]
W	Weight	[kN]
z	Eccentricity of the Equivalent Masonry Strut	[m]
α	Mass Related Damping Coefficient	[]
β	Stiffness Related Damping Coefficient	[]
γ_i	Building Importance Factor	[]
γ_m	Material Factor	[]
θ	Angle of Diagonal Strut	[rad]
λ_h	Panel Stiffness Factor	[]
ξ	Damping Ratio	[]
ρ	Redundancy Factor	[]
ρ	Density	[kg/m ³]
σ	Normal Stress	[MPa]
τ	Shear Stress	[MPa]
Ψ_i	Combination Factor	[]
ω	Angular Frequency	[]

Subscripts

NOMENCLATURE

xvii

<i>c</i>	Concrete	[]
<i>m</i>	Masonry	[]
<i>n</i>	Masonry	[]
<i>s</i>	Steel	[]
<i>v</i>	Vertical Direction	[]
<i>x</i>	X-Direction	[]
<i>y</i>	Y-Direction	[]

Chapter 1

Introduction

1.1 Introduction to the Problem

The area around the City of Cape Town is populated with numerous apartment blocks constructed of reinforced concrete frames with masonry infill. Due to the probability of moderate seismicity in the area, all buildings are susceptible to damage from an earthquake and should therefore be designed to sustain such loading. The loading applied to the structure was first determined by the South African Bureau of Standards (SABS) 0160-1989 which was superseded by the South African National Standards(SANS) 10160-4 in 2010. Structural engineers considered the provisions set by SABS 0160 pertaining to seismic loads as conservative and therefore did not apply the clauses related to seismic loading correctly. This raised concerns amongst structural engineers (Wium and van Zijl, 2005). Since the first seismic code was only implemented in 1989, a concern was also raised that buildings constructed prior to this date may not meet the new code requirements. It is the purpose of this thesis to determine if a representative reinforced concrete framed building in the Cape Town region can withstand seismic loading as required by SANS 10160-4. This will be achieved through the use of analytical modelling of a representative structure found in the area. This structure will be subjected to a multitude of earthquakes to verify if the building meets the new code requirements.

1.2 The Effect of Earthquakes on Structures

As earthquakes are regular occurrences, it is important to study their effect on structures. Earthquakes cause different responses to structures compared with its other loading such as self-weight and wind. This is due the earthquakes causing a displacement which results in a force, rather than the traditional force that causes a displacement. The resultant force is caused when the seismic wave displaces the foundation, while due to inertia the rest of the building remains momentarily static (Chopra, 2007). Figure 1.1 shows a simplified response of a structure to ground movement. As shown by Figure 1.1, all the displacement and resultant load acts at the base of the column.

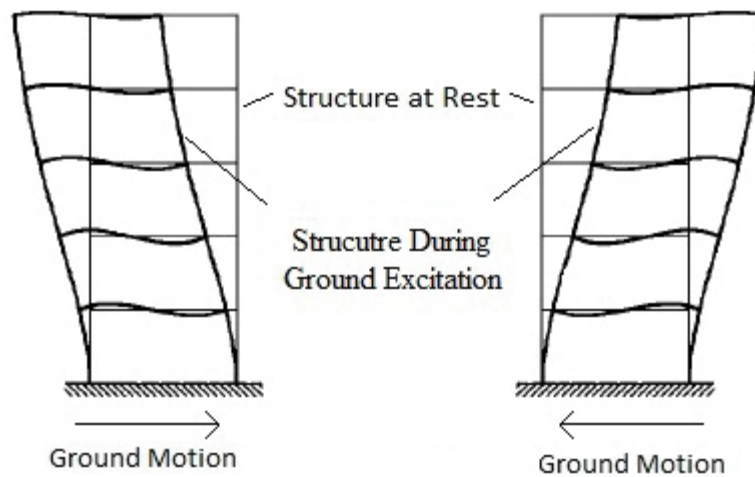


Figure 1.1: Response of a Structure to Ground Motion

(Chopra, 2007)

As with any dynamic loading, resonance is a phenomenon that must be avoided. Resonance occurs when the frequency of oscillation matches the systems' natural frequency, therefore resulting in an amplified response and possible failure of the structure (Buchholdt and Nejad, 2011). The significance of this is that if an earthquake causes a wave with the same period as that of the structure, the displacements of the building will be amplified which will result in larger loads (Chopra, 2007). As with any type of loading, all elements and the complete system must resist the seismic forces applied to it. Figure 1.2

shows a common column failure when subjected to earthquake loading. It should be noted that although the element failed, the structure has not collapsed. Figure 1.3 shows a set of columns that failed which led to the complete collapse of the building.



Figure 1.2: The Failure of a Column at Olive View Hospital in 1971

Source: Earthquake Engineering Research Institute



Figure 1.3: The Failure of a California State University Structure in 1994

Source: Photography by M. Celebi

1.3 Reinforced Concrete Framed Buildings in Earthquakes

Reinforced concrete framed buildings are one of the most common building types found in the Cape Town region. The frame is constructed of reinforced concrete columns, beams and slabs as shown in Figure 1.4. These frames are normally filled with masonry panels in order to insulate the inside from the outside environment. During the design process, the masonry infill panels are not normally considered to add stiffness to the structure. However, in the case of lateral loading, the masonry infill adds significant stiffness (Paulay and Priestley, 1992). This additional stiffness is significantly important in determining the natural frequency of a structure and will result in a more realistic response when subjected to a lateral load (Retief and Dunaiski, 2009).

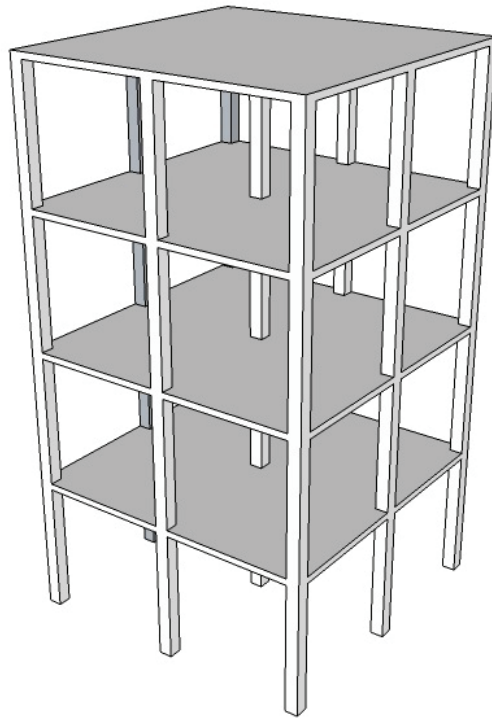


Figure 1.4: Example of a Reinforced Concrete Frame

1.4 Failure Modes of Reinforced Concrete Framed Buildings under Seismic Loading

The failure of reinforced concrete framed buildings is dependent on many factors (Paulay and Priestley, 1992). As this thesis only considers global failure of a structure, only the failure of elements leading to a global failure are considered.

1.4.1 Failure Modes without Masonry Infills

When a reinforced concrete framed building is subjected to seismic excitation, the foundation of the structure will displace while the rest of the structure remains momentarily stationary as shown in Figure 1.1. When this occurs, the steel reinforcing usually exceeds the yield limit and becomes plastic, leading to plastic hinges forming as shown in Figure 1.5 (Sung *et al.*, 2013). Although plastic hinges that form between the columns and beams, shown by the red markers on Figure 1.5, could be troublesome, they do not cause a global failure as those connections should be designed with a high level of ductility (Sung *et al.*, 2013). The markers points on Figure 1.5 represents a dangerous plastic hinge. The column at this point is normally not designed to become plastic, thus any yielding could lead to failure of this key component and cause global failure. (Paulay and Priestley, 1992).

1.4.2 Failure Modes with a Stiffness Discontinuity

A stiffness discontinuity is defined as a structure that has different lateral stiffnesses between adjacent floors (Guevara-Perez, 2012). This can occur when a shear wall does not span the full height of the building or when panels of masonry infill are omitted. A structure of uniform lateral stiffness is beneficial because the displacement caused by the earthquake is distributed evenly between the floors as shown in Figure 1.6. The result of a discontinuity is that a large portion of the displacement occurs at the point of the discontinuity rather than evenly divided throughout the structure (Guevara-Perez, 2012). It is for this reason that buildings in earthquake prone areas are designed with as few discontinuities as possible. A common example of a stiffness discontinuity is a building containing a soft-storey. A soft-storey is the complete

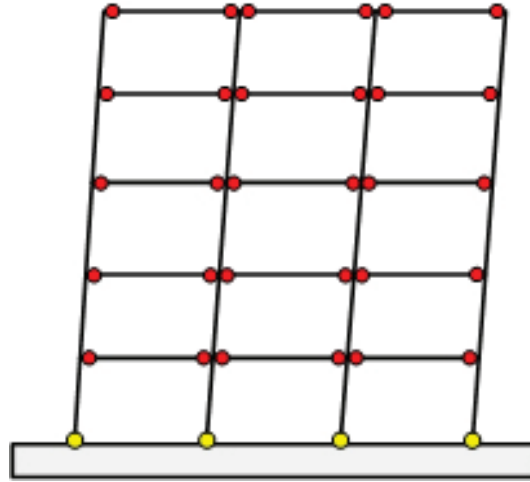


Figure 1.5: Plastic Hinges on a Frame Subjected to Seismic Excitation

(Sung *et al.*, 2013)

absence of infill stiffness as shown in Figure 1.7. Although soft-storeys can be found anywhere in a structure, the majority is usually located on the ground floor of the structure which is usually used for parking. With the displacement concentrated at one floor, the column on that floor receives all the load of the earthquake. The resulting plastic hinges at the top and bottom of the column are therefore required to carry far more load than they were designed for. The resulting failure will constitute global failure of the structure with either partial or complete collapse.

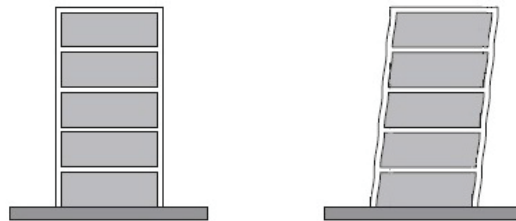


Figure 1.6: The Response of a Structure with Uniform Stiffness Subjected to Seismic Excitation

(Guevara-Perez, 2012)

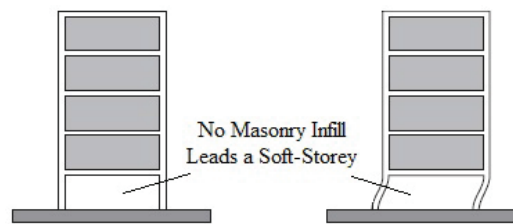


Figure 1.7: The Response of a Structure with a Stiffness Discontinuity Subjected to Seismic Excitation

(Guevara-Perez, 2012)

1.4.3 Failure Modes with Masonry Infill

Masonry infills could also contribute to the failure of the reinforced concrete frame when subjected to seismic loading. As the structure is laterally loaded, the frame will displace resulting in the closure of the gap with the masonry panel as illustrated in Figure 1.8. This gap is usually filled with a gypsum board between 20 and 40mm thick. Once this situation arise, the masonry infill starts to act on the column and beam. The infill will cause plastic hinges in the frame at the contact points which will lead to a multitude of failure modes (Paulay and Priestley, 1992). The failure of the masonry infill panel is not of concern in this study as it would not constitute global failure of the structure. The various failure modes of the reinforced concrete frame is shown in Figure 1.9. The circles signify the location of a plastic hinge

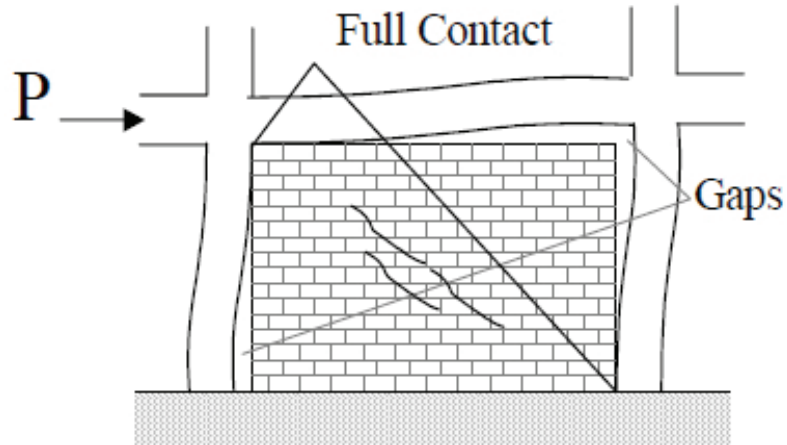


Figure 1.8: Response to Lateral Loading in an Infilled Reinforced Concrete Frame

(Al-Chaar *et al.*, 2002)

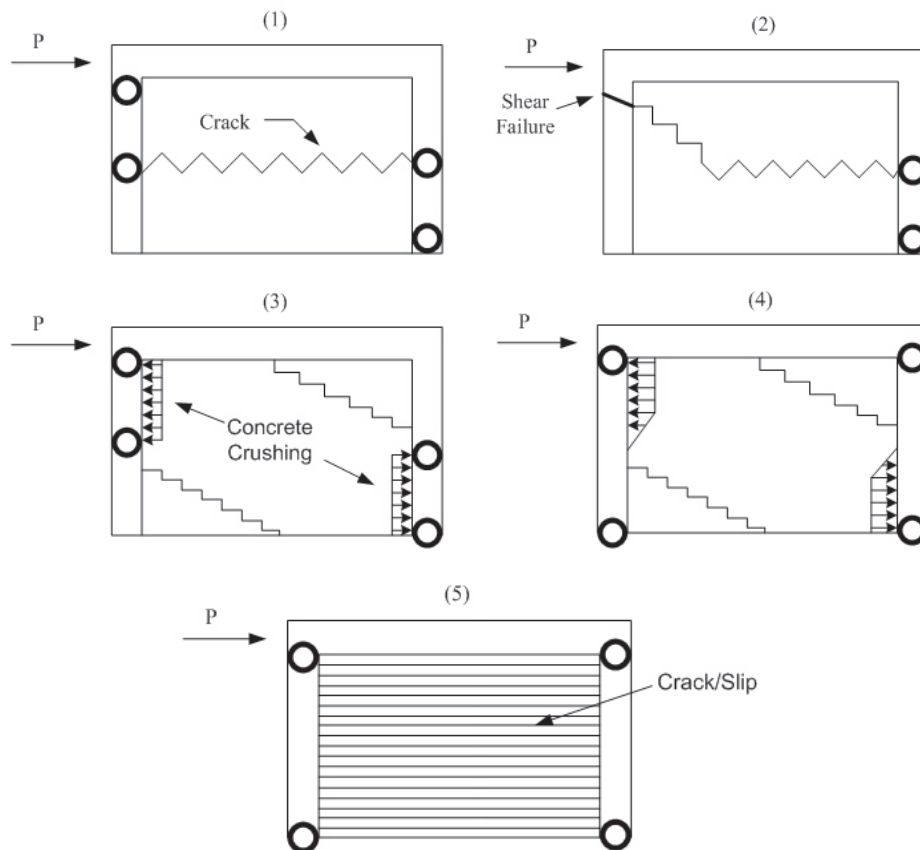


Figure 1.9: Failure Modes Caused by Infill Masonry

(Mehrabi, 1994)

Figure 1.9 shows the five most common failure mechanisms of the frame caused by the masonry infill. The two materials used in the masonry panel are masonry bricks and mortar. The combined strength of these two materials with the strength of the frame will cause various failure modes to occur (Daknakhni *et al.*, 2004). Figure 1.9 (1) occurs when the mortar is weak and the frame is strong. This results in the mortar failing along a horizontal plane causing a short column effect which in turn results in plastic hinges in the column at the point of failure which could lead to global failure of the structure (Mehrabi, 1994). Figure 1.9 (2) is a failure mode associated with weak frame joints and strong members with a strong infill. This failure mode causes a brittle shear failure in the column which could result in global failure of the structure (Daknakhni *et al.*, 2004). Concrete crushing, as shown in Figure 1.9 (3), results from a strong frame with a weak masonry brick panel. Due to the failure of the masonry bricks at the corners, a short column develops, which in turn results in plastic hinges in the columns (Mehrabi, 1994). The final two situations shown in Figure 1.9 are variations of the first two situation. Figure 1.9(4) is caused by the frame having weak joints in relation to the panel which results in plastic hinges developing at the joints. Figure 1.9(5) occurs similarly to Figure 1.9(1) due to weak mortar which in turn results in plastic hinges occurring at the joints (Mehrabi, 1994). The goal of this project is to determine if a structure would fail under seismic loading. It is for this reason that the failure of the columns is the focus of this study as a local failure in multiple columns or on important columns could lead to global failure.

Chapter 2

Theory

2.1 Earthquakes in South Africa

In order to study the effect that an earthquake has on a structure, it is necessary to understand how an earthquake is propagated and the effect it has on the earth's surface.

2.1.1 Introduction to Earthquakes

An earthquake is the geological event in which ground movement or shaking is caused by a wave of energy traveling through the earth's crust (Simpson *et al.*, 1989). It is estimated by the United States Geological Survey (USGS) that over 500,000 earthquakes occur annually, however only 100,000 of these are felt by human beings and only about a hundred cause damage (USGS, 2012). The origins of earthquakes can be traced to natural or induced causes. The majority of naturally caused earthquakes is due to the release of energy by the earth's crust when there is a slip along a fault line due to the movement of the tectonic plates (McSaveney, 2012). Man-made causes originate from different situations such as mining and fracking, all of which involve either rapidly released energy such as an explosion or increased pressure often due to a column of water (USDE, 2012).

2.1.2 Seismic Waves

There are three main types of energy waves that occur during a seismic event as shown in Figure 2.1. These waves all emanate outwards from the epicenter

of the earthquake. The first type is known as pressure waves (P-Wave). A P-Wave compresses and decompresses the soil in the direction of travel. P-Waves also travel through both solids and liquids, and is the fastest moving wave (Smithsonian, 2014). The second is known as shear waves (S-Wave). S-Waves move the soil in an upward and downward direction as the wave passes through it. The movement is perpendicular to the direction of the wave and can only travel through soil (Smithsonian, 2014). The final type is known as surface waves. Surface waves cause a rolling motion in the direction of travel. They are also the slowest type of wave (Smithsonian, 2014). The shapes of the three waves are shown in Figure 2.1. From these diagrams, it is clear that all three waves will have varying effects on a structure. The type of wave that causes the greatest destructive effect on a structure is the surface waves.

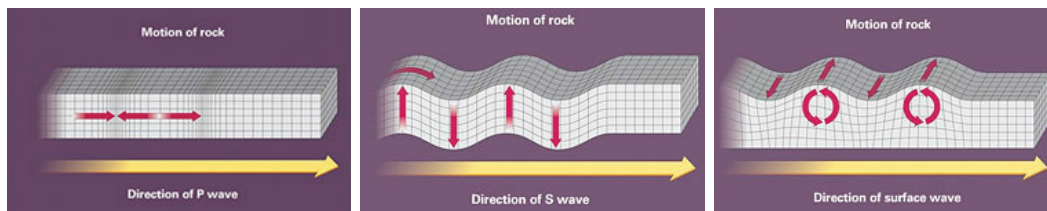


Figure 2.1: Types of Seismic Waves

(Smithsonian, 2014)

2.1.3 History of Earthquakes in South Africa

The first seismologists in South Africa commenced operations in 1910 and the current network of seismic stations was first established in 1971 (Brandt *et al.*, 2005). Table 2.1 shows the recent significant earthquakes in southern Africa which resulted in damage to infrastructure. The Council for Geoscience recently compiled a seismic history of South Africa dating back as far as 1620. Although there were no instruments to detect seismic activity during these times, it is evident from reports that there were major seismic events during this period. It is estimated from historical accounts that between 1620 and 1966 there were at least forty-three moderate intensity earthquakes. A moderate intensity earthquake has a magnitude of between 4.0 and 5.9 on the Richter Scale (USGS, 2012). Ten of these earthquakes are predicted to have

a magnitude greater than 4.5 on the Richter scale, while four clearly exceeded 5.1 in magnitude (Brandt *et al.*, 2005).

Table 2.1: Noteworthy Earthquakes of the 20th Century in South Africa

Date	Region	Magnitude
31/12/1932	St. Lucia, KwaZulu- Natal	6.0-6.5
29/09/1969	Tulbagh, Western Cape	6.3
14/04/1970	Tulbagh, Western Cape	5.7
08/12/1976	Welkom, Free State	5.2
07/03/1992	Carletonville, Gauteng	4.7

(Brandt *et al.*, 2005)

Figure 2.2 shows a map of the epicenters, or origins, and magnitude of the earthquakes that occurred in the analysis of historical data (Brandt *et al.*, 2005). Figure 2.2 shows the abundance of seismicity throughout South Africa. However, only in a few regions do the intensity of the seismic activity present a cause for alarm.

Table 2.2 shows the number of earthquakes recorded in the different provinces of South Africa. It is noticed that Gauteng, the North West, and Free State provinces have the majority of seismic activity in South Africa. This is due to the large mining activity in these regions which produces minor earthquakes.

Table 2.2: Provincial Breakdown of South African Earthquakes

Province	Number of Seismic Events	Percentage
Eastern Cape	102	0.3
Free State	3921	11.5
Gauteng	21414	62.7
KwaZulu Natal	156	0.4
Limpopo	192	0.6
Mpumalanga	121	0.4
Northern Cape	364	1.1
Northwest	7530	22.0
Western Cape	353	1.0
Total	34153	100

(Harrison, 2012)

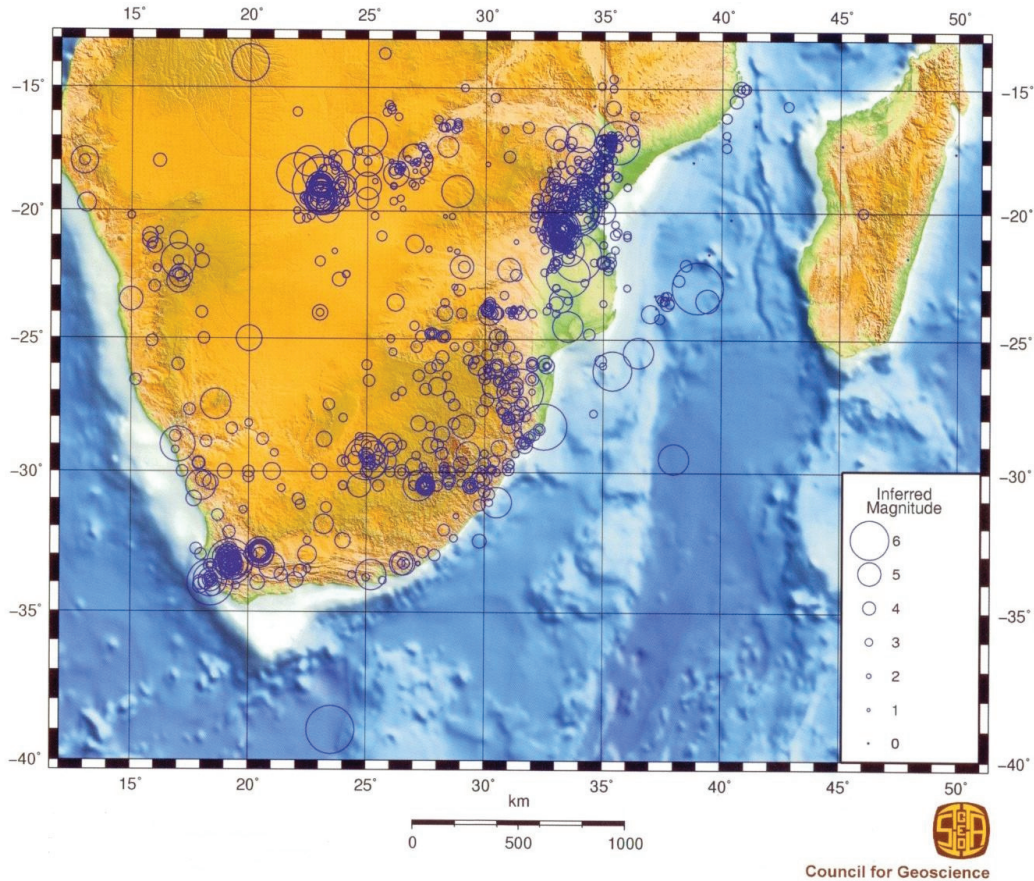


Figure 2.2: History of Earthquakes in Southern Africa from 1620 to 2005
(Brandt *et al.*, 2005)

This is evident in Table 2.3 which illustrates that although over 96% of all earthquakes occur in these three provinces, only 35% of the earthquakes with a magnitude greater five occur in these provinces. Although the percentage of seismic activity in the Western Cape is insignificant, it contributes nearly 30% of the magnitude five intensity earthquakes.

Table 2.3: Provincial Breakdown of Earthquakes with a Seismic Intensity Greater than Five

Province	Number of Seismic Events	Percentage
Eastern Cape	6	10.9
Free State	12	21.9
Gauteng	0	0.0
KwaZulu Natal	2	3.6
Limpopo	2	3.6
Mpumalanga	2	3.6
Northern Cape	8	14.5
Northwest	7	12.7
Western Cape	16	29.2
Total	55	100

(Harrison, 2012)

2.2 Seismic Design Code for South Africa

Although all regions of South Africa experiences seismicity, only certain parts are considered to be at risk of moderate seismicity. For these regions, it is apparent that a seismic design code is required. The first seismic code for South Africa was published in 1989 as part of the SABS 0160 loading code which set out the following method (SABS, 1989).

2.2.1 Design Methodology in SABS 0160-1989

The code specifies two zones of earthquake activity where the ground acceleration is significant to require seismic design. These zones are shown in Figure 2.3. Zone I is defined as the area effected by natural seismicity while Zone II is defined as the area in which mining induced seismicity can be expected.

The reaction as a result of ground motion for which the structure must be designed to resist is referred to as "seismic base shear". According to SABS 0160, the seismic base shear, V_n , is calculated using Equation 2.2.1,

$$V_n = C_s W_n \quad (2.2.1)$$

where C_s is the nominal seismic base shear coefficient and W_n is the nominal sustained vertical load acting on the structure. The nominal seismic base shear

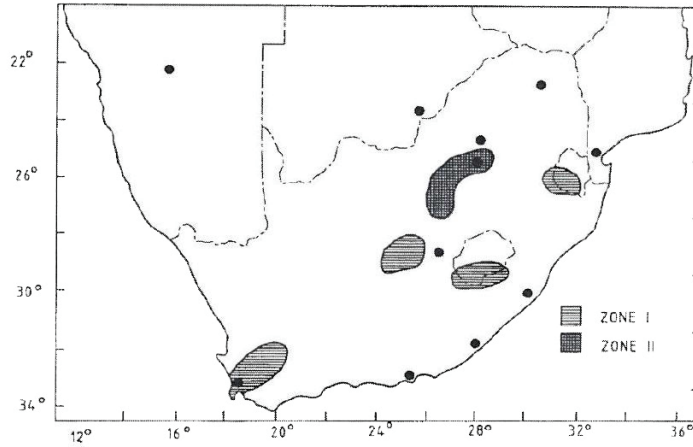


Figure 2.3: Seismic Hazard Zones of South Africa - 1989
(SABS, 1989)

coefficient is calculated using Equation 2.2.2 when the natural period of the building is known,

$$C_s = \frac{a_n R(T)}{K} \quad (2.2.2)$$

where

a_n = nominal ground acceleration defined by Figure 2.4, $a_n = 0.1g$ in Zone 1

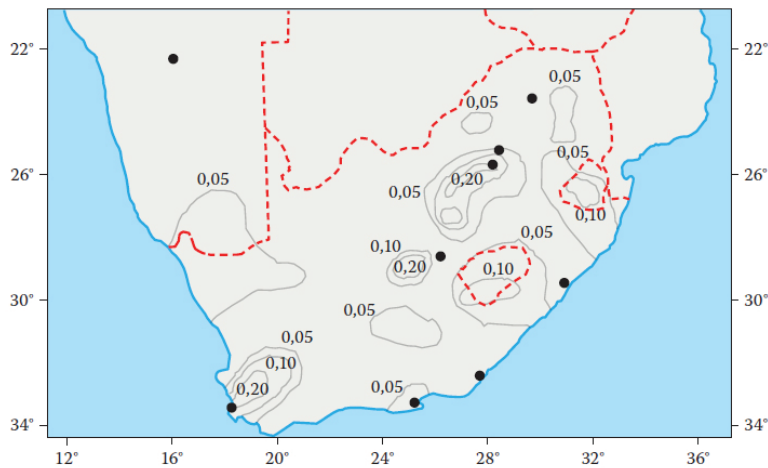


Figure 2.4: Peak Ground Acceleration of South Africa - 1989
(SABS, 1989)

$R(T)$ = normalized design response spectrum which is defined by Equations 2.2.3 and 2.2.4

$$R(T) = R_0 \text{ for } 0 \leq T \leq T_0 \quad (2.2.3)$$

$$R(T) = R_0 \times \left(\frac{T_0}{T}\right)^\beta \text{ and } R(T) \geq 0.3R_0 \text{ for } T \geq T_0 \quad (2.2.4)$$

These functions are shown in Figure 2.5 for the three soil types described in SABS 0160. Table 2.4 provides magnitudes of the different constants for the soils. The Figure 2.5 is developed by applying many earthquakes to a single degree of freedom structure and a statistical analysis is applied to yield the presented curves. This analysis leads to an exceedance probability of 5% (Dazio, 2013).

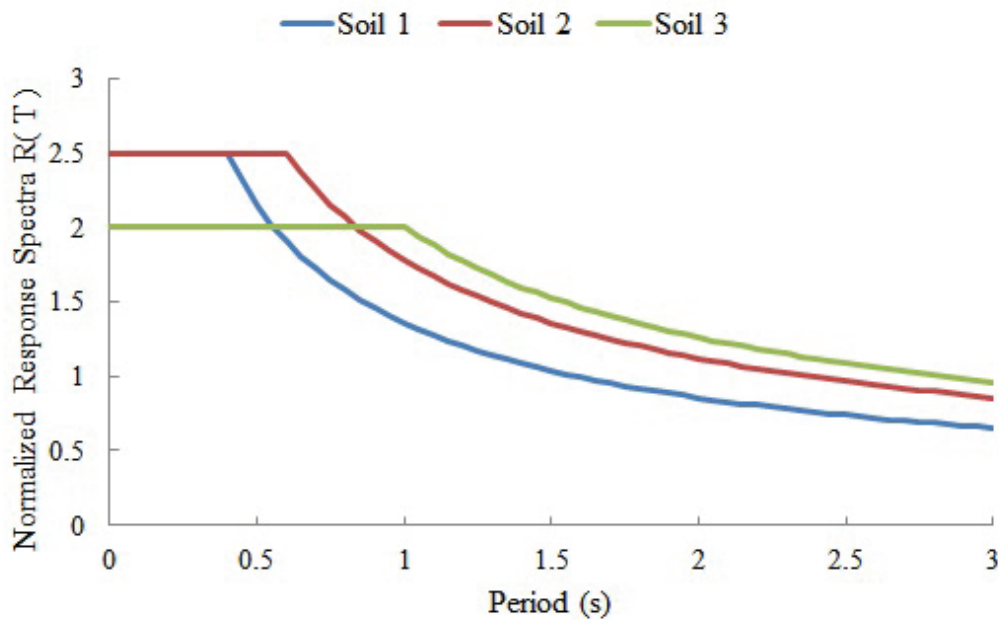


Figure 2.5: Normalized Response Spectra - 1989

(SABS, 1989)

where T = fundamental period of vibration of the structure as defined by Equation 2.2.5

$$T = C_T h_t^{\frac{3}{4}} \quad (2.2.5)$$

where

$$C_t = 0.09 \text{ for steel frames}$$

Table 2.4: Normalized Response Spectrum Parameters from SABS 0160

Soil	R_0	T_0	β
S1	2.5	0.4	$\frac{2}{3}$
S2	2.5	0.6	$\frac{2}{3}$
S3	2.0	1.0	$\frac{3}{3}$

(SABS, 1989)

 $C_t = 0.06$ for concrete frames h_t = height above the base to the highest level of the frame of the buildingand finally where K = behaviour factor as defined by Table 2.5**Table 2.5:** Behaviour Factors - 1989

Structural System	Behaviour Factor K
Bearing Wall System:	
Unreinforced Masonry Walls:	1.5
Reinforced Concrete or Reinforce Masonry Walls or Braced Frames:	3.5
One-, Two-, or Three-Storey Steel Frame Systems:	5.0
Building Frame System:	5.0
Moment-Resisting Frame System:	
Ordinary Concrete Frames:	2.0
Ordinary Steel Frames:	5.0
Elevated Tanks and Inverted Pendulum Type Structures:	
Structures Required to Remain Elastic:	1.0

(SABS, 1989)

When the natural period of the building is unknown, then Equation 2.2.6 is applied.

$$C_s = \frac{a_n R_0}{K} \quad (2.2.6)$$

where R_0 is defined in Table 2.4

The sustained vertical load, described in Equation 2.2.1, is defined as

$$W = D_n + \sum_i \Psi_i L_{ni} \quad (2.2.7)$$

where

D_n = nominal self-weight

L_{ni} = imposed vertical loads

Ψ_i = load combination factor.

2.2.2 Changes in SABS 0160-1989 to SANS 10160-2010

The changes made from SABS 0160-1989 to SANS 10160-2010 reflect both the improvements of previous design methods as well as the implementation of new methods and concepts. The updating of the code was also a reflection that engineers in practice considered the method in SABS 0160 to be too conservative and applied the rules to suit the economic pressures applied by the client. Some engineers used a combination of international codes with the peak ground acceleration from SABS 0160. This necessitated the revision of the code to SANS 10160-4 (Wium, 2010). A committee was formed in 2003 comprising of both academics and practicing engineers whose responsibility it was to update the code (Retief and Dunaiski, 2009).

2.2.2.1 The Updating of the Peak Ground Acceleration Map

The peak ground acceleration map from SABS 0160-1989, Figure 2.4, shows a maximum ground acceleration, a_n of $0.2g$. However, the code specifies in clause 5.6.5.2 that a value of $a_n = 0.1g$ should be used. This was accepted to satisfy concerns from practicing engineers that a magnitude of $a_n = 0.2g$ is unlikely to occur (Retief and Dunaiski, 2009). Figure 2.6 shows the map which the Council of Geosciences provided in 2003 to the review committee which shows the revised peak ground acceleration (Wium, 2010). Figure 2.7 shows the peak ground acceleration map in SANS 10160-2010. The committee decided that a peak ground acceleration of $a_n = 0.1g$ should be applied to Zone I as Cape Town, the main source of infrastructure in this region, does not fall

within the boundary of $a_n = 0.15g$ (Retief and Dunaiski, 2009). The peak ground acceleration for areas effected by seismicity due to mining activity was not changed from the previous code. The area effected was however updated due to the expansion of the mining industry since 1989 as well as more sensitive measurement equipment.

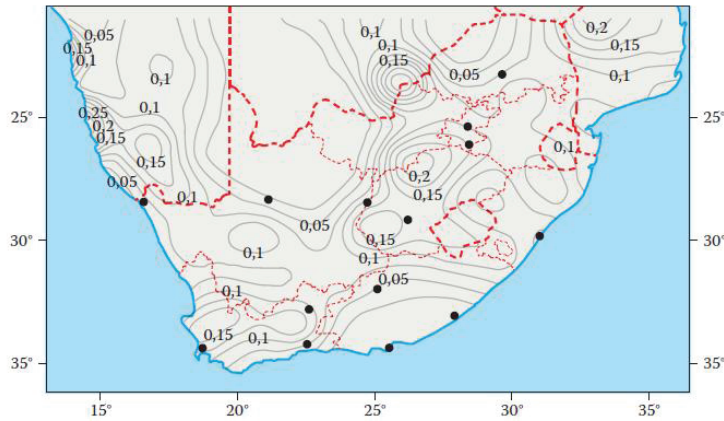


Figure 2.6: The Peak Ground Acceleration Map Provided by the Council of Geosciences - 2003

(Wium, 2010)

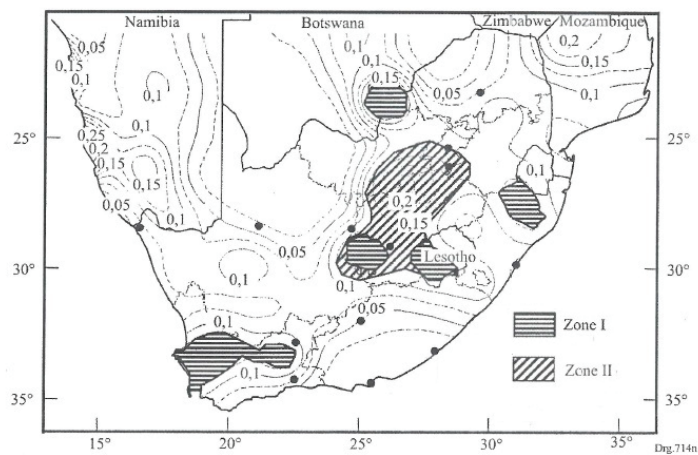


Figure 2.7: Seismic Hazard Zones Showing Peak Ground Acceleration and Earthquake Zones - 2010

(Wium, 2010)

2.2.2.2 The Response Spectra and Soil Types

The response spectra found in SABS 0160-1989 originated from the Applied Technology Council situated in the United States which developed response spectra for three soil types (USNBS, 1978). Since this initial publication, other international codes have made adjustments and refinements to the spectra. The revisions of SABS 0160-1989 response spectra was achieved by adopting the spectra from Eurocode 8-2004, since no information on South African conditions was available. The adopted information was the most conservative of the international codes at the time of 1989 (Wium, 2010). Figure 2.8 shows the comparison of the spectra from SABS 0160-1989 and SANS 10160-4-2010. As seen in Figure 2.8, the new response spectra chosen are conservative in comparison to the previous code. It is suggested that research into response spectra for mining induced earthquakes needs to be conducted as the shapes are different to that of naturally occurring earthquakes. It is also suggested that research should be conducted on different soils that occur in South Africa as it will have an effect on the response spectra (Wium, 2010).

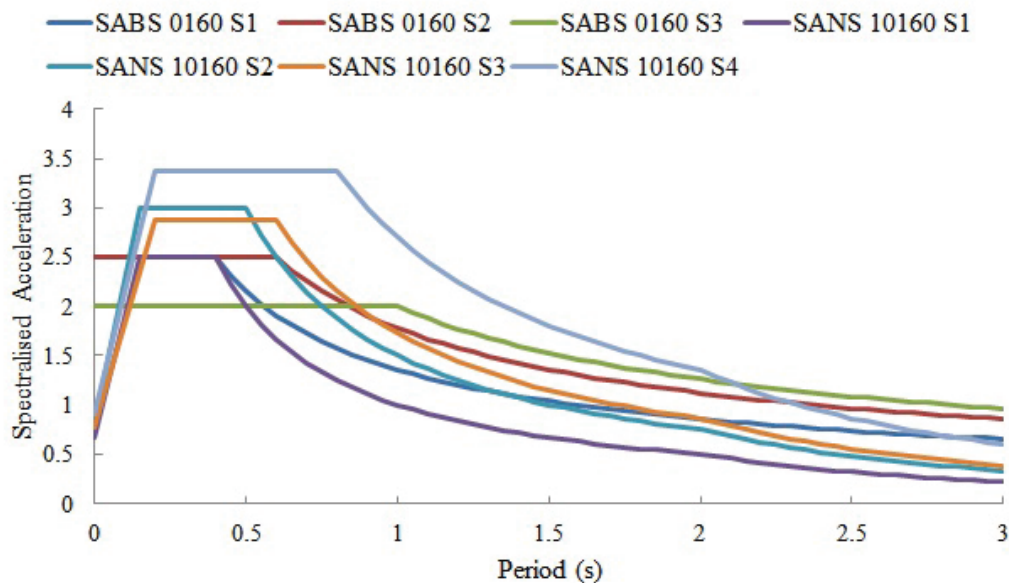


Figure 2.8: Comparison of Response Spectra of SABS 0160-1989 and SANS 10160-2010

(Wium, 2010)

2.2.2.3 The Adjustment of Load Factors, γ

The previous loading codes required the application of a combination of partial factors $\gamma_{earthquake} = 1.6$ and $\gamma_{dead} = 1.2$. This combination was considered conservative and was reduced to $\gamma_{earthquake} = 1.0$ and $\gamma_{dead} = 1.0$ (Wium, 2010). This change reflects the partial factors of international codes. A further factor called the redundancy factor, ρ , was added as a damage limitation criterion

2.2.2.4 The Addition of the Redundancy Factor, ρ

The redundancy factor, ρ , was added to Equation 2.2.8 for the equivalent lateral static force, E_k , known henceforth as ELSF.

$$E_k = \rho\gamma_1(E_x + 0.3E_y) + E_v \quad (2.2.8)$$

where γ_1 is the building importance factor, E_x , E_y and E_v are the seismic load in the two horizontal directions and the vertical direction, respectively. This redundancy factor was added to compensate for the reduction of peak ground acceleration from $0.15g$ to $0.1g$ in Zone I. It was also decided that ρ should vary from $1.2 \leq \rho \leq 1.5$ rather than $1.0 \leq \rho \leq 1.5$ as prescribed in the Uniform Building Code of 1997 (Wium, 2010). ρ is obtained by the Equation 2.2.9.

$$\rho = 2 - \frac{6.1}{r_{max}\sqrt{A_B}} \quad (2.2.9)$$

The redundancy factor allows engineers to reduce the ELSF by increasing the length of shear walls (Wium, 2010).

2.2.2.5 The Changes in Behaviour Factors, q

The changes to the behaviour factors were made to better reflect the factors found in international codes. It was decided by the committee to retain an approach of conservatism from SABS 0160-1989 (Wium, 2010). This approach would be maintained until research into South African building practices, materials and seismic activity can be performed to adjust the factors appropriately. The behaviour factors from SANS 10160-4 are shown in Table 2.6.

Table 2.6: The Behaviour Factors Specified in SANS 10160-4

Structural System	Detail	Behaviour Factor q
Bearing wall system	Unreinforced masonry walls:	1.5
	Reinforced concrete walls detailed correctly:	5.0
	Reinforced concrete walls detailed incorrectly:	2.5
	Reinforced masonry walls:	2.5
Building frame system	Reinforced concrete shear walls detailed correctly:	5.0
	Reinforced concrete shear walls detailed incorrectly:	2.0
	Ordinary braced steel frames:	5.0
Moment-resisting frame system	Ordinary concrete frames detailed correctly:	3.0
	Ordinary concrete frames detailed incorrectly:	2.0
	Ordinary braced steel frames:	4.5
Structures required to remain elastic:	All	1.0

(SANS, 2011)

2.2.2.6 The Calculation of Natural Period, T

The ELSF requires that the natural period of a building be determined. The change to the design calculation was required to be in line with Eurocode 8. The equation given in SANS 10160-2010 is conservative and as such, the use of dynamic analysis on the building would provide a more accurate value (Wium, 2010). The updated design prediction for the period T is specified by Equation 2.2.10

$$T = C_T h_t^{\frac{3}{4}} \quad (2.2.10)$$

where C_T is the constant relating to the type of structure and h_t is the height of the structure.

2.3 Modelling

In order to model the structure in an efficient manner, the full structure will be modelled using beam, truss and shell elements. Further more, it is important to model the additional lateral stiffness resulting from the masonry infill. There are a number of methods used to achieve this; however, for the purpose of this project, the Equivalent Strut Method was chosen due to its simplicity and accuracy for a global system (Crisafulli *et al.*, 2000).

2.3.1 The Conversion of 3D Members into Beam Elements

In order for the columns and beams of the structure to be modelled as beam elements, the cross-section must be reduced to a uniform section. This was achieved using the principle of transforming the section. Equation 2.3.1 is used to reduce the elastic moduli of the reinforced section to a single effective modulus \bar{E} (Craig, 2000). Equation 2.3.1 has been reduced to a formula that can be applied to a two dimensional cross-sectional area. The first material is concrete and the second material is steel. The same principle can be applied to calculate an effective density of the section, which is shown by Equation 2.3.2

$$\bar{E} = \frac{E_c A_c + E_s A_s}{A_c + A_s} \quad (2.3.1)$$

$$\bar{\rho} = \frac{\rho_c A_c + \rho_s A_s}{A_c + A_s} \quad (2.3.2)$$

2.3.2 The Equivalent Strut Method

The first author to study the effects of masonry infill on the lateral stiffness was conducted by Polyakov (1963). From his experimental results, he suggested that when masonry infill is loaded laterally it would form a strut as illustrated in Figure 2.9. From this insight, he suggested that the masonry infill could be replaced with an equivalent strut. Polyakov did not specify the properties of the strut. This was specified by Holmes who proposed that the strut should have a width of one-third of the diagonal length of the panel (Donea *et al.*, 1991). After a series of experiments, Paulay and Priestley (1992) suggested that Holmes strut was too conservative and they suggested that the width of

the strut should be reduced to a quarter of the panel's diagonal length. As more research was performed on the properties of the strut, more complex equations were generated taking into account all aspects from elastic moduli, moments of inertia and whether the panel was damaged or had openings (Crisafulli *et al.*, 2000). The equivalent strut method also assumes that the strut only works in compression as the masonry is joined with mortar which has a very low tensile capacity (Crisafulli *et al.*, 2000).

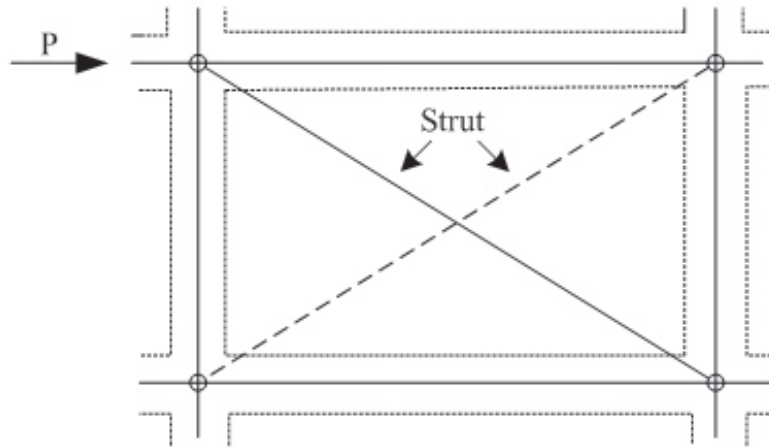


Figure 2.9: The Development of a Strut in Infilled Frames
(Crisafulli *et al.*, 2000)

2.3.2.1 The Modified Equivalent Strut Method

The first equivalent strut method that describes a strut as a diagonal between the adjacent corners of a bay is shown in Figure 2.9. This method accurately predicts the lateral stiffness of the structure; however, it fails to develop the correct shear and moment forces in the column (Crisafulli *et al.*, 2000). This method is therefore ideal for simulating the static loading of a structure. Since an earthquake results in multiple loadings, it becomes important to analyse the response of individual elements under cyclic loading. It is for this reason that various modified equivalent strut methods were proposed. Figure 2.10 shows some examples of the proposed methods. Each model that was proposed targets a specific failure mode of the frame as discussed in Chapter 1. As this project targets the global failure mechanism, the failure modes which include

column failure are of interest. The simplest model that correctly predicts the behaviour of the column is (d) of Figure 2.10 and it is for this reason that this model will be used in the thesis (Crisafulli *et al.*, 2000). A more complicated model could have been chosen, however this thesis did not require the additional accuracy of a complex model.

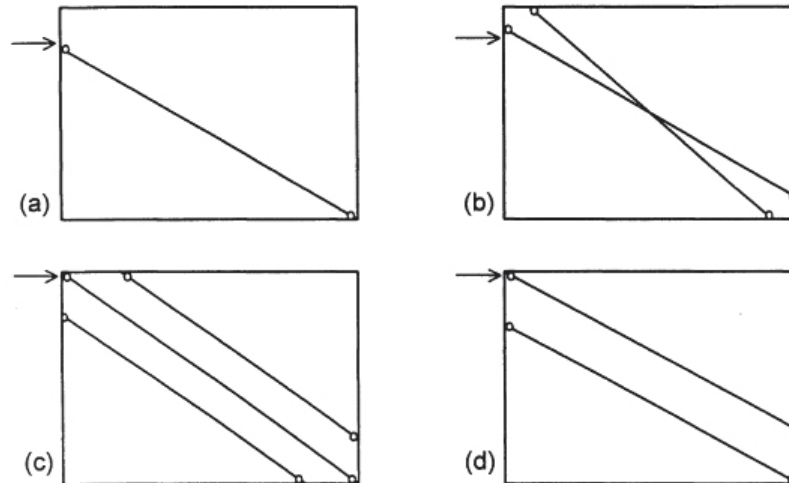


Figure 2.10: Proposed Modified Equivalent Strut Methods
(Crisafulli *et al.*, 2000)

2.3.2.2 The Properties of the Strut

As previously discussed, various proposals on the width of the strut were suggested after experimental work. Paulay and Priestley (1992) suggested a conservative width defined by Equation 2.3.3 with variables defined by Figure 2.11.

$$w = 0.25d_m \quad (2.3.3)$$

Research conducted by Stafford-Smith (1962) through a series of experiments determined a parameter which related the stiffness of the frame to that of the masonry panel. This parameter is obtained using Equation 2.3.4.

$$\lambda_h = h \sqrt[4]{\frac{E_m t \sin 2\theta}{4E_c I_c h_m}} \quad (2.3.4)$$

where t is the effective thickness of the masonry panel. Further widths were proposed based on the work of Stafford-Smith by Mainstone (1971), Liauw

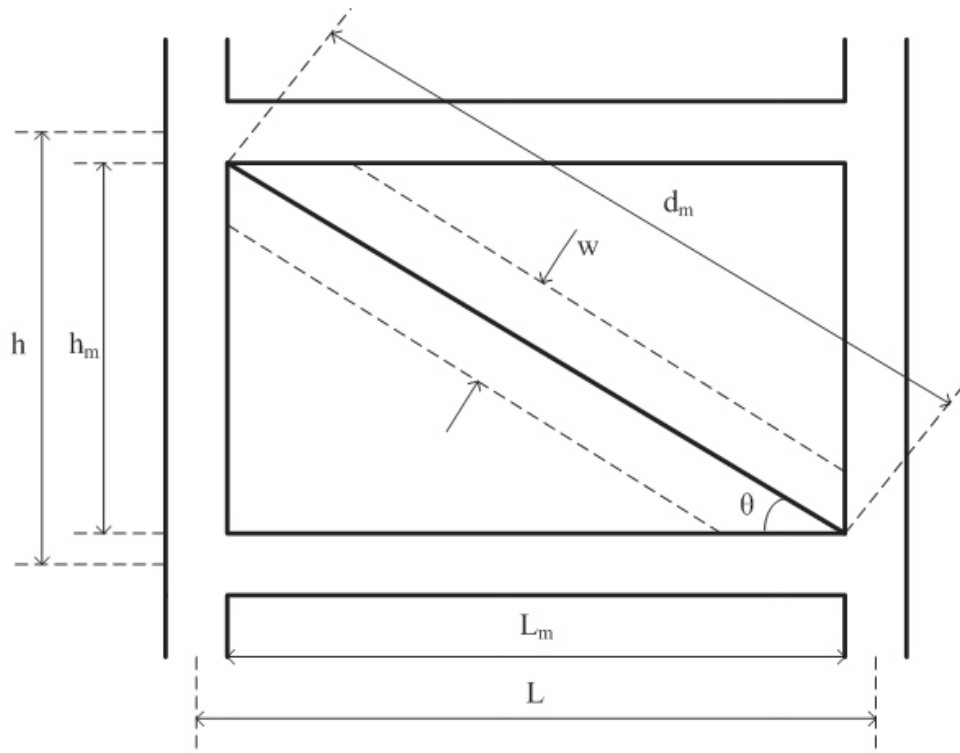


Figure 2.11: Defining the Diagonal Strut

(Crisafulli *et al.*, 2000)

and Kwan (1984) following their own experimental work which resulted in Equations 2.3.5 and 2.3.6, respectively.

$$w = 0.16\lambda_h^{-0.3}d_m \quad (2.3.5)$$

$$w = \frac{0.95h_m \cos \theta}{\sqrt{\lambda_h}} \quad (2.3.6)$$

Unfortunately, not all masonry panels completely fill the frame. It is suggested that a reduction factor be applied to the width. This factor is determined by the Equation 2.3.7 (Al-Chaar *et al.*, 2002).

$$R = 0.6\left(\frac{A_{open}}{A_{panel}}\right)^2 - 1.6\left(\frac{A_{open}}{A_{panel}}\right) + 1.0 \quad (2.3.7)$$

where A_{open} is the area of the openings and A_{panel} is the area of the infill panel. With the use of the width and the panel's effective thickness, the cross sectional area of the strut can be calculated. Many masonry panels have a

cavity in-between the two layers of masonry, therefore the effective thickness should not include this gap.

The equivalent strut method selected, shown in Figure 2.12, requires that an eccentricity of the second strut which is known as z and is defined by Equation 2.3.8 (Crisafulli *et al.*, 2000). As the struts would be modelled as a single truss element, they require a uniform area along the length of the strut. With this in mind, it was decided that the two struts would get half of the stiffness of the masonry panel.

$$z = \frac{\pi}{2\lambda_h} h \quad (2.3.8)$$

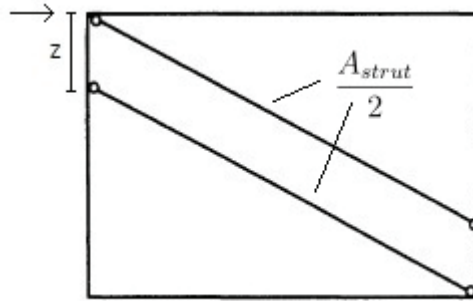


Figure 2.12: The Equivalent Strut Method Selected with Eccentricity
(Crisafulli *et al.*, 2000)

Chapter 3

Model

3.1 Introduction

The aim of this thesis is to establish whether a representative reinforced concrete framed structure from the greater Cape Town area can sustain a moderate intensity earthquake. This will be achieved through the study of the structure under different earthquakes. Due to the destructive nature of the shaking, it became necessary to conduct numerical simulations of the structure rather than build numerous test specimens. ABAQUS, a finite element analysis software package, was used for the numerical simulations. The use of ABAQUS for the simulations does not ensure that the results obtained are correct. This is due to the numerous modelling techniques and simplifications made of the structure. Therefore, it is necessary to calibrate the finite element model to either existing data or experimental tests. Section 3.2 explains how the calibration was achieved while Section 3.3 discusses the modelling of the representative structure.

3.2 Test Structure

The experimental tests performed by Stavridis *et al.* (2012) was considered adequate for the calibration process since it is representative of the reinforced concrete framed building in the Cape Town region. The necessary information for the calibration process is now presented. The calibration process begins with the mass of the structure, then moves to the stiffness, and then onto the acceleration and finally to the base shear force.

3.2.1 Information on the Test Specimen

The test specimen was constructed to a two-thirds scale of a three storey, two bay reinforced concrete frame with unreinforced masonry infill panels. The masonry panels of the left-hand bays, as shown in Figure 3.1, were without openings whereas the panels of the right-hand bays had openings that represent windows. The test specimen is shown in Figure 3.1. The specimen was designed to be nonductile which would accurately represent older buildings built in the 1920s (Stavridis *et al.*, 2012).

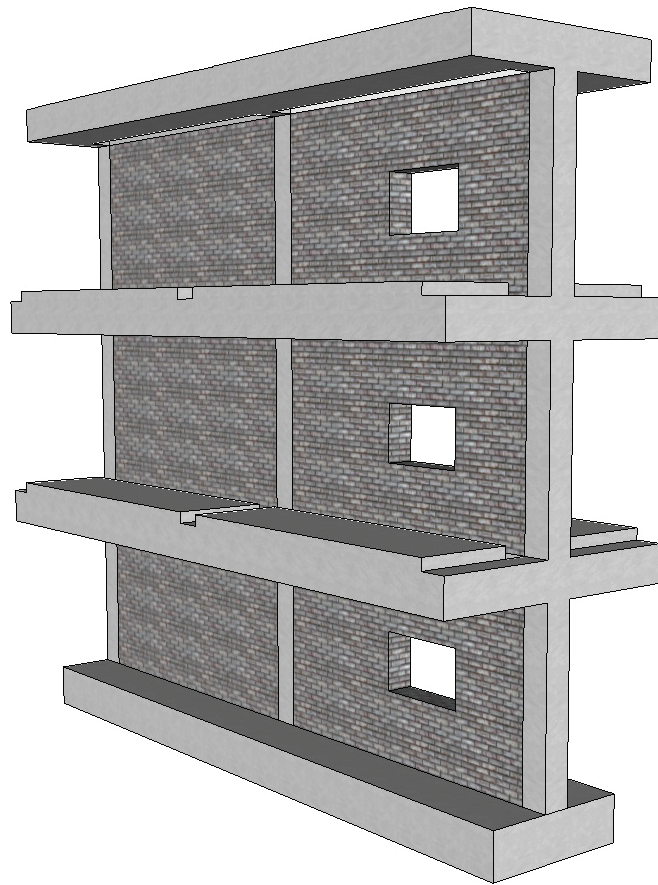


Figure 3.1: The Frame Used for Calibration
(Stavridis *et al.*, 2012)

3.2.1.1 Structural Information

The frame was designed to be representative of the structures found in the 1920s in California. This resulted in the use of percentage reinforcement values for the columns and beams rather than the traditional deem to satisfy method found in design codes. With this in mind, the columns of the first, second and third floor had 2, 1.5 and 1% reinforcement, respectively. The structural detail of the test specimen is shown in Figures 3.2 and 3.3. The reinforcement follow the United States' size designation. Table 3.1 shows the necessary bar sizes in metric. Grade 60 steel with a yield strength of $420MPa$, reinforcing steel was used for this structure while the masonry panels were built with $60 \times 94 \times 197mm$ bricks. The masonry infills were two layers thick.

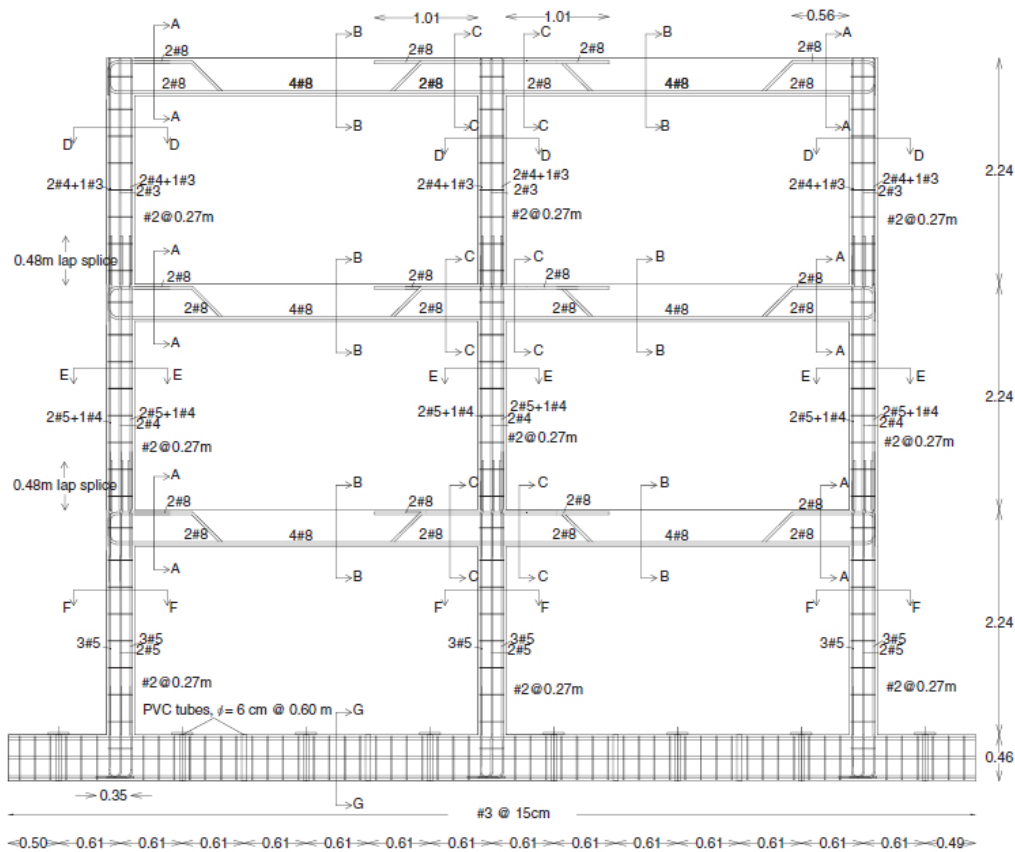


Figure 3.2: The Specimen (Dimensions in m)

(Stavridis *et al.*, 2012)

In addition to the frame, transverse beams were added to each level with slabs spanning between the beams to simulate the correct mass. These beams

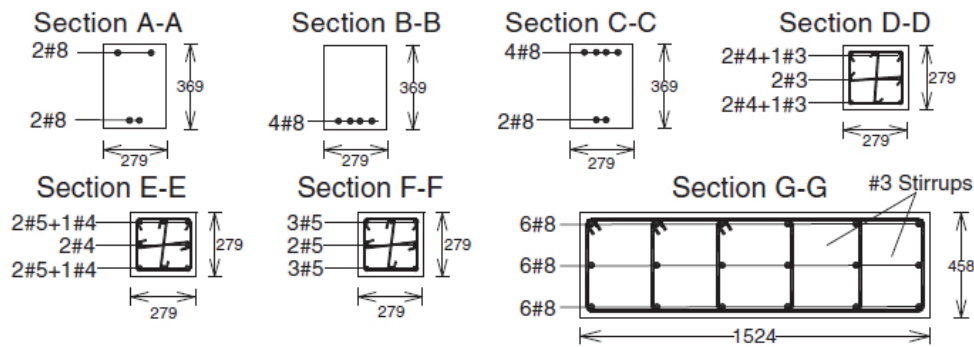


Figure 3.3: The Reinforcement Detail (Dimensions in mm)
(Stavridis *et al.*, 2012)

Table 3.1: Conversion of American Reinforcement Designation to Metric

Bar Designation	Size in <i>mm</i>
#3	9.5
#4	12.7
#5	15.9
#8	25.4

are located at all the intersections of the beams and columns of the frame. The slabs connected to the first and second floor on the frame have the dimensions of $3.28 \times 0.97 \times 0.48m$. The reason for the slab's large thickness was the need to reduce the length of the cantilever while maintaining the correct mass. The roof slab's smaller size was to reflect the smaller load that was applied to the roof. The roof slab has the dimensions $3.28 \times 0.71 \times 0.37m$. The layout of the slab is shown in Figure 3.4 and the reinforcing detail of the transverse beam and slab is shown in Figure 3.5.

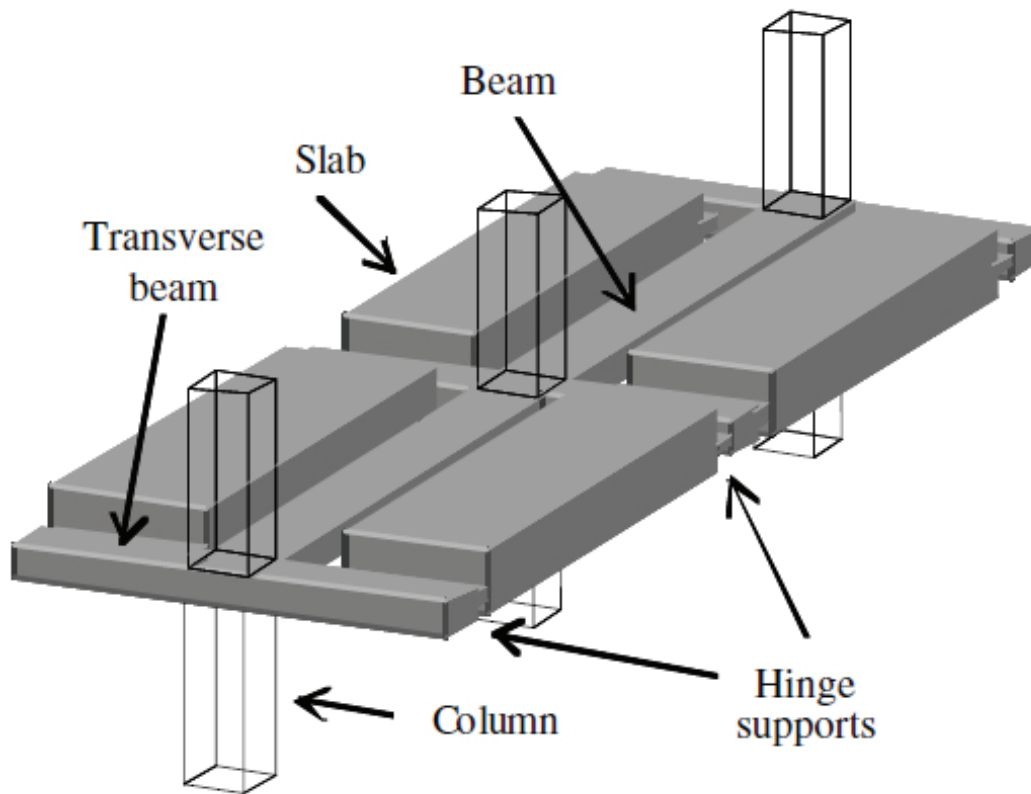


Figure 3.4: The Transverse Beams and Slab
(Stavridis *et al.*, 2012)

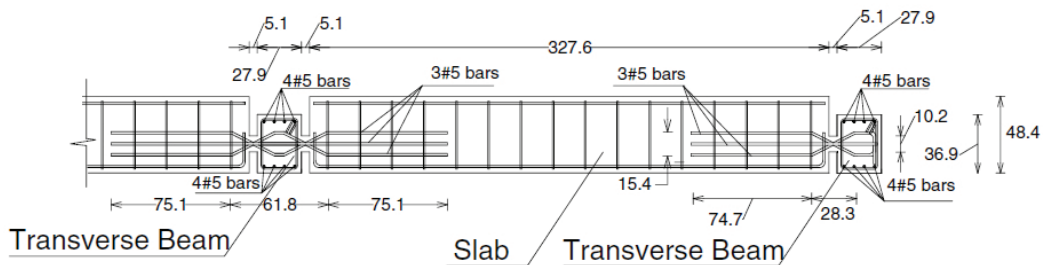


Figure 3.5: The Transverse Beams and Slab Reinforcement Detail
(Stavridis *et al.*, 2012)

3.2.2 Material Properties

Stavridis *et al.* (2012) performed tests on the materials of the test specimen. The results presented in this section were obtained from there. The concrete properties were determined from $15.2 \times 30.4\text{cm}$ cylinder compression tests at 28 days. The tension strength was obtained through split-cylinder tests. The

results of tests are presented in Table 3.2.

Table 3.2: The Material Properties of the Concrete at 28 Days

	Compressive Strength	Tensile Strength	Elastic Modulus	Strain at Peak Stress
Storey	[MPa]	[MPa]	[GPa]	$\left[\frac{m}{m}\right]$
1 st	37.99	3.47	15.14	0.0032
2 nd	41.95	3.96	17.44	0.0033
3 rd	39.17	4.04	16.98	0.0032
Average	39.70	3.82	16.52	0.00323

(Stavridis *et al.*, 2012)

The properties of the masonry were also obtained through various tests and are presented in Table 3.3.

Table 3.3: The Material Properties of the Masonry at 28 Days

	Compressive Strength	Elastic Modulus
Storey	[MPa]	[GPa]
1 st	19.80	5.41
2 nd	23.61	6.82
3 rd	22.81	6.52
Average	22.07	6.25

(Stavridis *et al.*, 2012)

The properties of Grade 60 reinforcement bars are defined in the ASTM A615M - 13 code (ASTM, 2003). These average values are given in Table 3.4.

Table 3.4: The Properties of Grade 60 Reinforcement

Tensile Strength	Density	Elastic Modulus	Poisson Ratio
[MPa]	$[kgm^{-3}]$	[GPa]	
420	7850	200	0.3

(ASTM, 2003)

3.2.3 The Earthquake Applied to the Test Structure

Stavridis *et al.* (2012) applied the 1989 Loma Prieta earthquake to the test structure. Stavridis *et al.* (2012) applied 14 scaled versions of the earthquake to the test specimen. The unscaled ground acceleration is shown in Figure 3.6.

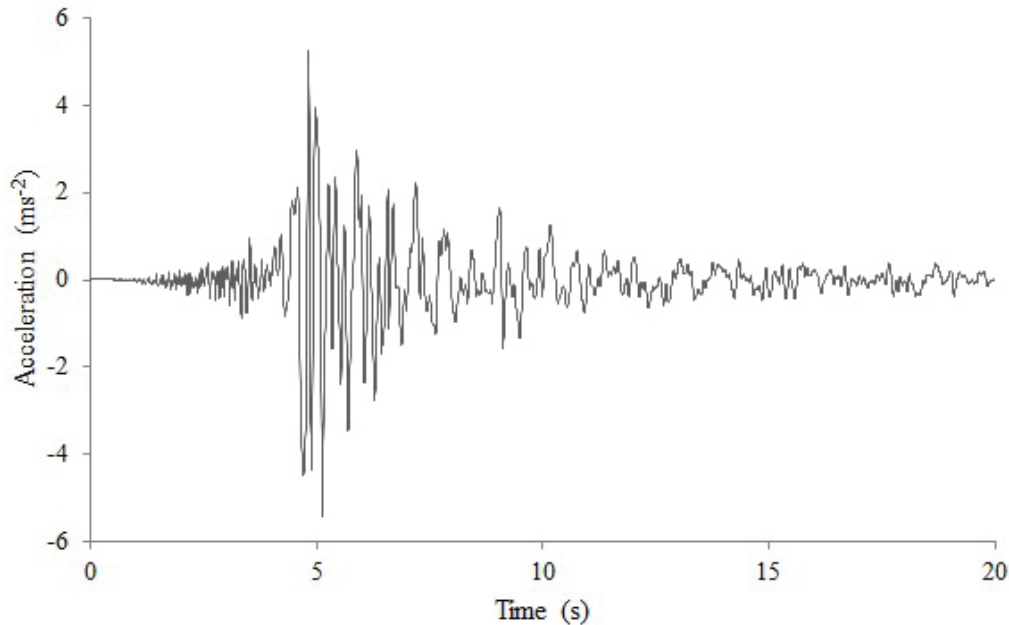


Figure 3.6: The Unscaled Ground Acceleration of the Loma Prieta Earthquake Measured at the Gilroy 3 Station

Stavridis *et al.* (2012) performed tests with various scaled versions of the Loma Prieta earthquake. The scaling ranged from 10% to 120% of the ground acceleration. For the purpose of this thesis, the results of the test using the 40% scaled earthquake was used. This was because it was the largest scaling of the earthquake which did not cause damage to the structure and therefore it remained elastic.

3.2.4 The Calibration of the Numerical Model of the Test Structure

The calibration of the model was performed in four steps. The first step was to obtain the correct weight of the structure which was achieved through manipulation of the densities of the materials. The second step was to obtain

the correct frequency. If the mass is correct, the changes made to the stiffness of the structure would result in the correct frequency. The third step was to obtain the correct acceleration of the roof when applying the scaled earthquake, which involved the adjustment of the damping ratio. The final step was to obtain the correct base shear ratio from the scaled earthquake.

3.2.4.1 The Structure Setup

The beams and columns of the structure were modelled as beam elements while the slabs were modelled as shell elements. The diagonal members that represent the masonry are truss elements. The resulting structure can be seen in Figure 3.7. It was assumed that the connection between the columns and the beams was fixed, while the connection of the slab to the beam was pinned. It was assumed that the connection to the base beam was fixed. Finally, the connection between the frame and the equivalent struts were modelled as pins as they only take axial load. These assumptions were made based on the anchorage of the reinforcement at the connections.

3.2.4.2 The Weight of the Structure

In Section 3.2.2 various materials of the model were discussed. The reinforcement steel used was Grade 60 rebar with a density of 7850 kgm^{-3} , which is specified by the ASTM A615M - 13 code. Unfortunately, the density of the concrete and the masonry are both unspecified in Stavridis *et al.* (2012) paper. Concrete can have a density between $1800\text{-}2400 \text{ kgm}^{-3}$ while masonry's density can range from 650 to 1500 kgm^{-3} (The Concrete Society of the United Kingdom, 2013). For this calibration, the density of the masonry was assumed equal to 1000 kgm^{-3} . With that assumption made, it was possible to vary the density of concrete until the correct mass was obtained. Using the Equation 3.2.1, the relative densities of the beam elements were found.

$$\bar{\rho} = \frac{\rho_c A_c + \rho_s A_s}{A_c + A_s} \quad (3.2.1)$$

Since the masonry was only modelled as struts and not a full panel, the density of the panels were added to the beams. The weights obtained from various densities are shown in Table 3.5 and graphically in Figure 3.8. The

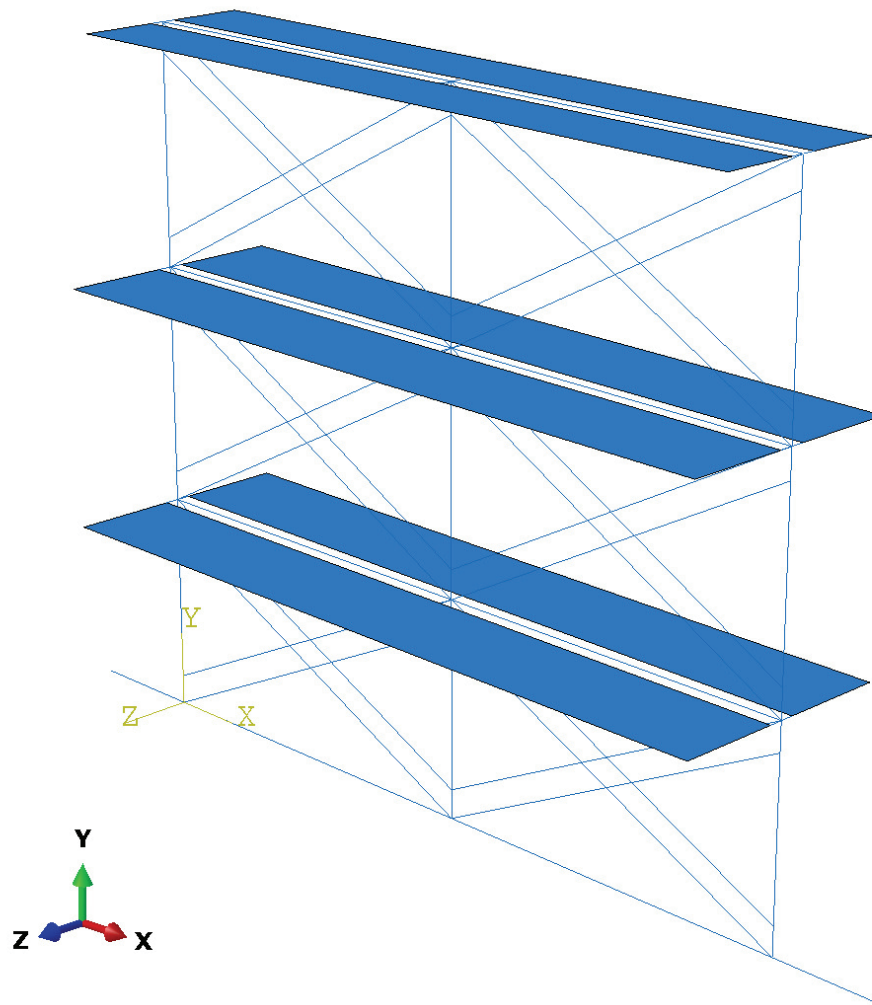


Figure 3.7: The Structure as Modelled in Abaqus

target weight of the structure is $645kN$ which is presented as the horizontal line on Figure 3.8

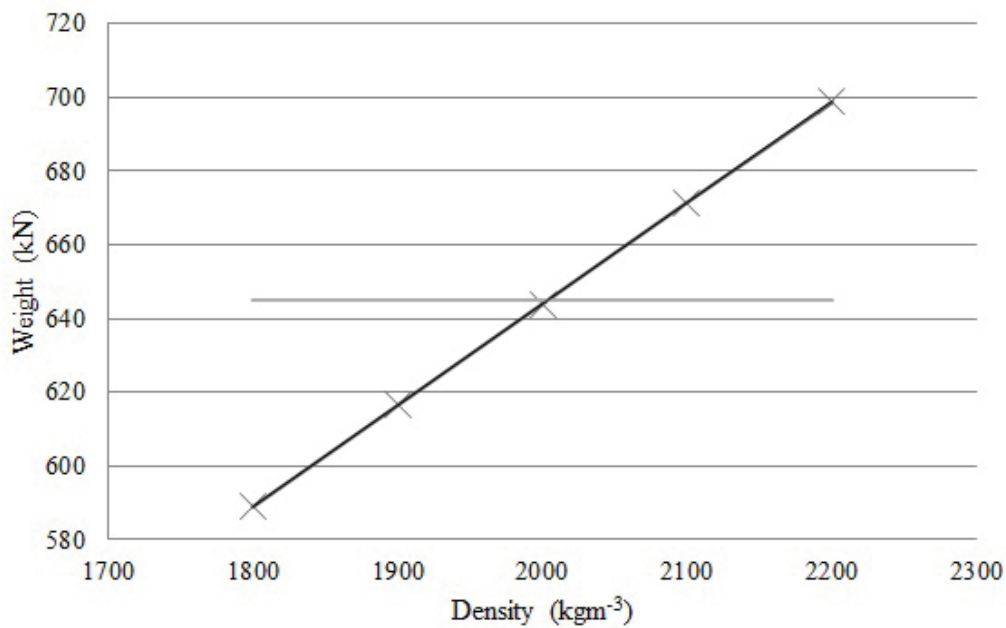
Figure 3.8 illustrates that the weight is linearly dependent on the density of the concrete defined by the Equation 3.2.2 where W is the weight of the structure and ρ is the density of concrete.

$$W = 0.2751\rho + 93.83 \quad (3.2.2)$$

From Equation 3.2.2, it was determined that a concrete density of $2004kgm^{-3}$ will lead to a weight of $645kN$ when the masonry panel's density is assumed equal to $1000kgm^{-3}$. The density of the concrete could be considered low, however if a masonry density of $650kgm^{-3}$ was used, it would result in a den-

Table 3.5: The Weight of the Structure Given Different Concrete Densities

Density	Weight
$[kgm^{-3}]$	$[kN]$
1800	588.9
1900	616.5
2000	643.9
2100	671.5
2200	698.9

**Figure 3.8:** The Weight of the Structure at Various Densities

sity of concrete of $2100kgm^{-3}$. It was felt that although this density is more reasonable, the lower density of the masonry would be unlikely in the building modelled from the 1970s.

3.2.4.3 The Frequency of the Structure

After the weight of the structure was calibrated, it was necessary to calibrate the stiffness of the structure in order to obtain its frequency. Equation 3.2.3 defines the angular frequency ω , while $[K]$ and $[M]$ are the stiffness and mass matrices of the structure, respectively (Chopra, 2007).

$$\det([K] - \omega^2[M]) = 0 \quad (3.2.3)$$

ω can be related to frequency by Equation 3.2.4.

$$f = \frac{\omega}{2\pi} \quad (3.2.4)$$

The first step to obtaining the stiffness of the structure was to calculate the stiffness of elements.

3.2.4.3.1 Beam Element Stiffness

The columns and beams of the structure are all composed of reinforced concrete. As these elements are modelled as homogenous materials, it was necessary to reduce the composite section elastic moduli into a single value \bar{E} . This was achieved with the use of Equation 3.2.5.

$$\bar{E} = \frac{E_c A_c + E_s A_s}{A_c + A_s} \quad (3.2.5)$$

With the detail of the cross-sections of the elements given in Figure 3.3 and the average elastic moduli given in Section 3.2.2, the resulting stiffness for each element is given in Table 3.6.

Table 3.6: The Equivalent Elastic Modulus of the Cross-Sections

Section	Area of Concrete	Area of Steel	Elastic Modulus of Concrete	Elastic Modulus of Steel	Elastic Modulus of Section
Section	A_c [mm^2]	A_s [mm^2]	E_c [GPa]	E_s [GPa]	\bar{E} [GPa]
A	100924	2027	16.5	200.0	20.1
B	100924	2027	16.5	200.0	20.1
C	99911	3040	16.5	200.0	21.9
D	77049	792	16.5	200.0	18.4
E	76543	1298	16.5	200.0	19.6
F	76258	1583	16.5	200.0	20.3
G	691912	6080	16.5	200.0	18.1
Transverse Beam	101368	1583	16.5	200.0	19.3

Sections A through G and the transverse beams is given in Figure 3.3 and 3.5.

3.2.4.3.2 The Masonry Panel Stiffness

The stiffness of the masonry panel is dependent on the area and elastic modulus of the compression truss element. When initial tests performed on the model, it was determined that the stiffness of the masonry panel was best represented using the width proposed by Paulay and Priestley (1992). The other methods for determining the width all led to results which were unrealistic. Paulay and Priestley's width w was calculated using Equation 3.2.6 where d_m is defined as the distance between two opposite corners of the masonry panel.

$$w = \frac{d_m}{4} \quad (3.2.6)$$

The area of effective strut A was then determined with Equation 3.2.9, where t is the thickness of the panel.

$$A = wt \quad (3.2.7)$$

Finally, the area of the effective strut must be divided equally between the two struts that constitute the modelling technique. The area of the struts used to simulate the panels with openings must be reduced with the opening factor R given in Equation 3.2.8 (Al-Chaar *et al.*, 2008). The resulting opening reduction factor is shown in Table 3.7.

$$R = 0.6\left(\frac{A_{open}}{A_{panel}}\right)^2 - 1.6\left(\frac{A_{open}}{A_{panel}}\right) + 1.0 \quad (3.2.8)$$

This reduction factor is then applied to the area of the strut resulting in Equation 3.2.8.

$$A_{red} = Rwt \quad (3.2.9)$$

Table 3.7: The Opening Factor of the Masonry Panel

Area of Masonry Panel	Area of Opening	Opening Factor R
$[m^2]$	$[m^2]$	
6.326	0.527	0.871

The elastic modulus of the element was given in Section 3.2.2. The properties of the masonry used in the model are given in Table 3.8

Table 3.8: The Properties of the Masonry Strut

Area of Each Strut Without an Opening	Area of Each Strut With an Opening	Elastic Modulus
$[mm^2]$ 90808	$[mm^2]$ 79079	$[GPa]$ 6.5

3.2.4.3.3 The Resulting Frequency Using Initial Stiffness

Stavridis *et al.* (2012) measured the frequency of the structure as $17.85Hz$. With the properties given in the previous sections, the numerical model resulting in a frequency of $13.07Hz$. The difference between the target frequency and the frequency of the numerical model differed significantly enough not to be accepted. As the mass of the model, geometry and connections are correct, this could only mean that the moduli of elasticity are incorrect. As the elastic modulus of Grade 60 steel is known, it meant that the moduli of the concrete and masonry was incorrect.

3.2.4.3.4 The Recalibration of the Beam Stiffness

The modulus of elasticity of the concrete is given in Section 3.2.2 as $16.52GPa$. The American Concrete Institute (2008) suggests that the elastic modulus, E_c , of concrete can be approximated by Equation 3.2.10 where ρ_c is the density of the concrete given in kgm^{-3} and f_c is the compressive strength of the concrete given in MPa .

$$E_c = 0.043\rho_c^{1.5}f_c^{0.5} \quad (3.2.10)$$

Using Equation 3.2.10, the value of E_c was obtained as $24.4GPa$. Using this value for the elastic modulus of concrete, the resultant stiffness of the cross-sections are presented in Table 3.9

Table 3.9: The Equivalent Elastic Modulus of the Cross-Sections with New Concrete Elastic Modulus

Section	Area of Concrete	Area of Steel	Elastic Modulus of Concrete	Elastic Modulus of Steel	Elastic Modulus of Section
Variable	A_c [mm^2]	A_s [mm^2]	E_c [GPa]	E_s [GPa]	\bar{E} [GPa]
A	100924	2027	24.4	200.0	27.9
B	100924	2027	24.4	200.0	27.9
C	99911	3040	24.4	200.0	29.6
D	77049	792	24.4	200.0	26.2
E	76543	1298	24.4	200.0	27.3
F	76258	1583	24.4	200.0	28.0
G	691912	6080	24.4	200.0	25.9
Transverse Beam	101368	1583	24.4	200.0	27.1

3.2.4.3.5 Resulting Frequency Using the Changed Beam Stiffness

The new beam stiffness resulted in a frequency of $13.856Hz$. The difference between this frequency and that given by for the structure by Stavridis *et al.* (2012) is still unacceptable. As both the elastic moduli of steel and concrete are defined, the stiffness of the masonry must therefore be adjusted.

3.2.4.3.6 The Recalibration of the Masonry Stiffness

The masonry strut's stiffness is governed by the area and the elastic modulus of the strut. As stated in Section 3.2.4.3.2, the area of the strut was determined using Paulay and Priestley (1992)'s method which is considered as conservative. It is for this reason that the elastic modulus of the masonry was changed to obtain the correct frequency of the structure. The frequency at various elastic moduli for masonry is presented in Table 3.10.

A final elastic modulus of masonry was chosen as $14.9GPa$. This resulted in a frequency of the numerical model of $17.849Hz$ which is comparable to $17.85Hz$ obtained by Stavridis *et al.* (2012).

3.2.4.3.7 The Mesh Size of the Elements

Once the final value was obtained, the mesh size of the elements was reduced

Table 3.10: The Frequency of the Structure at Various Elastic Modulii of Masonry

Elastic Modulus of Masonry	Frequency of the Structure
[<i>GPa</i>]	[<i>Hz</i>]
6.25	13.856
13.00	17.258
14.00	17.582
15.00	17.878
16.00	18.148

until there was an insignificant change to the frequency obtained. This process resulted in a mesh size of $0.25m$.

3.2.4.3.8 Comments on the Calibration of the Frequency

The changes to the elastic modulii of the concrete and the masonry from those given by Stavridis *et al.* (2012) was necessary to obtain the correct stiffness. The change in the stiffness of the concrete was found to be justified through the use of Equation 3.2.10 provided by American Concrete Institute (2008). The stiffness of the masonry was measured through a masonry prism test (Stavridis *et al.*, 2012). This test did not take into account the masonry panel's confinement by the frame as well as influence of the mortar in the panel. It is for these two reasons that the value given for the elastic modulus of the masonry is questionable thereby allowing for the changes in the value during the modelling process.

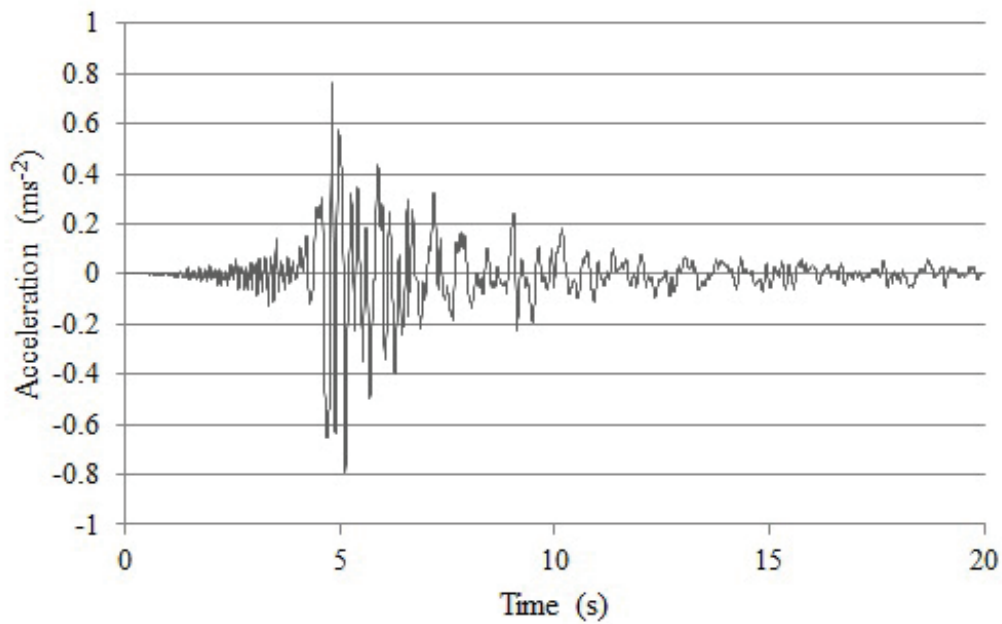
3.2.4.4 The Acceleration of the Roof

After the mass and the stiffness of the structure was calibrated, it was necessary calibrate the model in terms of acceleration, velocity and displacement. This was done by comparing the maximum acceleration value of the center of the roof from the model and the experimental results. First it was necessary to establish that the results obtained from the model are correct.

3.2.4.4.1 Acceleration, Velocity and Displacement of the Excitation Point

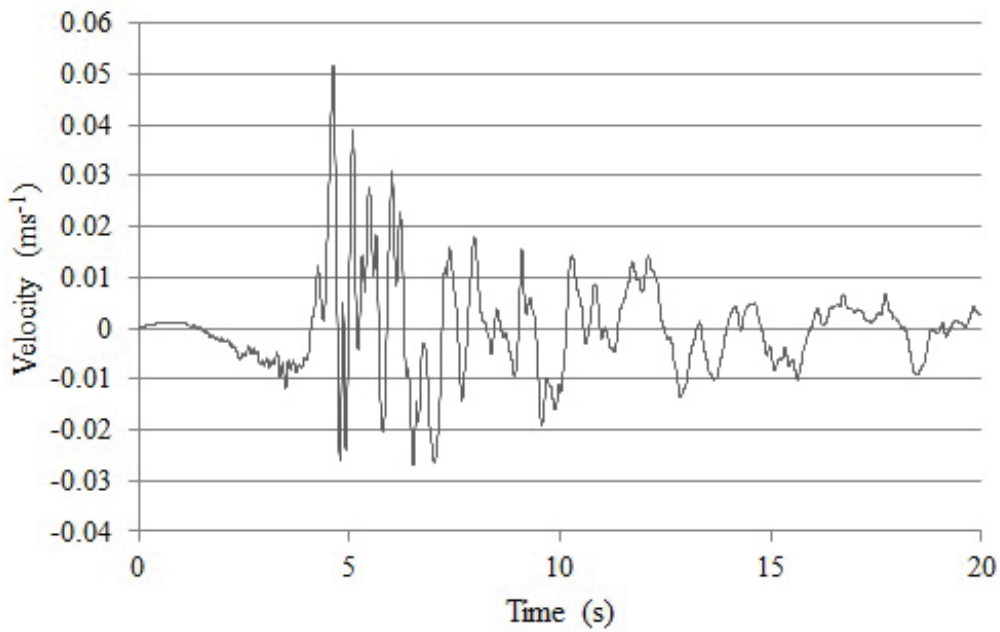
The excitation is the point where the ground acceleration data of the earth-

quake is applied to the model. In order to be confident of the results, the acceleration, velocity and displacement results obtained at the excitation point of the finite element model must match the expected values. Figure 3.9 shows the experimental ground acceleration. Figure 3.10 and Figure 3.11 shows the graphs for the velocity and displacement, respectively. The results obtained from Abaqus show that at the excitation point the acceleration, velocity and displacement are identical. This shows that the model yields correct accelerations, velocities and displacements responses at the base of the structure.



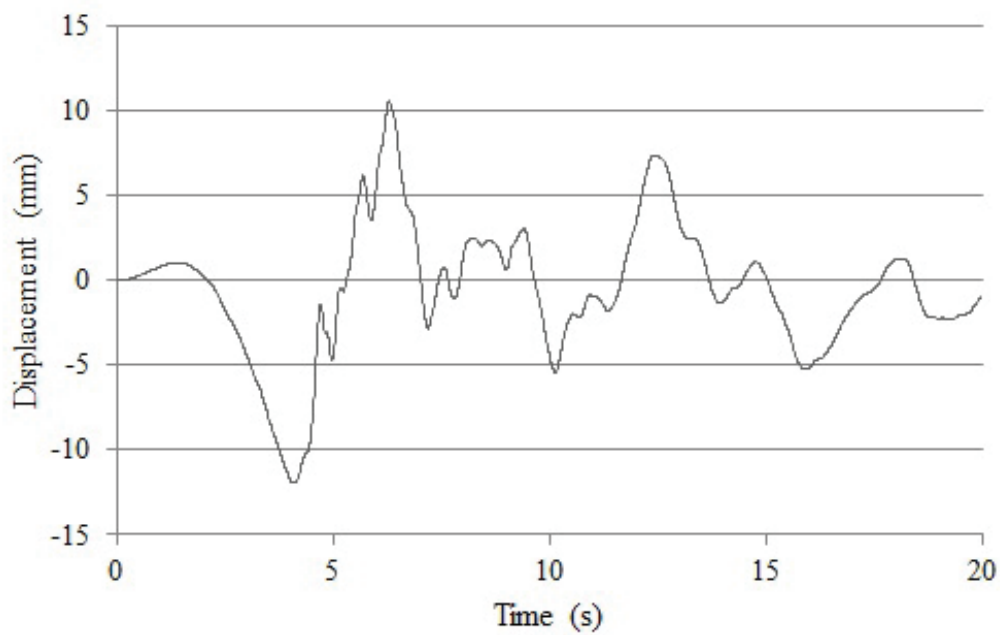
(a) The Experimental Applied Ground Acceleration

Figure 3.9: The Acceleration at the Excitation Point



(a) The Experimental Applied Ground Velocity

Figure 3.10: The Velocity at the Excitation Point



(a) The Experimental Applied Ground Displacement

Figure 3.11: The Displacement at the Excitation Point

3.2.4.4.2 The Acceleration of the Roof without Damping

After the calibration, it was necessary to compare the accelerations obtained of the roof to the value given by Stavridis *et al.* (2012). Figure 3.12 shows the graph of the acceleration as measured at the top of the middle column. The graph shows that there is no absorption of energy from the structure. In order for the model to partially absorb the energy given by the earthquake, damping must be included into the material properties.

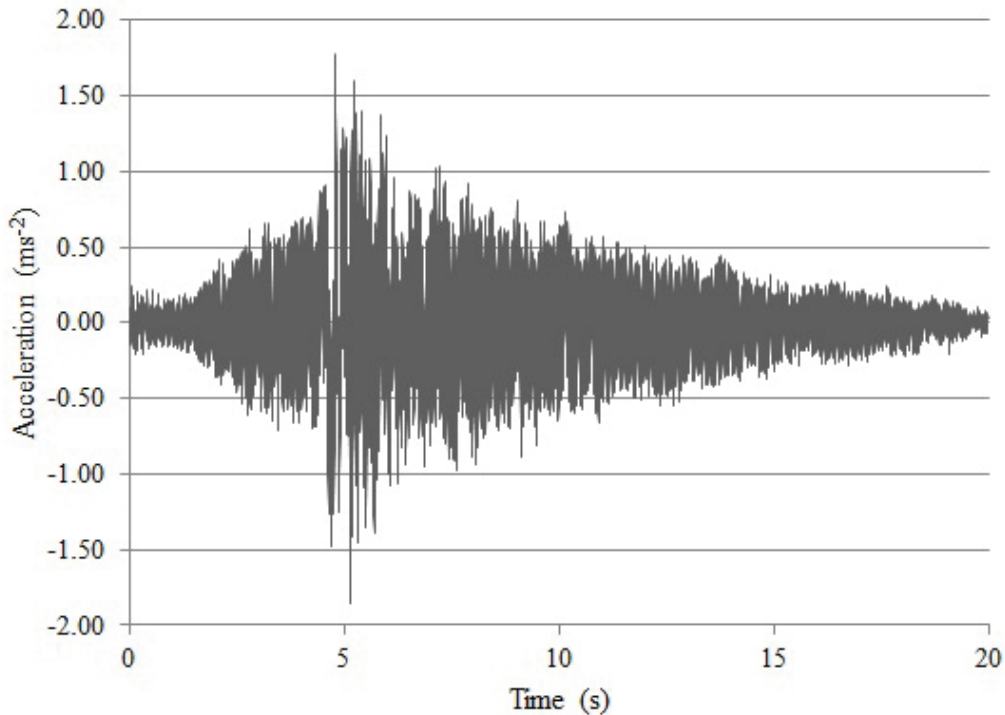


Figure 3.12: The Acceleration of the Roof without Damping

3.2.4.4.3 Rayleigh Damping

ABAQUS uses a method of damping called Rayleigh damping. To define Rayleigh damping, factors α and β must be defined. α is the factor related to mass damping and β is related to stiffness damping. The formula for the fraction of the critical damping ξ is given in Equation 3.2.11 where ω is the angular velocity of the mode in question.

$$\xi = \frac{\alpha}{2\omega} + \frac{\beta\omega}{2} \quad (3.2.11)$$

3.2.4.4.4 The Acceleration of the Roof at Different Damping Factor Values

The first attempt at including damping in this model was performed using only the mass damping with $\alpha = 0.55$, which resulted in an insignificant decrease in the acceleration of the roof. The numerical results were not within an acceptable range compared to the acceleration of $1.27ms^{-1}$. As the change in acceleration was insignificant when altering the α values, it was decided to fix the value of α at 0.4 while varying the β factor. The resulting values for the acceleration of the roof at various β values is shown in Table 3.11. The ξ values were calculated using $\omega = 2.841 \frac{rad}{s}$ which is the angular velocity associated to the frequency of the structure.

Table 3.11: The Acceleration of the Roof at Various β Values

α	β	ξ	Roof Acceleration
		[%]	$[ms^{-1}]$
0.4	0.00676	8.000	1.1982
0.4	0.00600	7.892	1.2065
0.4	0.00400	7.608	1.2297
0.4	0.00350	7.537	1.2349
0.4	0.00300	7.466	1.2437
0.4	0.00250	7.395	1.2549

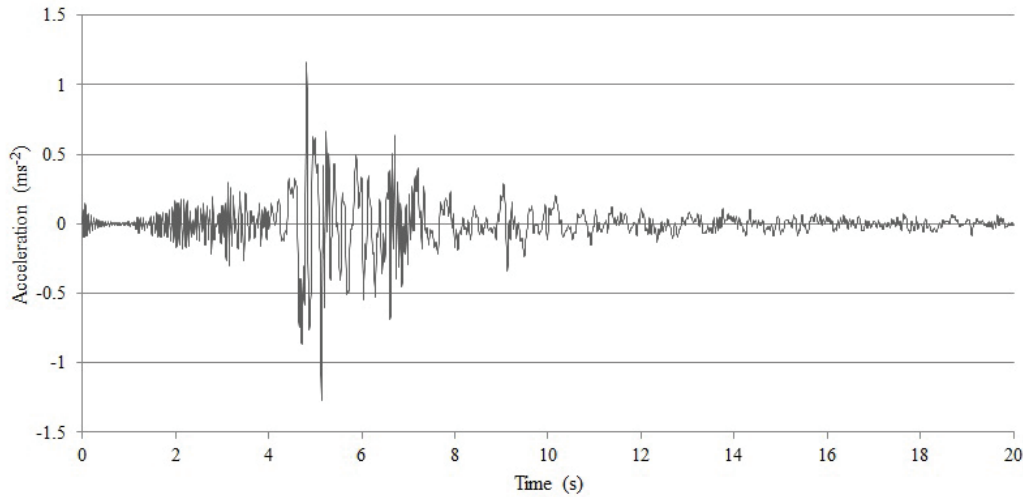
Upon reaching an acceleration for the roof of $1.25ms^{-1}$, it was decided to test whether a change in α still resulted in an insignificant change in the acceleration. Once this was established, it was decided that the final value for α should be 0.3 as it resulted in a ξ value closer to 5% which is deemed reasonable for a reinforced concrete framed structure with masonry infill. A further distinction must be made that although changing the α value to achieve a damping percentage of five seems significant, the change results in a small difference to the acceleration of the roof. A final change was made to the β value to yield more accurate results. This is presented in Table 3.12 while Figure 3.13 shows the acceleration experienced by the roof.

3.2.4.4.5 Comments on the Calibration of the Damping

As changes to the α factor does not result in large changes to the acceleration of the roof, the value of 0.3 was chosen such that ξ approached 5%. Changes

Table 3.12: The Acceleration of the Roof with Final Damping Factor Values

α	β	ξ	Roof Acceleration
		[%]	$[ms^{-1}]$
0.4	0.00250	7.395	1.2549
0.3	0.00250	5.635	1.2557
0.3	0.002	5.564	1.2665

**Figure 3.13:** The Acceleration of the Roof

in the β factor resulted in relatively small changes in the acceleration of the roof. As such, it was changed to a point where it yielded a difference of less than 1% from the acceleration given by Stavridis *et al.* (2012).

3.2.4.5 The Base Shear

The final parameter required for comparison was the base shear. This is the force measured at the foundation on the structure. This check is purely to confirm that the model is performing as expected. The value obtained by Stavridis *et al.* (2012) for the base shear is 0.97 of the weight of the structure. The base shear response obtained from the finite element model is presented in Figure 3.14.

Figure 3.14 shows that the maximum value of the base shear is $629.08kN$ which results in ratio of 0.975 to the weight. This ratio obtained is well within acceptable levels.

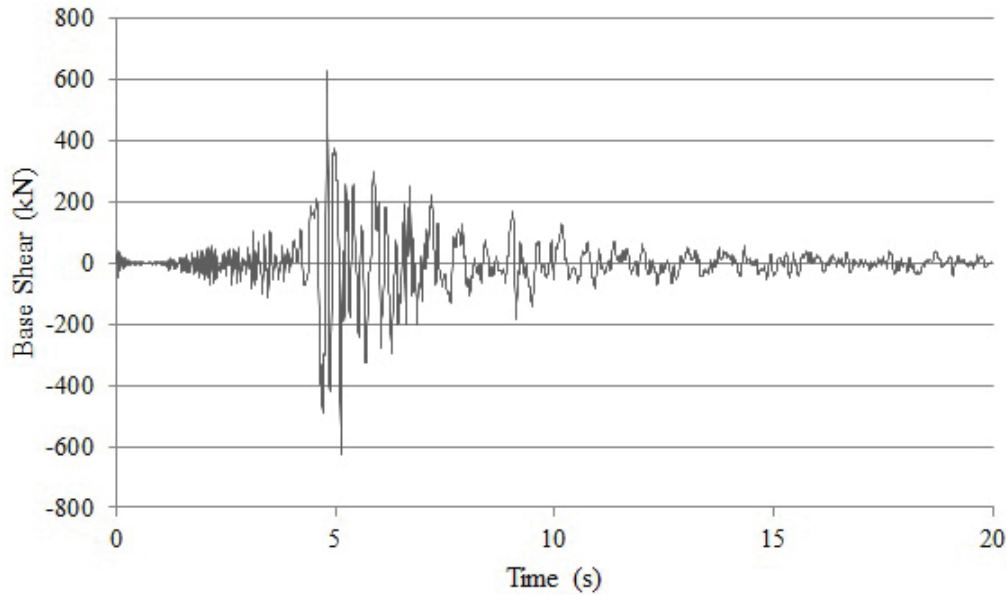


Figure 3.14: The Base Shear of the Test Structure

3.2.4.6 Comments on the Calibration of the Model

The purpose of the calibration model was to obtain material models that can be used confidently in the modelling of other reinforced concrete framed buildings. The limitations of the numerical model is that it was calibrated for an undamaged frame and undamaged masonry panels. The reality is that structures experience damage over time. As no two earthquakes are the same, the use of an earthquake which occurred in the United States does not invalidate the material model. Although there are limitations, the material model generated is sufficient to make the necessary conclusions on the concrete reinforced frames found in the greater Cape Town region.

3.3 The Representative Structure

The choice of a representative structure was made by evaluating the building's size and shape. It was important for the building to be similar to those found in the greater Cape Town region. With this in mind, the representative structure was based on a reinforced concrete framed building found in Stellenbosch.

3.3.1 Information on the Building

The building chosen was built in 1971 which pre-dates the first seismic code in South Africa. The structure is three storeys high with two bays on the short side and four bays on the long side as shown in Figure 3.15. The structure is currently used as a disaster management facility for the area of Stellenbosch and it is therefore important for it to remain undamaged during an earthquake.

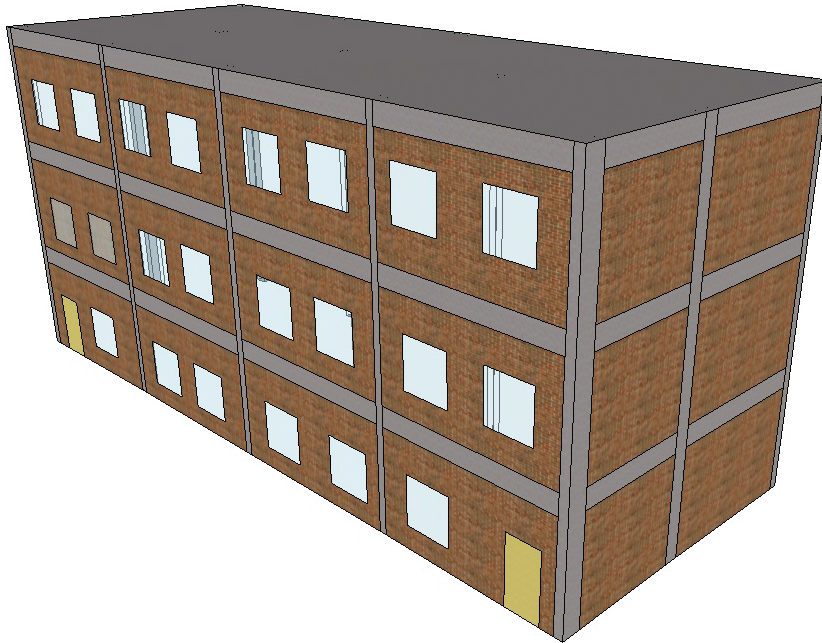


Figure 3.15: A 3D Representation of the Representative Structure

3.3.2 Structural Information

The only available information of the building was a plan layout. It was however possible to make certain assumptions regarding other values needed without compromising the conclusions of the thesis. The plan layout of the structure is presented in Figure 3.16 with the red lines representing the masonry infill panes. The cross-sectional dimensions of the columns is presented in Table 3.13. Table 3.13 refers to beams B1 and B2. Beam B1 spans along grid lines 1-5 while beam B2 spans along grid lines A-C. The floors are spaced at $3.8m$ intervals.

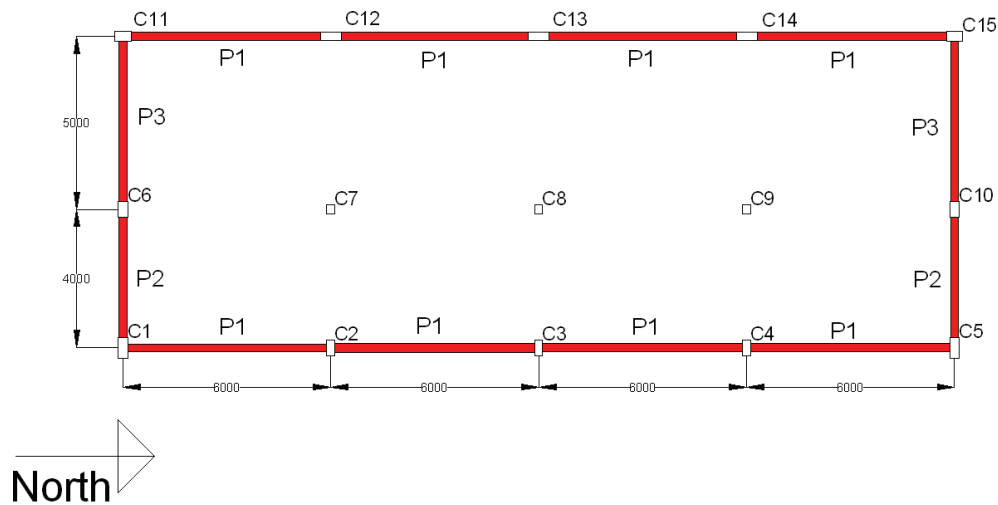


Figure 3.16: The Plan View of the Representative Structure

As the reinforcement detail was not available, the reinforcement of the beams and columns had to be assumed. As was shown in Section 3.2.4.3.4, a change to the stiffness of the columns and beams would result in a small change in the stiffness of the structure. It is for this reason that the reinforcement detail could be assumed. The vertical reinforcement in the column was assumed at 2% for the ground floor, 1.5% for the second floor and 1% for the top floor. These values were used as they correspond to the reinforcement in the calibration process. With regard to the reinforcement in the beams and slabs, a value of 2% and 1% were assumed, respectively, which also reflect the values of the calibration process. It is important to note that the structure is not sensitive to changes in column stiffness and as such the reinforcement assumed could be a wide range of values. The values chosen here reflect the values used in the calibration process. The values are within the range suggested by current concrete design code SANS 10100 for columns which specifies the minimum reinforcement of 0.4% and a maximum of 6%. The corresponding values for beams are 0.26% and 4%. The suggested values for slabs are 0.13% and 4% (SANS 10100-1, 2000).

Table 3.13: The Dimensions of the Columns

	b	h
Column	[<i>mm</i>]	[<i>mm</i>]
C1	280	600
C2	230	460
C3	230	460
C4	230	460
C5	280	600
C6	280	465
C7	230	280
C8	230	280
C9	230	280
C10	280	465
C11	465	280
C12	600	230
C13	600	230
C14	600	230
C15	465	280
B1	230	600
B2	280	600

3.3.3 Material Properties

The same material properties that were used in the calibration process were used for the model of the representative structure. The properties of the concrete, masonry and steel used are presented in Table 3.14, Table 3.15 and Table 3.16 respectively.

Table 3.14: The Concrete Properties

Compressive Strength	Elastic Modulus	Density	Poisson Ratio
[<i>MPa</i>]	[<i>GPa</i>]	[<i>kgm⁻³</i>]	
39.7	24.4	2004	0.21

3.3.4 Beam Element Stiffness

As the vertical reinforcement was assumed as a percentage of the column cross-sectional area, it was possible to calculate the effective elastic modulus

Table 3.15: The Masonry Properties

Compressive Strength	Elastic Modulus	Density	Poisson Ratio
[MPa]	[GPa]	[kgm ⁻³]	
22.07	14.9	1000	0.21

Table 3.16: The Steel Properties

Tensile Strength	Density	Elastic Modulus	Poisson Ratio
[MPa]	[kgm ⁻³]	[GPa]	
420	7850	200	0.3

\bar{E} for the ground, first and second floor. The effective stiffness is presented in Table 3.17. The stiffness of the beams were calculated in the same manner.

Table 3.17: The Effective Stiffness of the Columns for Various Floor

	A_c	A_s	E_c	E_s	\bar{E}
Floor	[%]	[%]	[GPa]	[GPa]	[GPa]
Ground	98.0	2.0	24.4	200	27.91
First	98.5	1.5	24.4	200	27.03
Second	99.0	1.0	24.4	200	26.16

3.3.5 Masonry Struts

This structure contains three different masonry panels. The first panel, referred to as p_1 is found in the North-South direction, i.e. the long side of the building. They are all the same size with doors and windows in each panel. The second and third panels, p_2 and p_3 respectively, both occur on the East-West direction, i.e. the short side of the structure. The positions of the different panels is shown in Figure 3.16. Both panels p_2 and p_3 do not have openings and the only difference is their size. The information with respect to the panels is presented in Table 3.18.

Although the areas of the doors and windows in each panel are not exactly the same, their magnitudes are within 2% of each other and therefore a single

value for the opening reduction factor was used. The opening reduction factor, R , was determined using Equation 2.3.7.

Table 3.18: The Information on the Masonry Panels

	Area of Panel Face	Area of Opening	Opening Reduction Factor R
Panel	$[m^2]$	$[m^2]$	
p_1	17.50	4.56	0.62
p_2	11.33	0.00	1.00
p_3	14.53	0.00	1.00

The method for calculating the properties of the struts was presented in the calibration process. The same method was applied to get the properties presented in Table 3.19. The area of each strut was determined by Equations 3.3.1 and 3.3.2 while applying the reduction factors shown in Table 3.18.

$$w = \frac{d_m}{4} \quad (3.3.1)$$

$$A = \frac{wt}{2} \quad (3.3.2)$$

Table 3.19: The Area of Each Masonry Panel's Strut

	Diagonal Length	Width	Thickness	Area per Strut
Variable	d_m	w	t	A
Panel	$[m]$	$[m]$	$[m]$	$[m^2]$
p_1	6.34	1.58	0.22	0.174
p_2	4.77	1.19	0.22	0.131
p_3	5.55	1.39	0.22	0.153

3.3.6 Representative Earthquakes Chosen

The buildings in the area under consideration must resist a moderate intensity earthquake. A moderate intensity earthquake has a magnitude between 4.0-5.9 on the Richter scale (USGS, 2012). As discussed in Section 2.1.3, an earthquake in Tulbagh, Western Cape resulted in a 6.3 magnitude. In Section

2.2.2.1, the peak ground acceleration evaluation by the Council of Geosciences specified a value of $0.15g$ for the area under consideration. With a Richter magnitude range of 5.5-6.5 and peak ground acceleration of between $0.1-0.15g$, a search was performed on the PEER Strong Motion Database maintained by Pacific Earthquake Engineering Research Center (2013) for earthquakes which satisfied these requirements. Although many earthquakes fulfilled these requirements, it was decided that only five of these would be used. The five earthquakes chosen are presented in Table 3.20. The resultant peak ground acceleration was calculated by combining both directions at each time step and choosing the maximum. Detailed information pertaining to these earthquakes is presented in Appendix A. It is worth noting that the earthquake applied to the calibration structure was only in a single direction. The earthquakes were applied to the representative structure in a combination of both the North-South and East-West seismographs in the appropriate directions. This was done to best simulate a real earthquake. Although the earthquakes chosen all occurred in the United States, they will still allow for conclusions to be made about structures in the Cape Town Region. As no two earthquakes are the same, the use of earthquakes that occur in the United States is just as good as using one from Cape Town.

3.3.7 Three Dimensional Frame Model

The representative structure was modelled in ABAQUS using the material properties described in the previous sections. The same damping constants of $\alpha = 0.3$ and $\beta = 0.002$, that were obtained from the calibration process, was used. The connections were all fixed with the exception of the masonry struts to the frame which was pinned. The frequency of this structure is different to the frequency of the calibration model. This model is designed to displace in two directions thus resulting in two natural frequencies. The two modes are shown in Figure 3.17 and Figure 3.18.

The two modes have frequencies of $6.20Hz$ and $8.97Hz$ for mode 1 and mode 2, respectively. Mode 1 results from movement in the East-West direction while mode 2 pertains to the North-South direction. It should also be noted that there is a torsional response in both modes as the structure is not symmetric in stiffness due to the different cross-sections of the columns. It was during process that the mesh size was determined such that the frequencies of

Table 3.20: The Five Representative Earthquakes Chosen

Earthquake	Magnitude	Date	Direction	Peak Ground Acceleration (g)
Coalinga	6.4	02/05/1983	North-South	0.098
			East-West	0.100
			Resultant	0.104
Coyota Lake	5.7	06/08/1979	North-South	0.108
			East-West	0.107
			Resultant	0.109
Morgan Hill	6.2	24/04/1984	North-South	0.069
			East-West	0.098
			Resultant	0.099
Palm Springs	6.0	08/07/1986	North-South	0.110
			East-West	0.095
			Resultant	0.111
Whittier Narrows	6.0	01/10/1987	North-South	0.109
			East-West	0.103
			Resultant	0.124

the structure changed insignificantly when the mesh size was reduced further.

3.3.7.1 Results of the Three Dimensional Frame Model

The earthquakes chosen to represent a possible ground motion found in the the greater Cape Town area was applied to the model. From this, the forces experienced by the columns were obtained. The structure has a total of fifteen columns however some have the same cross-section. As there is six different cross-sections, it was decided to chose six columns to represent the six cross-sections. The six columns chosen were C1, C3, C6, C8, C11 and C13. Figure 3.19 shows an example of the resultant forces in Column C13 when subjected to the Palm Springs earthquake. The rest of the force diagrams are given in Appendix B. Since the columns were previously modelled as beam elements, it was necessary to model the columns as 3D elements to obtain the stresses in concrete and the steel.

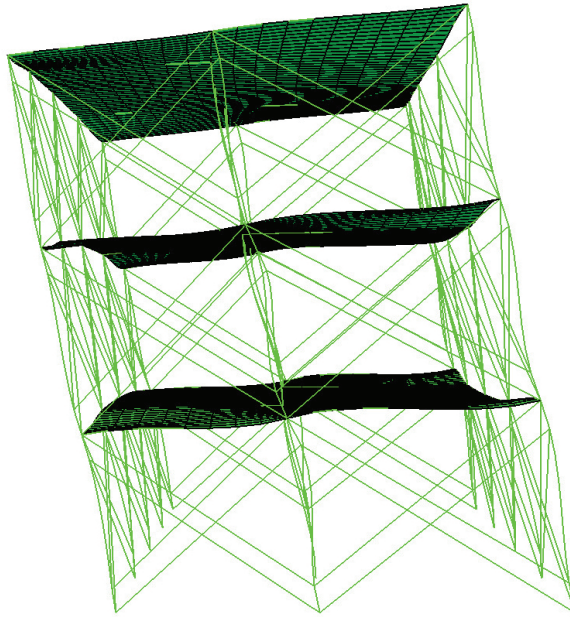


Figure 3.17: Frequency Mode 1 of Representative Structure

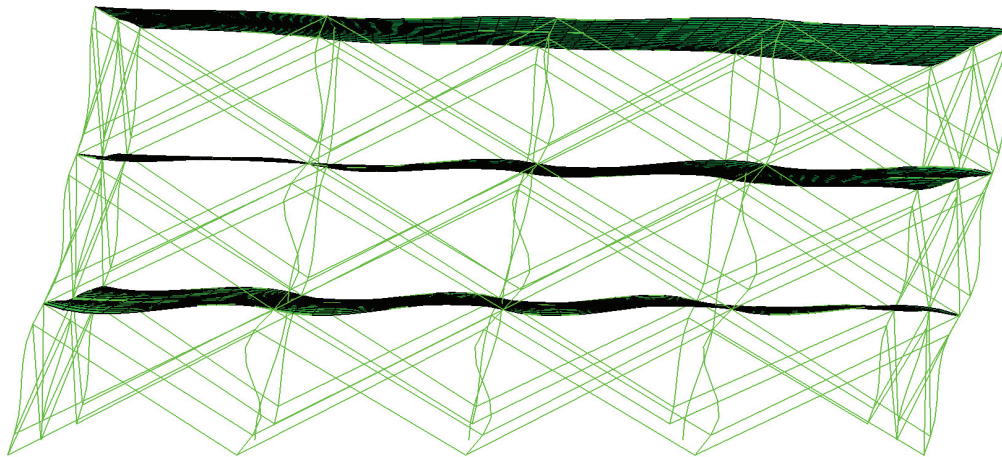
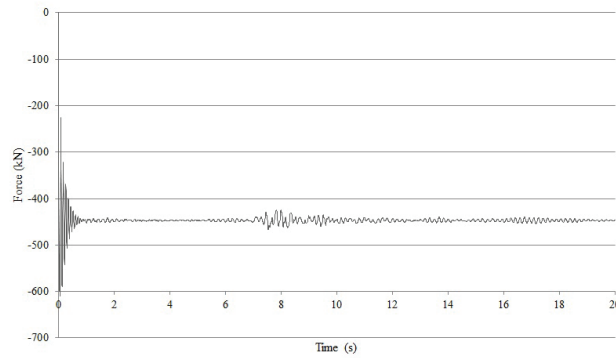


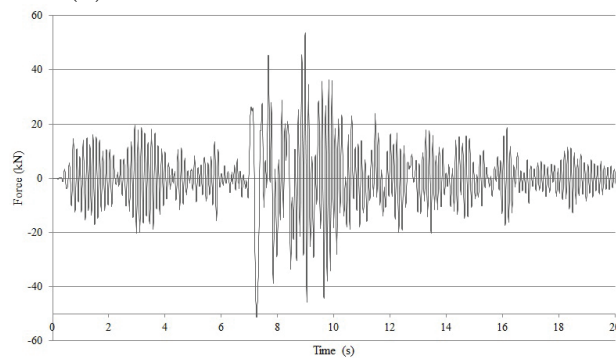
Figure 3.18: Frequency Mode 2 of Representative Structure

3.3.8 Modelling of an Individual Column

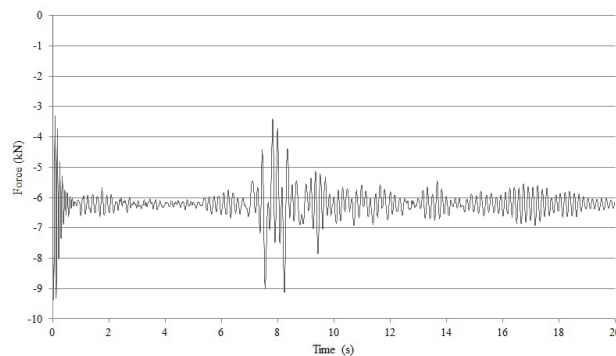
Modelling of the columns in three dimensions (3D) was necessary to obtain the stress values at specific points in the concrete as well as the steel. The concrete of the column was modelled using solid 3D elements through the cross section and height. The steel was modelled as a beam element. Since the steel was now modelled as an element, it was necessary to define its diameter which is presented in Table 3.21. The reinforcement in Table 3.21 was chosen to



(a) The Axial Force on Column C13



(b) The Shear Force on Column C13 in the Direction of the Long Side



(c) The Shear Force on Column C13 in the Direction of the Short Side

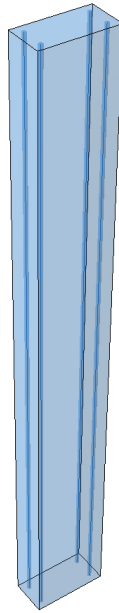
Figure 3.19: The Forces in Column C13 when the Palm Springs Earthquake is Applied

be as close as possible to the area of steel used during the 3D beam model. Figure 3.20 shows the ABAQUS model.

An important component of this model is the interaction between the steel and the concrete. This is to ensure that the forces are correctly transferred between the concrete and the steel. As this interaction is dependent on a multitude of variables, it was suggested that the steel is "embedded" into the

Table 3.21: Area of Steel for the Modelling of the Columns

	A_c	A_s Assumed	A_s Chosen	A_s Provided
Column	$[mm^2]$	$[mm^2]$		$[mm^2]$
C1	168000	3360	4Y32	3217
C3	106950	2139	4Y25	1963
C6	130200	2604	4Y32	3217
C8	55200	1104	4Y20	1257
C11	130200	2604	4Y32	3217
C13	138000	2760	4Y32	3217

**Figure 3.20:** The 3D Model of Column C3

concrete. By embedding the steel into the concrete, ABAQUS links the nodes of the elements where they intersect. Although this does not take into account the bond strength of the concrete to the steel, the results are accurate enough to be a fair representation of the situation (Dassault Systemes, 2013).

The forces obtained in the Section 3.3.7.1 were applied to the apex of the column while the bottom of the column was modelled as a fixed support. The elements in which the results were obtained were all found at the fixed support. The results of this model is presented in Chapter 4.

3.3.8.1 Mesh Sizes in the Modelling of the Individual Columns

The mesh size was chosen as $50mm$. This was done for two reasons. Firstly, the centroid of the steel was assumed to $50mm$ from the edge of the concrete. By choosing the mesh size to equal that of the cover, it allowed the embedment constraint to be efficient. The second reason was that the analysis of the column was time inefficient. The improved results of a finer mesh would not have justified the increase in analysis time.

3.3.9 Comments on the Modelling of the Representative Structure

The forces within the columns of the representative structure can be justified by the calibration process and therefore the results of this model are accepted. The modelling of the individual columns is less accurate. The interaction between the steel and the concrete is not entirely accurate. This inaccuracy will not cause significant errors though it should be considered when drawing conclusions. Unfortunately due to time constraints, it was not possible to rotate the building to different angles in order to check those loading conditions.

Chapter 4

Results

4.1 Introduction

The results of the columns that were modelled in 3D are presented in terms stresses. This chapter only represents the results from the analysis while the results will be discussed in Chapter 5.

4.2 Results of the Individual Column

The columns that were modelled in 3D are identified as C1, C3, C6, C8, C11, C13 shown in Figure 3.16. As each column has a different cross-section and placed in different positions in the building lead to different individual stresses in the concrete and steel.

4.2.1 The Resultant Stresses of the Concrete

The stress in the concrete varies through the height and cross-section and therefore it becomes important to obtain the stresses at critical points in the column as shown in Figure 4.1. These critical elements are all found on the bottom of the column as it is here where the maximum stresses were found. The identification numbers on Figure 4.1 represent the element numbering used.

A number of different types of stresses can be obtained from ABAQUS. In order to compare critical points, the principal stresses were obtained. The principal stresses is the maximum or minimum normal stress which act on an

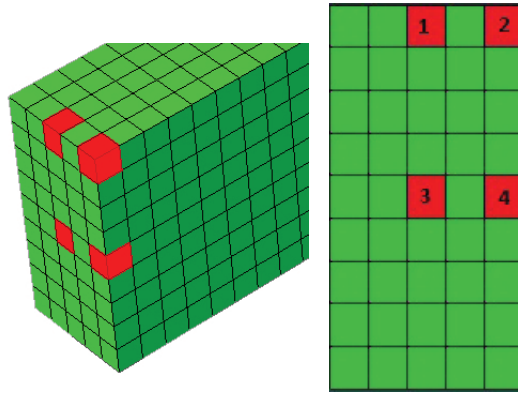


Figure 4.1: The Elements Where Stresses Were Obtained on Column C3

element (Craig, 2000). Since 3D elements were used to model the concrete, it will result in a principal stress in each of the three directions. From the principal stresses σ_p , the maximum shear stress, τ , on each plane can be found using Equation 4.2.1

$$\tau_{ij} = \frac{\sigma_{pj} - \sigma_{pi}}{2} \quad (4.2.1)$$

Where i and j are the directions of the principal stresses and $i \neq j$.

Tables 4.1, 4.2, 4.3, 4.4, 4.5 and 4.6 presents the principal and shear stresses of the columns. A negative principal stress means that the element is in compression in that direction. For each direction in the element two principal stresses were obtained. The first principal stress is the minimum stress experienced in that direction while the second is the maximum principal stress experienced in that direction.

4.2.2 The Resultant Stresses in the Steel

The reinforcing steel was modelled as beam elements. In order to obtain the stresses in the steel, it was necessary to obtain the forces and convert it into stresses. The simulations resulted in three forces per element, namely an axial force and two shear forces. These forces were converted into stress, namely the axial stress f_a and two shear stresses τ_1 and τ_2 . Tables 4.7, 4.8, 4.9, 4.10, 4.11 and 4.12 presents the maximum and minimum stresses of each reinforcement bar in each column. For each of the stresses, a minimum and maximum value was obtained. Once again, a negative value refers to compressive stresses.

Table 4.1: The Principal and Shear Stresses of Column C1

		σ_{p1}	σ_{p2}	σ_{p3}	τ_{12}	τ_{23}	τ_{13}
Earthquake	Element	[MPa]	[MPa]	[MPa]	[MPa]	[MPa]	[MPa]
Coalinga $a_{N-S} = 0.098g$ $a_{E-W} = 0.100g$ $a_{max} = 0.104g$	1	-10.9 -0.8	-1.9 -0.1	-1.0 0.3	4.5	0.5	4.9
	2	-18.4 0.3	-1.8 0.6	-1.3 6.8	8.3	3.1	8.5
	3	-3.4 0.0	-0.7 0.2	-0.6 1.2	1.3	0.5	1.4
	4	-11.5 0.8	-2.3 2.1	-0.9 10.3	4.6	4.1	5.3
Coyota Lake $a_{N-S} = 0.108g$ $a_{E-W} = 0.107g$ $a_{max} = 0.109g$	1	-14.4 0.0	-2.4 0.2	-1.3 2.0	6.0	0.9	6.6
	2	-23.1 0.7	-2.3 1.1	-1.6 11.6	10.4	5.3	10.8
	3	-4.3 0.2	-0.9 0.5	-0.7 2.5	1.7	1.0	1.8
	4	-38.2 1.0	-3.1 3.2	-1.2 15.7	17.7	6.2	18.6
Morgan Hill $a_{N-S} = 0.069g$ $a_{E-W} = 0.098g$ $a_{max} = 0.109g$	1	-33.1 0.4	-5.7 0.8	-2.9 4.6	13.7	2.0	15.1
	2	-48.7 1.3	-4.8 2.0	-3.4 21.6	21.9	9.8	22.6
	3	-5.5 0.2	-1.2 0.5	-0.8 2.8	2.2	1.1	2.3
	4	-21.8 1.7	-4.5 4.4	-1.7 21.4	8.7	8.5	10.0
Palm Springs $a_{N-S} = 0.110g$ $a_{E-W} = 0.095g$ $a_{max} = 0.111g$	1	-13.0 0.0	-2.3 0.1	-1.2 1.6	5.4	0.8	5.9
	2	-19.9 0.6	-1.9 1.0	-1.4 10.8	9.0	4.9	9.2
	3	-3.3 0.0	-0.7 0.2	-0.6 1.1	1.3	0.5	1.4
	4	-12.0 0.9	-2.5 2.3	-1.0 11.1	4.8	4.4	5.5
Whittier Narrows $a_{N-S} = 0.109$ $a_{E-W} = 0.103g$ $a_{max} = 0.124g$	1	-14.1 0.0	-2.4 0.2	-1.3 2.4	5.9	1.1	6.4
	2	-25.5 0.8	-2.5 1.2	-1.8 13.3	11.5	6.0	11.9
	3	-4.5 0.2	-1.0 0.4	-0.7 2.1	1.8	0.8	1.9
	4	-15.8 1.1	-3.2 3.0	-1.3 14.4	6.3	5.7	7.3

Table 4.2: The Principal and Shear Stresses of Column C3

		σ_{p1}	σ_{p2}	σ_{p3}	τ_{12}	τ_{23}	τ_{13}
Earthquake	Element	[MPa]	[MPa]	[MPa]	[MPa]	[MPa]	[MPa]
Coalinga $a_{N-S} = 0.098g$ $a_{E-W} = 0.100g$ $a_{max} = 0.104g$	1	-11.0 -0.1	-0.4 0.0	-0.3 21.2	5.4	10.7	16.1
	2	-96.5 5.9	-9.0 9.3	-5.8 99.7	43.7	45.2	46.9
	3	-8.0 -1.1	-0.8 -0.2	-0.7 5.2	3.8	2.8	6.6
	4	-99.1 7.3	-19.6 19.6	-5.6 94.4	39.8	37.4	46.8
Coyota Lake $a_{N-S} = 0.108g$ $a_{E-W} = 0.107g$ $a_{max} = 0.109g$	1	-19.9 0.0	-0.4 0.0	-0.3 18.5	9.8	9.3	18.7
	2	-194.3 11.3	-18.1 17.6	-11.6 189.3	88.1	85.8	91.3
	3	-13.3 0.0	-0.7 0.0	-0.6 11.1	6.4	5.8	12.2
	4	-196.0 13.9	-38.7 37.0	-14.6 187.3	78.7	75.1	90.7
Morgan Hill $a_{N-S} = 0.069g$ $a_{E-W} = 0.098g$ $a_{max} = 0.109g$	1	-14.7 0.3	-0.9 0.6	-0.5 15.1	7.2	7.4	13.4
	2	-139.0 8.4	-13.0 13.0	-8.3 140.1	63.0	63.5	65.8
	3	-10.3 0.0	-0.7 0.0	-0.6 8.0	4.9	4.2	8.9
	4	-140.6 10.0	-27.8 26.6	-10.5 134.7	56.4	54.1	65.0
Palm Springs $a_{N-S} = 0.110g$ $a_{E-W} = 0.095g$ $a_{max} = 0.111g$	1	-12.1 0.0	-0.4 0.0	-0.3 10.7	6.0	5.4	11.4
	2	-118.8 6.7	-11.1 10.5	-7.1 113.0	53.8	51.2	55.8
	3	-9.1 0.0	-0.7 0.0	-0.6 6.3	4.3	3.4	7.7
	4	-121.1 8.3	-23.9 22.1	-9.1 111.8	48.6	44.8	56.0
Whittier Narrows $a_{N-S} = 0.109$ $a_{E-W} = 0.103g$ $a_{max} = 0.124g$	1	-16.5 0.0	-0.6 0.0	-0.4 15.3	8.2	7.7	15.8
	2	-162.6 9.2	-15.1 14.5	-9.7 155.4	73.7	70.5	76.4
	3	-11.8 0.0	-0.7 0.0	-0.6 9.1	5.7	4.8	10.5
	4	-164.9 11.5	-32.6 30.6	-12.3 155.1	66.2	62.2	76.3

Table 4.3: The Principal and Shear Stresses of Column C6

		σ_{p1}	σ_{p2}	σ_{p3}	τ_{12}	τ_{23}	τ_{13}
Earthquake	Element	[MPa]	[MPa]	[MPa]	[MPa]	[MPa]	[MPa]
Coalinga $a_{N-S} = 0.098g$ $a_{E-W} = 0.100g$ $a_{max} = 0.104g$	1	-13.7 0.0	-2.3 0.0	-1.3 0.0	5.7	0.5	6.3
	2	-14.6 0.0	-1.5 0.0	-1.1 0.0	6.6	0.2	6.8
	3	-13.7 0.0	-2.6 0.0	-2.5 0.0	5.5	0.1	5.6
	4	-14.6 0.0	-2.5 0.0	-1.3 0.0	6.0	0.6	6.6
Coyota Lake $a_{N-S} = 0.108g$ $a_{E-W} = 0.107g$ $a_{max} = 0.109g$	1	-13.8 0.0	-2.3 0.0	-1.3 0.0	5.8	0.5	6.3
	2	-14.7 0.0	-1.5 0.0	-1.3 0.0	6.6	0.1	6.7
	3	-13.6 0.0	-2.6 0.0	-2.4 0.0	5.5	0.1	5.6
	4	-14.5 0.0	-2.5 0.0	-1.3 0.0	6.0	0.6	6.6
Morgan Hill $a_{N-S} = 0.069g$ $a_{E-W} = 0.098g$ $a_{max} = 0.109g$	1	-13.8 0.0	-2.3 0.0	-1.3 0.0	5.8	0.5	6.3
	2	-14.7 0.0	-1.5 0.0	-1.1 0.0	6.6	0.2	6.8
	3	-13.6 0.0	-2.6 0.0	-2.4 0.0	5.5	0.1	5.6
	4	-14.5 0.0	-2.5 0.0	-1.3 0.0	6.0	0.6	6.6
Palm Springs $a_{N-S} = 0.110g$ $a_{E-W} = 0.095g$ $a_{max} = 0.111g$	1	-31.8 2.4	-5.6 4.7	-2.8 26.9	13.1	11.1	14.5
	2	-35.6 1.9	-3.6 2.7	-2.6 26.8	16.0	12.1	16.5
	3	-3.2 0.0	-0.7 0.0	-0.6 0.0	1.3	0.1	1.3
	4	-8.3 0.0	-1.6 0.0	-0.7 0.2	3.3	0.5	3.8
Whittier Narrows $a_{N-S} = 0.109$ $a_{E-W} = 0.103g$ $a_{max} = 0.124g$	1	-13.6 0.0	-2.3 0.0	-1.4 0.0	5.6	0.5	6.1
	2	-14.5 0.0	-1.6 0.0	-1.2 0.0	6.5	0.2	6.7
	3	-13.7 0.0	-2.6 0.0	-2.5 0.0	5.5	0.1	5.6
	4	-14.5 0.0	-2.6 0.0	-1.4 0.0	6.0	0.6	6.6

Table 4.4: The Principal and Shear Stresses of Column C8

		σ_{p1}	σ_{p2}	σ_{p3}	τ_{12}	τ_{23}	τ_{13}
Earthquake	Element	[MPa]	[MPa]	[MPa]	[MPa]	[MPa]	[MPa]
Coalinga $a_{N-S} = 0.098g$ $a_{E-W} = 0.100g$ $a_{max} = 0.104g$	1	-13.7 0.0	-2.3 0.0	-1.3 0.0	5.7	0.5	6.3
	2	-14.6 0.0	-1.5 0.0	-1.1 0.0	6.6	0.2	6.8
	3	-13.7 0.0	-2.6 0.0	-2.5 0.0	5.5	0.1	5.6
	4	-14.6 0.0	-2.5 0.0	-1.3 0.0	6.0	0.6	6.6
Coyota Lake $a_{N-S} = 0.108g$ $a_{E-W} = 0.107g$ $a_{max} = 0.109g$	1	-13.8 0.0	-2.3 0.0	-1.3 0.0	5.8	0.5	6.3
	2	-14.7 0.0	-1.5 0.0	-1.3 0.0	6.6	0.1	6.7
	3	-13.6 0.0	-2.6 0.0	-2.4 0.0	5.5	0.1	5.6
	4	-14.5 0.0	-2.5 0.0	-1.3 0.0	6.0	0.6	6.6
Morgan Hill $a_{N-S} = 0.069g$ $a_{E-W} = 0.098g$ $a_{max} = 0.109g$	1	-13.8 0.0	-2.3 0.0	-1.3 0.0	5.8	0.5	6.3
	2	-14.7 0.0	-1.5 0.0	-1.1 0.0	6.6	0.2	6.8
	3	-13.6 0.0	-2.6 0.0	-2.4 0.0	5.5	0.1	5.6
	4	-14.5 0.0	-2.5 0.0	-1.3 0.0	6.0	0.6	6.6
Palm Springs $a_{N-S} = 0.110g$ $a_{E-W} = 0.095g$ $a_{max} = 0.111g$	1	-13.8 0.0	-2.3 0.0	-1.3 0.0	5.8	0.5	6.3
	2	-14.7 0.0	-1.5 0.0	-1.1 0.0	6.6	0.2	6.8
	3	-13.6 0.0	-2.6 0.0	-2.4 0.0	5.5	0.1	5.6
	4	-12.7 0.0	-2.5 0.0	-1.3 0.0	5.1	0.6	5.7
Whittier Narrows $a_{N-S} = 0.109$ $a_{E-W} = 0.103g$ $a_{max} = 0.124g$	1	-13.6 0.0	-2.3 0.0	-1.4 0.0	5.6	0.5	6.1
	2	-14.5 0.0	-1.6 0.0	-1.2 0.0	6.5	0.2	6.7
	3	-13.7 0.0	-2.6 0.0	-2.5 0.0	5.5	0.1	5.6
	4	-14.5 0.0	-2.6 0.0	-1.4 0.0	6.0	0.6	6.6

Table 4.5: The Principal and Shear Stresses of Column C11

		σ_{p1}	σ_{p2}	σ_{p3}	τ_{12}	τ_{23}	τ_{13}
Earthquake	Element	[MPa]	[MPa]	[MPa]	[MPa]	[MPa]	[MPa]
Coalinga $a_{N-S} = 0.098g$ $a_{E-W} = 0.100g$ $a_{max} = 0.104g$	1	-12.1 2.1	-2.4 5.2	-1.0 26.7	4.9	10.8	12.3
	2	-12.8 1.8	-1.3 2.6	-0.9 27.0	5.8	12.2	12.6
	3	-4.2 0.5	-0.9 0.9	-0.7 4.5	1.6	1.8	2.0
	4	-4.9 0.4	-0.8 0.8	-0.4 5.4	2.1	2.4	2.9
Coyota Lake $a_{N-S} = 0.108g$ $a_{E-W} = 0.107g$ $a_{max} = 0.109g$	1	-32.4 4.0	-6.3 10.1	-2.6 51.6	13.1	20.8	23.8
	2	-34.1 3.4	-3.3 5.0	-2.3 52.2	15.4	23.6	24.4
	3	-8.5 1.3	-1.8 2.0	-1.3 9.8	3.4	3.9	4.3
	4	-10.3 1.1	-1.5 1.9	-0.8 12.7	4.4	5.6	6.1
Morgan Hill $a_{N-S} = 0.069g$ $a_{E-W} = 0.098g$ $a_{max} = 0.109g$	1	-75.6 14.1	-14.7 35.1	-6.0 180.2	30.4	72.6	83.1
	2	-76.7 12.3	-7.4 17.7	-5.1 185.3	34.7	83.8	86.5
	3	-16.6 5.0	-3.5 7.6	-2.3 36.5	6.6	14.4	15.8
	4	-18.5 1.3	-2.4 5.2	-0.9 43.7	8.1	19.2	21.4
Palm Springs $a_{N-S} = 0.110g$ $a_{E-W} = 0.095g$ $a_{max} = 0.111g$	1	-10.8 0.8	-2.1 2.1	-0.9 11.0	4.4	4.4	5.1
	2	-12.1 1.0	-1.2 1.3	-0.8 14.1	5.4	6.4	6.6
	3	-3.6 0.2	-0.8 0.3	-0.6 1.7	1.4	0.7	1.5
	4	-6.0 0.4	-1.0 0.8	-0.6 5.1	2.5	2.1	2.7
Whittier Narrows $a_{N-S} = 0.109$ $a_{E-W} = 0.103g$ $a_{max} = 0.124g$	1	-18.3 3.5	-3.6 8.7	-1.5 44.5	7.3	17.9	20.5
	2	-18.7 2.7	-1.8 4.0	-1.3 42.6	8.4	19.3	20.0
	3	-5.4 0.9	-1.1 1.6	-0.9 7.7	2.1	3.1	3.4
	4	-8.6 0.8	-1.5 1.5	-0.8 9.8	3.5	4.1	4.5

Table 4.6: The Principal and Shear Stresses of Column C13

		σ_{p1}	σ_{p2}	σ_{p3}	τ_{12}	τ_{23}	τ_{13}
Earthquake	Element	[MPa]	[MPa]	[MPa]	[MPa]	[MPa]	[MPa]
Coalinga $a_{N-S} = 0.098g$ $a_{E-W} = 0.100g$ $a_{max} = 0.104g$	1	-6.2 0.5	-1.3 1.6	-0.5 7.5	2.5	3.0	3.5
	2	-10.5 0.8	-1.1 1.1	-0.7 11.9	4.7	5.4	5.5
	3	-3.6 -1.1	-0.8 -0.2	-0.7 -0.2	1.4	0.1	1.5
	4	-13.0 0.7	-2.2 1.4	-1.2 8.4	5.4	3.5	5.9
Coyota Lake $a_{N-S} = 0.108g$ $a_{E-W} = 0.107g$ $a_{max} = 0.109g$	1	-6.6 0.6	-1.3 1.6	-0.5 7.9	2.6	3.1	3.7
	2	-17.0 1.1	-1.8 1.5	-1.2 15.7	7.6	7.1	7.9
	3	-3.8 0.0	-0.8 0.0	-0.7 0.0	1.5	0.1	1.5
	4	-19.7 0.9	-3.3 1.8	-1.8 10.7	8.2	4.5	9.0
Morgan Hill $a_{N-S} = 0.069g$ $a_{E-W} = 0.098g$ $a_{max} = 0.109g$	1	-6.8 0.6	-2.8 2.1	-0.6 8.0	3.0	4.2	3.7
	2	-15.1 1.3	-1.5 1.8	-1.1 18.7	6.8	8.5	8.7
	3	-3.6 0.0	-0.8 0.0	-0.6 0.0	1.4	0.1	1.5
	4	-16.4 1.1	-2.8 2.1	-1.5 12.5	6.8	5.2	7.4
Palm Springs $a_{N-S} = 0.110g$ $a_{E-W} = 0.095g$ $a_{max} = 0.111g$	1	-6.6 0.6	-1.3 1.6	-0.5 7.9	2.6	3.1	3.7
	2	-12.1 0.7	-1.3 1.0	-0.9 10.3	5.4	4.6	5.6
	3	-3.4 0.0	-0.8 0.0	-0.6 0.0	1.3	0.1	1.4
	4	-14.1 0.6	-2.4 1.2	-1.3 7.1	5.9	3.0	6.4
Whittier Narrows $a_{N-S} = 0.109$ $a_{E-W} = 0.103g$ $a_{max} = 0.124g$	1	-5.7 0.5	-1.2 1.5	-0.5 7.0	2.3	2.8	3.3
	2	-17.5 1.1	-1.8 1.5	-1.2 15.4	7.8	7.0	8.1
	3	-3.8 0.0	-0.8 0.0	-0.7 0.0	1.5	0.1	1.6
	4	-19.7 1.0	-3.3 2.0	-1.8 11.9	8.2	4.9	9.0

Table 4.7: The Stresses in the Reinforcing Steel in Column C1

	f_a	τ_1	τ_2
Earthquake	[MPa]	[MPa]	[MPa]
Coalinga	14.7	0.2	0.9
	-102.6	-0.3	-0.8
Coyota Lake	41.9	0.3	1.1
	-148.3	-0.4	-1.1
Morgan Hill	88.3	0.5	2.0
	-275.0	-1.0	-1.8
Palm Springs	14.8	0.3	1.0
	-91.4	-0.4	-0.9
Whittier Narrows	39.5	0.3	1.2
	-141.9	-0.4	-1.1

Table 4.8: The Stresses in the Reinforcing Steel in Column C3

	f_a	τ_1	τ_2
Earthquake	[MPa]	[MPa]	[MPa]
Coalinga	510.8	0.0	0.0
	-550.2	1.4	1.4
Coyota Lake	1001.0	0.0	0.0
	-1007.6	2.6	14.1
Morgan Hill	711.3	0.0	0.0
	-711.4	2.0	10.1
Palm Springs	613.3	0.0	0.0
	-619.4	1.6	8.7
Whittier Narrows	873.5	0.0	0.0
	-854.2	2.2	12.2

Table 4.9: The Stresses in the Reinforcing Steel in Column C6

	f_a	τ_1	τ_2
Earthquake	[MPa]	[MPa]	[MPa]
Coalinga	171.6	0.9	0.7
	-152.8	-0.8	-0.3
Coyota Lake	206.3	1.1	1.0
	-213.1	-1.2	-0.5
Morgan Hill	496.6	2.6	1.9
	-514.0	-2.8	-1.3
Palm Springs	192.4	1.1	0.9
	-195.3	-1.1	-0.4
Whittier Narrows	210.2	1.1	0.9
	-181.7	-1.0	-0.4

Table 4.10: The Stresses in the Reinforcing Steel in Column C8

	f_a	τ_1	τ_2
Earthquake	[MPa]	[MPa]	[MPa]
Coalinga	0.0	0.0	0.0
	-110.0	0.3	0.2
Coyota Lake	0.0	0.0	0.0
	-108.3	0.3	0.2
Morgan Hill	0.0	0.0	0.0
	-108.3	0.4	0.2
Palm Springs	0.0	0.0	0.0
	-108.3	0.3	0.2
Whittier Narrows	0.0	0.0	0.0
	-106.8	0.3	0.2

Table 4.11: The Stresses in the Reinforcing Steel in Column C11

	f_a	τ_1	τ_2
Earthquake	[MPa]	[MPa]	[MPa]
Coalinga	156.2	2.2	0.3
	-97.6	-0.8	-0.5
Coyota Lake	314.9	4.1	0.7
	-191.8	-2.3	-1.0
Morgan Hill	1035.3	13.9	1.5
	-461.9	-5.7	-3.5
Palm Springs	39.0	1.0	0.3
	-71.8	-0.7	-0.3
Whittier Narrows	287.6	3.5	0.4
	-150.0	-1.2	-0.7

Table 4.12: The Stresses in the Reinforcing Steel in Column C13

	f_a	τ_1	τ_2
Earthquake	[MPa]	[MPa]	[MPa]
Coalinga	63.4	1.0	0.2
	-81.3	-0.2	-0.2
Coyota Lake	112.8	1.0	0.4
	-97.4	-0.2	-0.3
Morgan Hill	109.6	1.3	0.3
	-131.1	-0.5	-0.4
Palm Springs	70.2	1.0	0.3
	-73.9	-0.2	-0.2
Whittier Narrows	116.7	0.9	0.4
	-111.3	-0.2	-0.3

4.2.3 The Summary of the Stresses in the Concrete and the Steel

Tables 4.13 and 4.14 summarises the maximum and minimum stresses found in each column.

Table 4.13: A Summary of the Stress in the Concrete

Column	σ_{p1}		σ_{p2}		σ_{p3}		τ_{12}	τ_{23}	τ_{31}
	[MPa]		[MPa]		[MPa]		[MPa]	[MPa]	[MPa]
	Min	Max	Min	Max	Min	Max	Max	Max	Max
1	-48.7	1.7	-5.7	4.4	-3.4	21.6	21.9	9.8	22.6
3	-196.0	13.9	-38.7	37.0	-14.6	189.3	88.1	85.8	91.3
6	-35.6	2.4	-5.6	4.7	-2.8	26.9	16.0	12.1	16.5
8	-14.7	0.0	-2.6	0.0	-2.5	0.0	6.6	0.6	6.8
11	-76.7	14.1	-14.7	35.1	-6.0	185.3	34.7	83.8	86.5
13	-19.7	1.3	-3.3	2.1	-1.8	18.7	8.2	8.5	9.0

Table 4.14: A Summary of the Stress in the Steel

Column	Tension Stress	Compression Stress
	[MPa]	[MPa]
1	88.3	-275.0
3	1001.0	-1007.6
6	496.6	-514.0
8	0.0	-110.0
11	1035.3	-461.9
13	116.7	-131.1

Chapter 5

Discussions

5.1 Introduction

The column's principal and shear stresses obtained from the numerical simulations will be used to determine whether the column will fail. This will be achieved by comparing the stresses to the code requirements. Figure 5.1 shows the column reference number of the critical columns which were modelled in 3D.

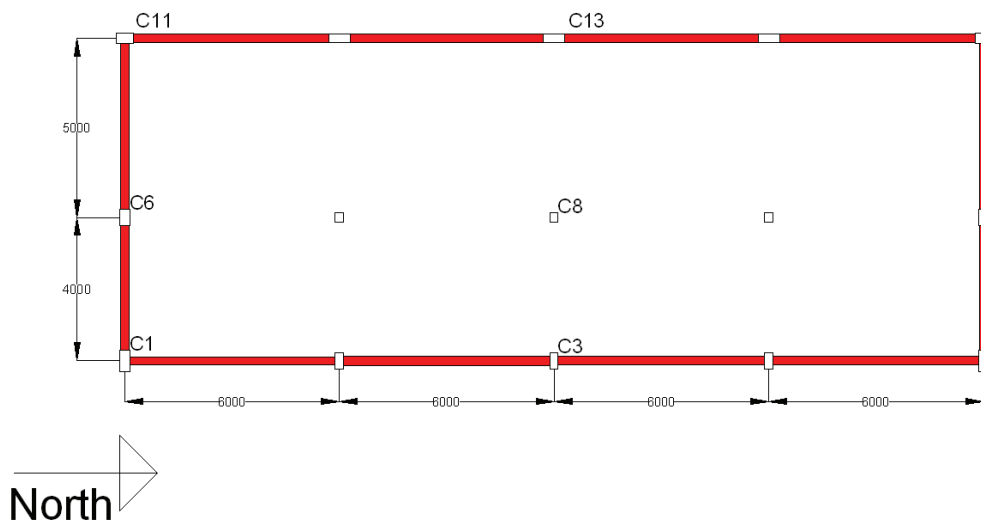


Figure 5.1: The Columns Numbers Chosen for Modelling

5.1.1 The Failure Criteria

The failure criteria that was considered covers the modes of failure that the columns experience during an earthquake. The first failure criteria considered whether the concrete's compression resistance was exceeded. For this model, an average concrete compressive strength of 40MPa was assumed. SANS 10100-1 (2000) clause 3.3.3.2 states that the concrete strength should be divided by a material factor of $\gamma_m = 1.5$. Therefore the maximum compression strength of the concrete should be limited to $f_c = \frac{40}{1.5} = 26.6\text{MPa}$. SANS 10100-1 (2000) also states that concrete should not have tensile strength.

Another failure criteria to be considered is shear stress. As shear reinforcement is not included in the model, the only test which can be considered is to use clause 4.3.4.1.1 of SAN 10100-1 which states *"the design shear stress at any cross-section of the beam should in no case exceed a value of the lesser of $0.75\sqrt{f_{cu}}$ or 4.75MPa regardless of any shear reinforcement provided."* In the case of this model, the shear is limited to $0.75\sqrt{f_{cu}} = 4.74\text{MPa}$. Therefore, any shear force experienced by the column that is larger than 4.74MPa will lead to the failure of the cross-section (SANS 10100-1, 2000).

Since reinforced concrete elements were used, it is important to compare the stresses in the steel to codified requirements. Steel is used as both tensile and compression elements. The longitudinal reinforcement used in the columns have a tensile yield strength of $f_y = 391\text{MPa}$, which accounts for the material factor of $\gamma_m = 1.15$. The longitudinal reinforcement has a compression strength of $f_{yc} = 327\text{MPa}$ which also includes the steel's material factor (South African Reinforced Concrete Engineers' Association, 2013). If these strengths are exceeded, the material will yield which could lead to failure of the element.

Although the code does not dictate whether an element will fail, it does show when an element is not deemed to be reliable in the eyes of designers.

5.1.2 Stresses in the Columns

Since each column developed different stresses during the simulations, it was required that they be individually assessed to determine if failure would occur. Once all the columns were individually assessed, a conclusion could then be deduced regarding the global structure's collapsibility.

5.1.2.1 Stresses in Column C1

Column C1 is located at the bottom left-hand side of the structure and has the cross-section shown in Figure 5.2. The first aspect reviewed was the normal stresses in the elements. Any region in the concrete exceeding a compression stress of 26.6MPa would result in a violation of the code requirements, indicating that the concrete is susceptible to damage. The reinforcing steel has a yield stress of 391MPa in tension and 327MPa in compression. Figure 5.3 presents the maximum compression and tensile stresses in the concrete of Column C1 in the different elements. The element numbers are shown in Figure 4.1. Figure 5.4 presents the maximum compression and tensile stresses in the reinforcement in Column C1.

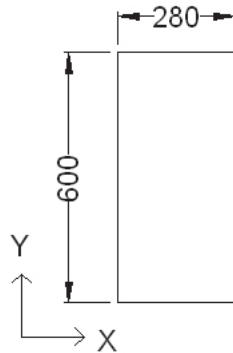


Figure 5.2: The Cross-Section of Column C1

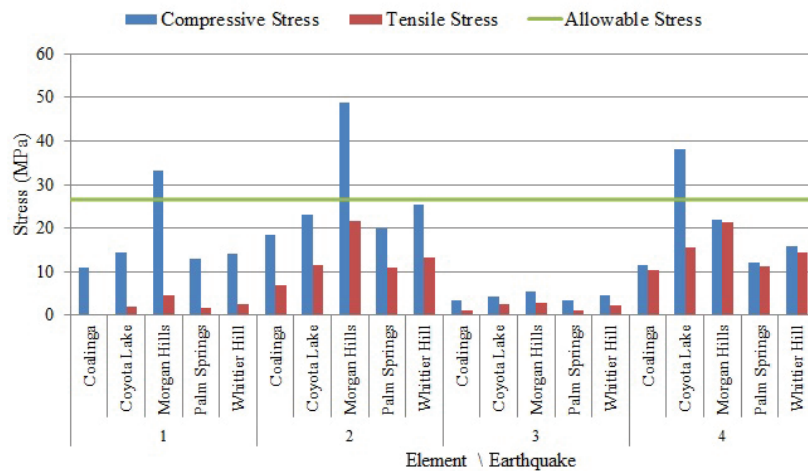


Figure 5.3: The Maximum Normal Stresses in Column C1 in the Concrete

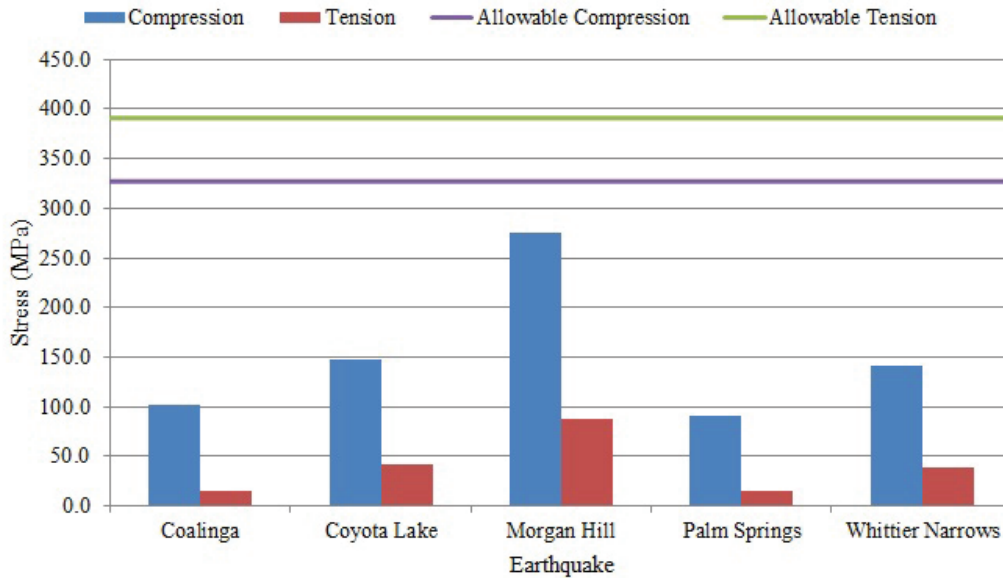


Figure 5.4: The Maximum Axial Stresses in Column C1 in the Reinforcement

As Figure 5.3 shows, there are three elements in which the concrete's compressive strength of $26.6MPa$ was exceeded. This occurs in element 1 and 2 during the Morgan Hills earthquake and in element 4 during the Coyota Lake earthquake. The simulation shows that the Morgan Hill Earthquake results in bending about the X-Axis which results in failure along the top and bottom edges of the column. From this it can be concluded that Column C1 will be damaged during the Morgan Hill earthquake. The column could be damaged in the Coyota Lake earthquake, however the reinforcing steel has not yet yielded and therefore the column could withstand the stress. The next aspect considered was to determine if the concrete would fail in tension. Figure 5.3 shows that there are tensile stress present in the concrete. In order to resist significant damage due to the earthquakes, the tensile stresses in the concrete is redistributed to the reinforcing steel. In order for the column to avoid damage in tension, an additional tensile stress, that was previously carried by the concrete, of $412MPa$ at maximum must be carried by the steel. This additional stress is beyond the yield strength of the steel in tension will thus result in damage to the column.

The final aspect to consider is whether the shear stress of the cross-section exceeds $4.74MPa$. The Figure 5.5 presents the shear stresses experienced by the column during the earthquakes.

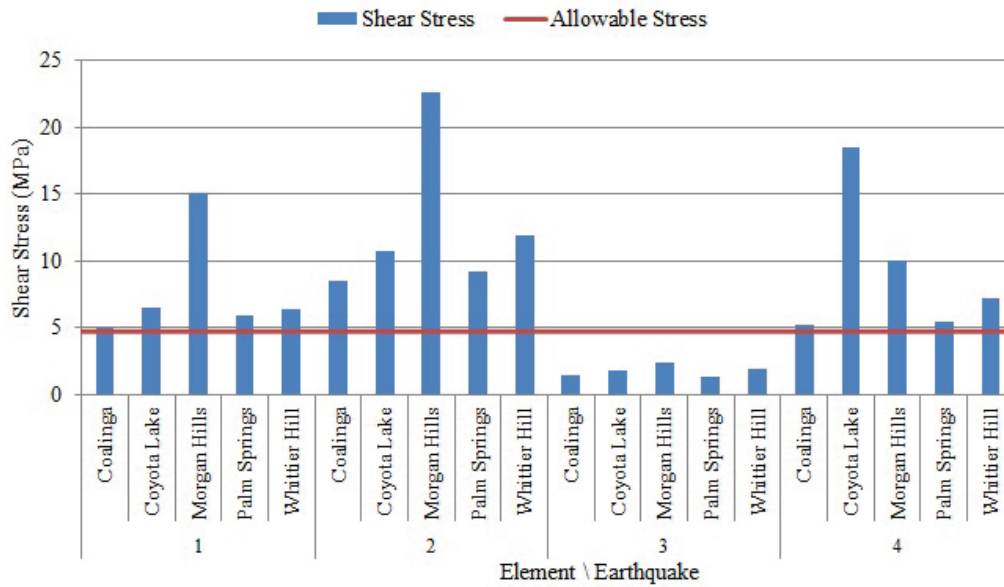


Figure 5.5: The Maximum Shear Stresses in Column C1 in the Concrete

Since the average shear stress exceeds the allowable codified limit indicates that the concrete is likely to fail in shear.

To summarise, Column C1 will be damaged in compression during two of the earthquakes considered in this study. All of the earthquakes would cause failure in tension and shear.

5.1.2.2 Stresses in Column C3

Column C3 is located in the middle of the long-side of the structure and has a cross-section shown in Figure 5.6. The first aspect reviewed was the normal stresses in the elements. Figure 5.7 presents the maximum compression and tensile stresses in Column C3 for different elements. Figure 5.8 presents the maximum compression and tensile stresses in the reinforcement in Column C3.

For this case, the Figure 5.7 and 5.8 shows that there are large stresses in elements 2 and 4 that significantly exceeds the yield stress of the concrete and the reinforcement. This would indicate that there is bending stress about the Y-Axis of the column. The magnitude of the stress is due the the column's orientation which results in the weak axis resisting the bending generated by the masonry panels. These significantly large stresses in the elements will result in failure of the column.

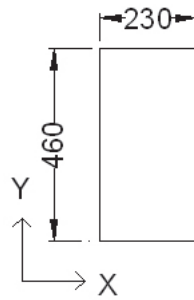


Figure 5.6: The Cross-Section of Column C3

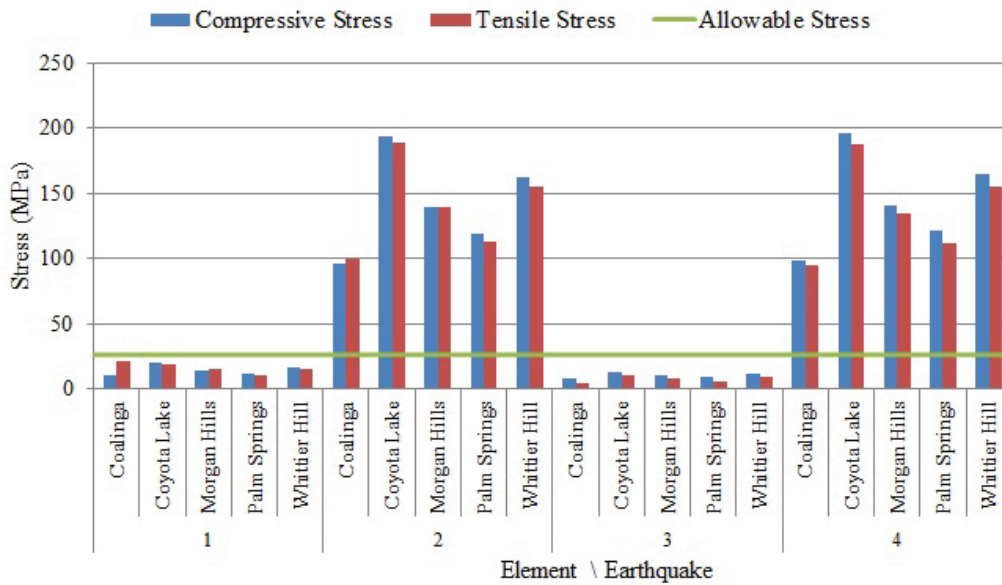


Figure 5.7: The Maximum Compression Stresses in Column C3 in the Concrete

The second aspect to consider is whether the shear stress of the cross-section exceeds $4.74MPa$. The Figure 5.9 presents the shear stresses experienced by the column during the different earthquakes.

The average shear stress experienced by the column significantly exceeds the codified value of $4.74MPa$ and therefore the column is likely to fail in shear.

To summarise, the Column C3 will probably fail in compression, tension and in shear. This is due to the orientation of the column which requires the weak axis to resist the load.

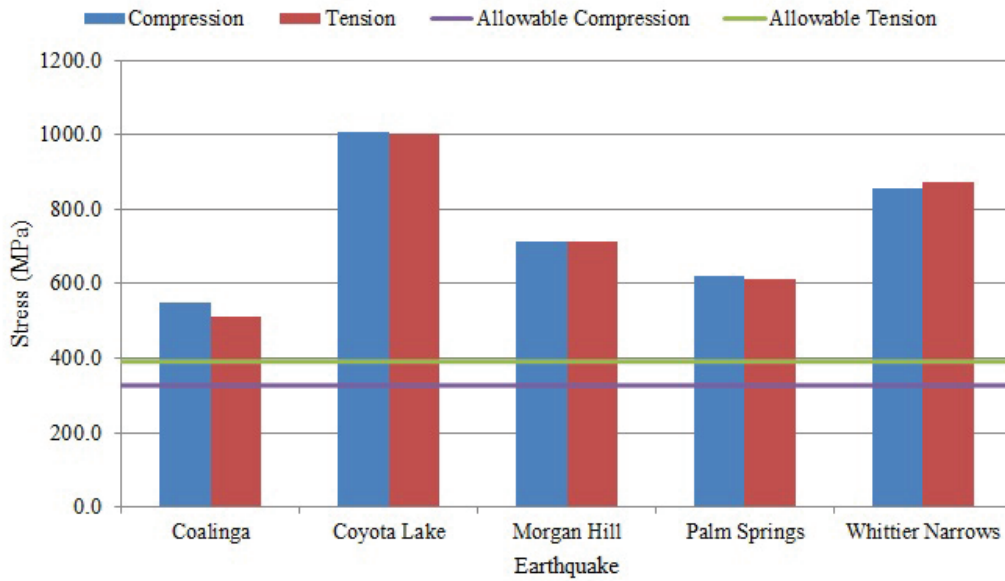


Figure 5.8: The Maximum Axial Stresses in Column C3 in the Reinforcement

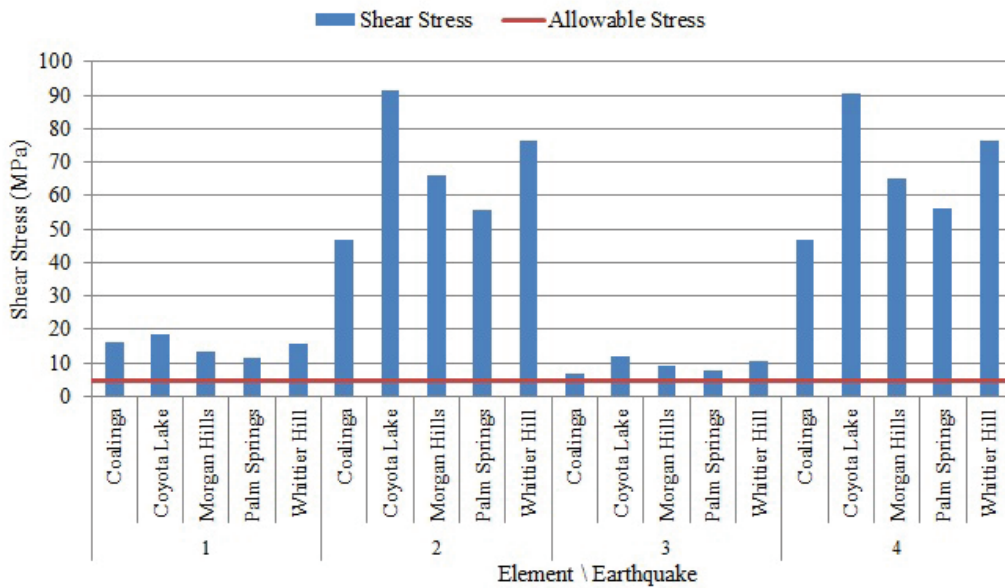


Figure 5.9: The Maximum Shear Stresses in Column C3 in the Concrete

5.1.2.3 Stresses in Column C6

Column C6 is located in the middle of the short-side of the structure and has the cross-section shown in Figure 5.10. The first aspect reviewed was the normal stresses in the elements. Figure 5.11 presents the maximum compression and tensile stresses in Column C6 for different elements. Figure 5.12 presents the maximum compression and tensile stresses in the reinforcement in Column C6.

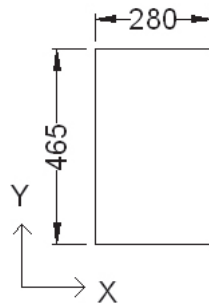


Figure 5.10: The Cross-Section of Column C6

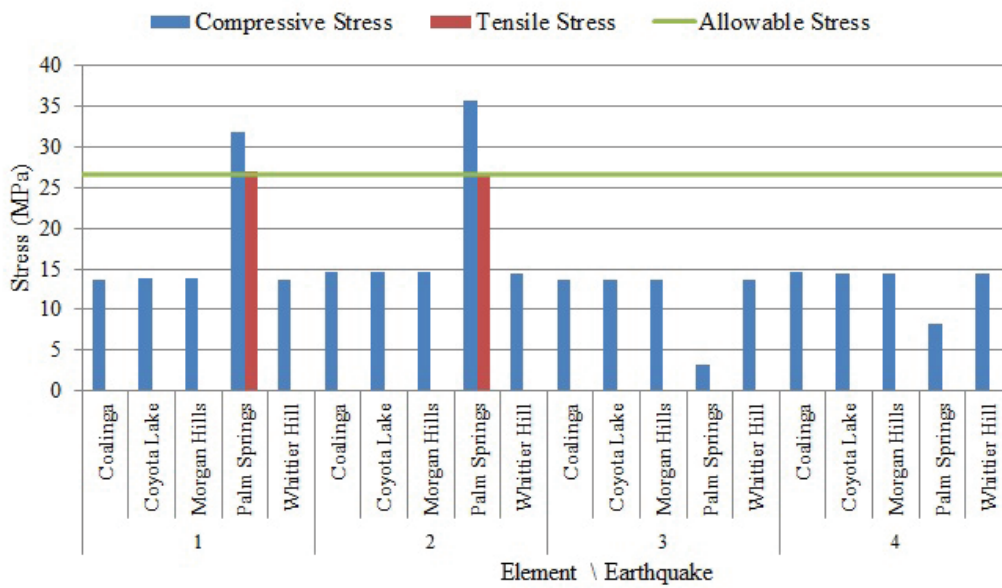


Figure 5.11: The Maximum Stresses in Column C6 in the Concrete

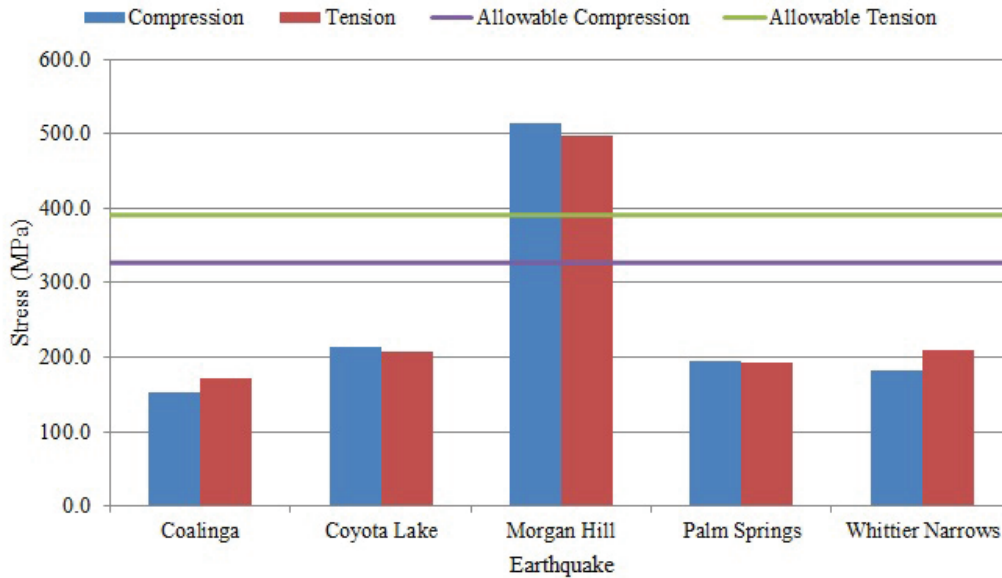


Figure 5.12: The Maximum Axial Stresses in Column C6 in the Reinforcement

The only two elements that exceed the yield stress of the concrete are elements 1 and 2 during the Palm Springs earthquake. These stresses occurred due to a resonance effect during this earthquake. As there was resonance, the stresses are amplified beyond the yield stress. The reinforcing steel during this earthquake does not yield and therefore can carry the redistributed load from the concrete. This would cause a maximum redistributed stress of $1012MPa$ in the steel. This value is obtained by calculating the tension force in the concrete and divided equally between the four reinforcement bars. This would exceed the yield stress of the steel and therefore fail. Furthermore, the steel would also yield during the Morgan Hill earthquake.

The second aspect to consider is whether the shear stress of the cross-section exceeds $4.74MPa$. Figure 5.13 presents the shear stresses experienced by the column during the earthquakes.

The shear in the column during all earthquakes exceeds the limit of $4.74MPa$ and therefore the column will possibly fail in shear.

To summarise, Column C6 will fail in compression and tension during the Palm Springs earthquake. The column would not fail in compression in the other earthquakes while it would fail in tension only during the Morgan Hill earthquake. All the earthquakes will cause failure shear in the member.

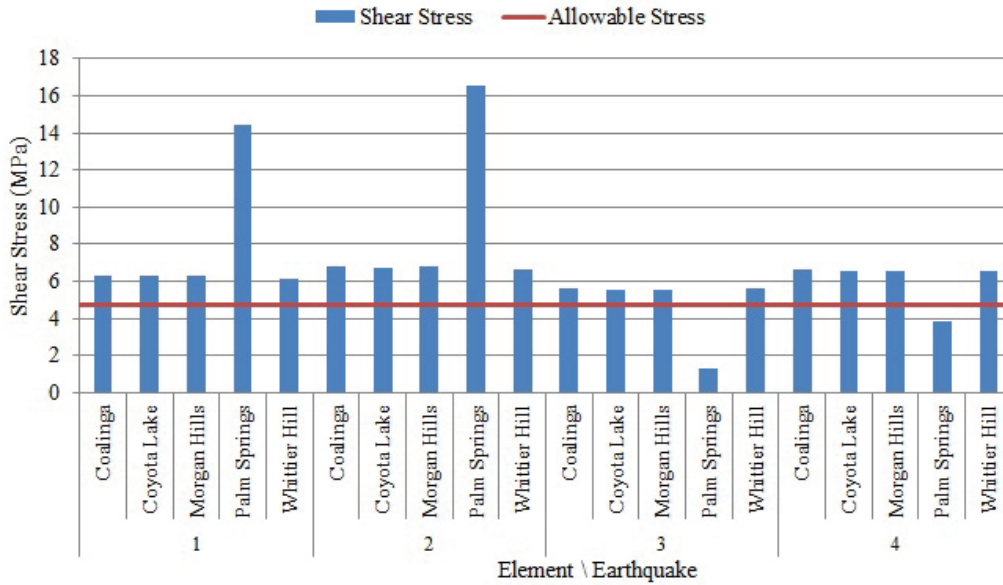


Figure 5.13: The Maximum Shear Stresses in Column C6 in the Concrete

5.1.2.4 Stresses in Column C8

Column C8 is located in the center of the structure and has the cross-section shown in Figure 5.14. The first aspect reviewed was the normal stresses in the elements. Figure 5.15 presents the maximum compression stress in Column C8 for different elements. This column does not experience any tensile stress. Figure 5.16 presents the maximum compression stress in the reinforcement in Column C8.

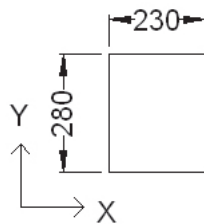


Figure 5.14: The Cross-Section of Column C8

The concrete does not exceed its yield stress and as such it will not fail. This column never has elements which results in tensile stresses. The reason for this is lack of masonry panels that influence the column directly. This results in small lateral forces and therefore minimal bending stresses. The

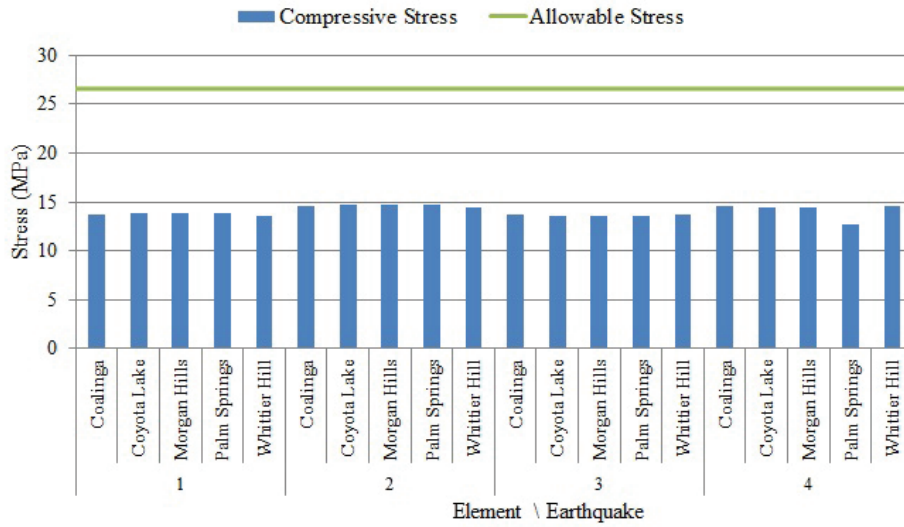


Figure 5.15: The Maximum Compression Stresses in Column C8 in the Concrete

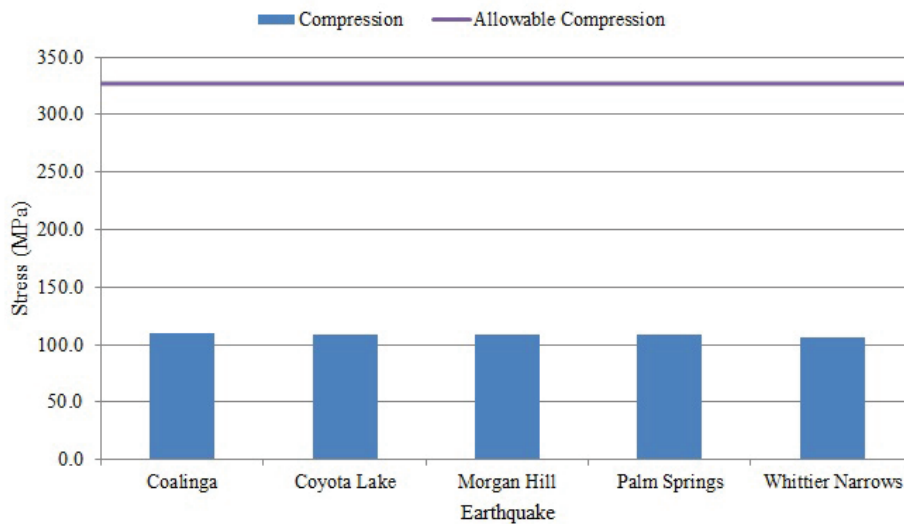


Figure 5.16: The Maximum Axial Stresses in Column C8 in the Reinforcement

reinforcement also only experiences compressive stress and these values do not exceed the yield stress.

The second aspect to consider is whether the shear stress of the cross-section exceeds $4.74MPa$. The Figure 5.17 presents the shear stresses experienced by the column during the earthquakes.

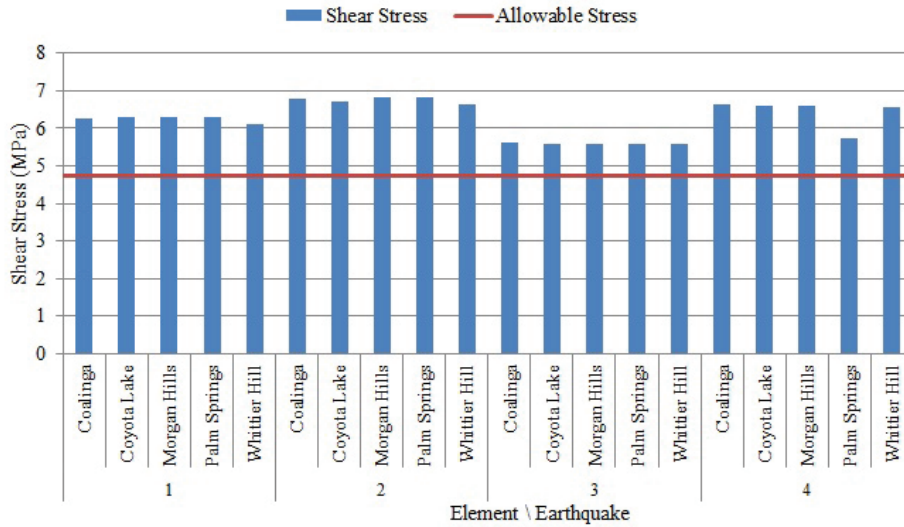


Figure 5.17: The Maximum Shear Stresses in Column C8 in the Concrete

The average shear stress experienced by the column is 6.25MPa . Since this value exceeds 4.74MPa , the column is at risk of failing.

To summarise, the Column C8 is able to resist the earthquake forces in compression and in tension, while the column shows a high probability of failure in shear.

5.1.2.5 Stresses in Column C11

Column C11 is located at the top right-hand side of the structure and has the cross-section shown in Figure 5.18. The first aspect reviewed was the normal stresses in the elements. Figure 5.19 presents the maximum compression and tensile stresses in the Column C11 for different elements. Figure 5.20 presents the maximum compression and tensile stresses in the reinforcement in Column C11.

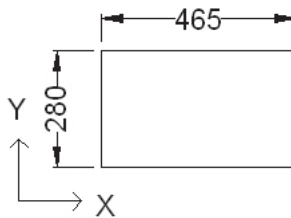


Figure 5.18: The Cross-Section of Column C11

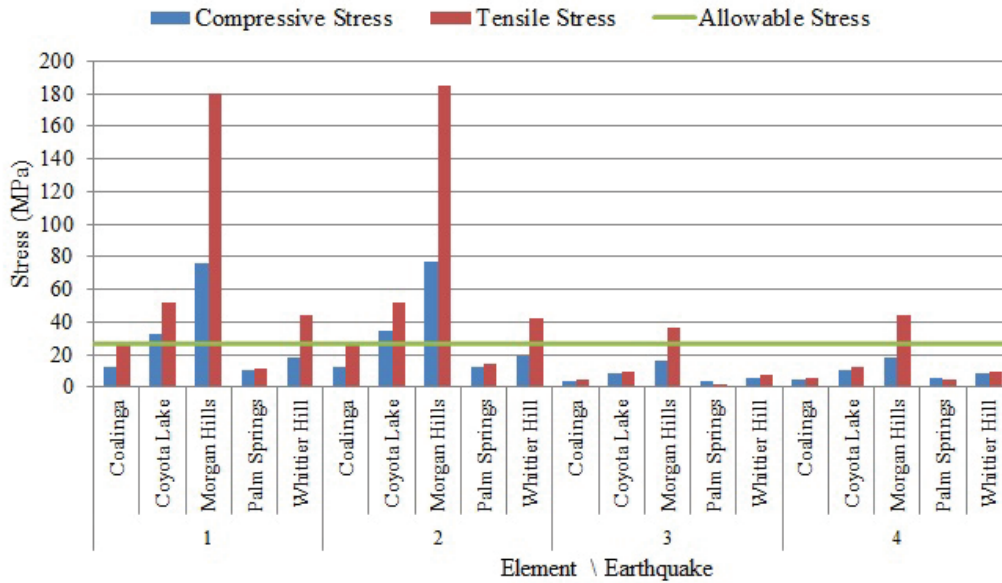


Figure 5.19: The Maximum Normal Stresses in Column C11 in the Concrete

The compressive stress of the concrete is significantly exceeded in elements 1 and 2 during the Morgan Hill earthquake. This is again due to resonance caused by the earthquake. This resonance leads to a large moment about the X-axis which results in these large stresses. The compressive stress is not exceeded by the other applied earthquakes. All columns experience tensile stresses in the concrete which must be redistributed to the reinforcing steel. Figure 5.20 shows the tensile stress of the steel has exceeded the yield limit in the Morgan Hill earthquake and it is reasonable to assume that the column will fail in tension for this earthquake if the stresses were redistributed. The other earthquakes will also lead to yielding of the reinforcement steel in tension after redistribution.

The second aspect to consider is whether the shear stress of the cross-section exceeds 4.74MPa . The Figure 5.21 presents the shear stresses experienced by the column during the earthquakes.

The shear stress experienced by the column significantly exceeds the limit of 4.74MPa and therefore the column will most likely fail in shear.

To summarise, the Column C11 will fail in compression during the Morgan Hills earthquake. The column will fail in tension during all the earthquakes. The column will also fail due to shear stress.

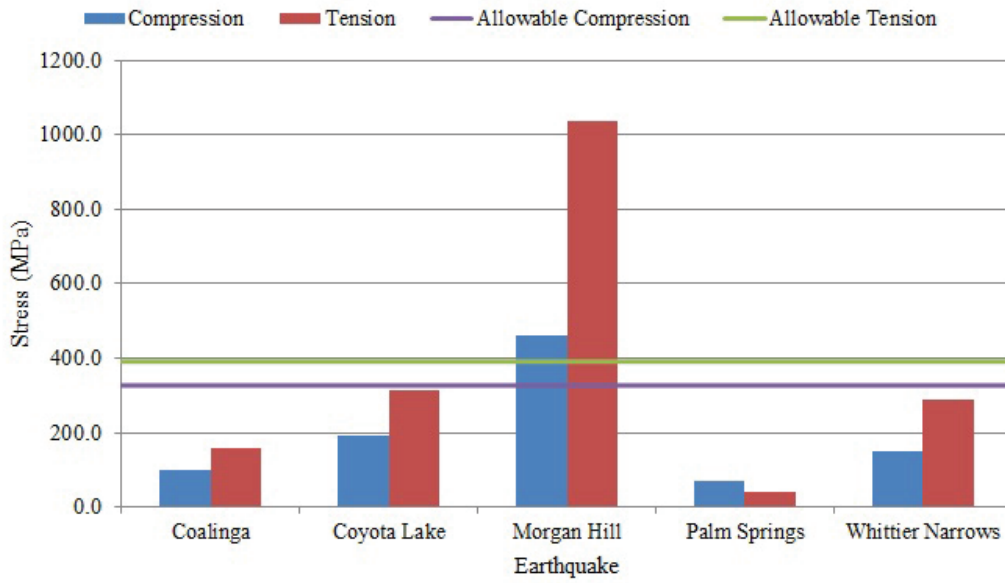


Figure 5.20: The Maximum Axial Stresses in Column C1 in the Reinforcement

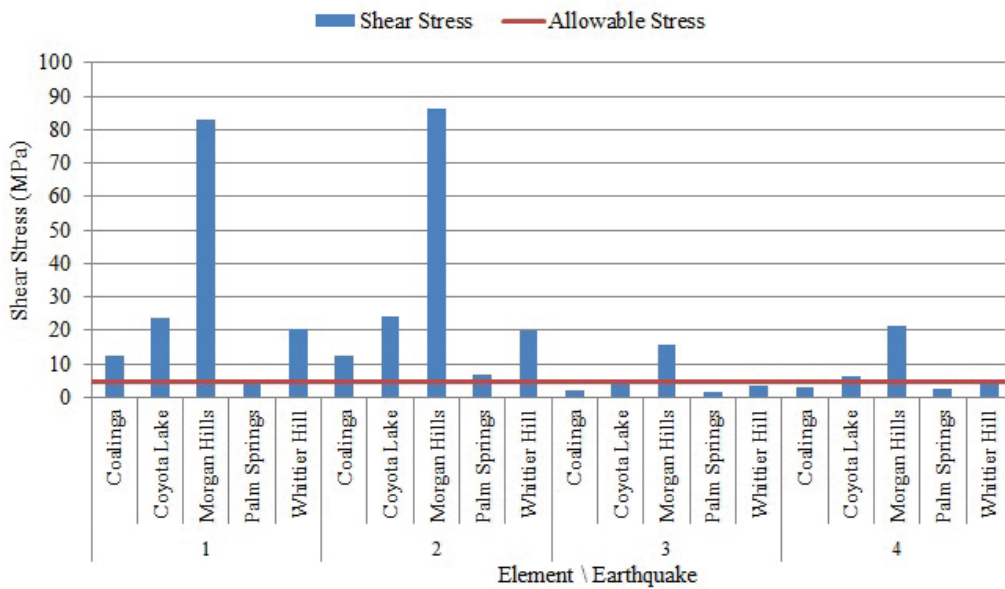


Figure 5.21: The Maximum Shear Stresses in Column C11 in the Concrete

5.1.2.6 Stresses in Column C13

Column C13 is located in the middle of the long-side of the structure and has the cross-section shown in Figure 5.22. The first aspect reviewed was the normal stresses in the elements. Figure 5.23 presents the maximum compression and tensile stresses in Column C13 for different elements. Figure 5.24 presents the maximum compression and tensile stresses in the reinforcement in Column C13.

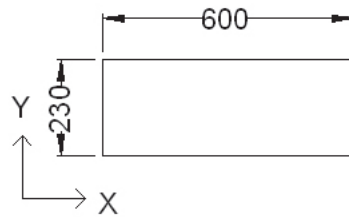


Figure 5.22: The Cross-Section of Column C13

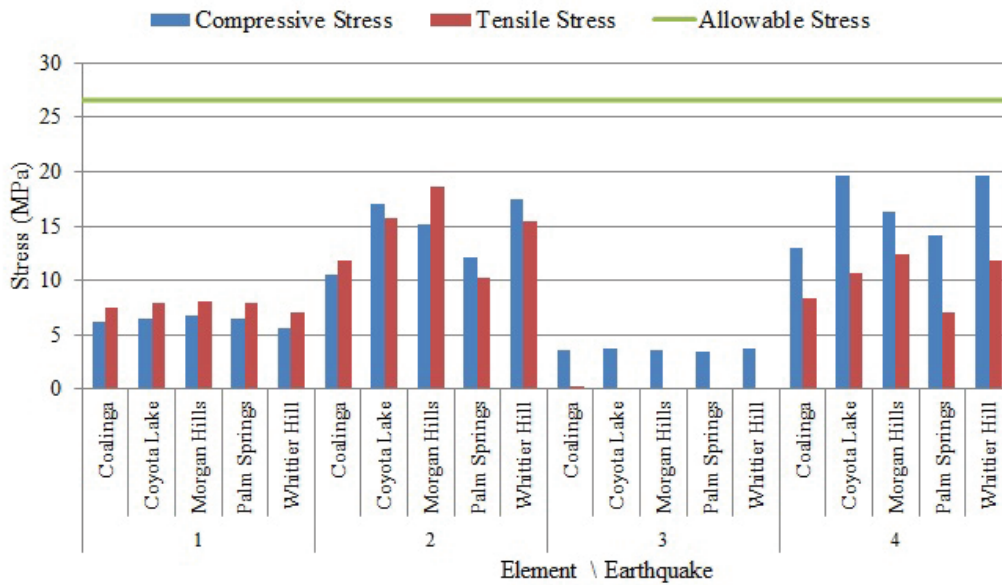


Figure 5.23: The Normal Compression Stresses in Column C13 in the Concrete

The compression yield stress of the concrete and the reinforcement is not exceeded during any of the earthquakes and therefore the column shows no

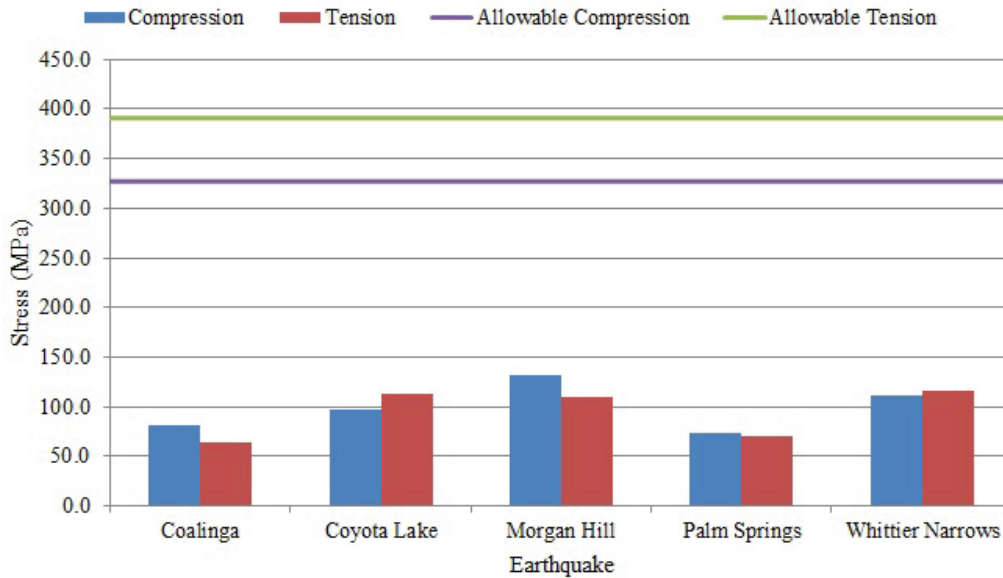


Figure 5.24: The Maximum Axial Stresses in Column C13 in the Reinforcement

sign of failure in compression. The concrete experiences tensile stresses which must be redistributed to the reinforcement. This would result in a maximum additional stress of 343MPa in the steel. This in combination with the stress already in the steel would lead to yielding of the reinforcement.

The second aspect to consider is whether the shear stress of the cross-section which cannot exceed 4.74MPa . The Figure 5.25 presents the shear stresses experienced by the column during the earthquakes.

Figure 5.25 shows that elements 1 and 3 would not exceed the shear limit while elements 2 and 4 would. As this resulted in a mixed result, further data was obtained from the model and the section was found to have an average shear value of 5.85MPa which would indicate the failure of the column in shear.

To summarise, the Column C13 will not fail in compression however the steel would yield in tension. Further more the section will fail in shear.

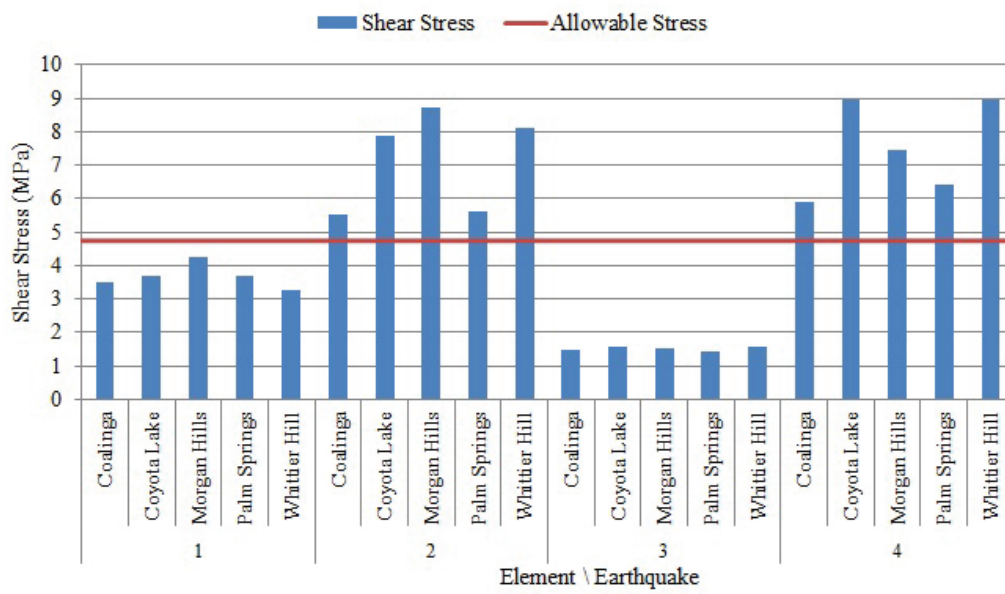


Figure 5.25: The Maximum Shear Stresses in Column C13 in the Concrete

Chapter 6

Conclusions

6.1 The Global Response of the Structure

Now that a selection of the columns were individually assessed, the structure must be considered as a whole. Table 6.1 summarises the different failures considered for each column. A "yes" signifies that the element has failed.

Table 6.1: The Summary of the Different Failures in the Columns

	Concrete			Steel	
Column	Compression	Tension	Shear	Tension	Compression
C1	Yes	Yes	Yes	Yes	No
C3	Yes	Yes	Yes	Yes	Yes
C6	Yes	Yes	Yes	Yes	No
C8	No	No	Yes	No	No
C11	Yes	Yes	Yes	Yes	No
C13	No	Yes	Yes	Yes	No

6.1.1 Compression Stress in the Columns

Columns C8 and C13 are the only columns that are able to resist the earthquake forces in compression. Column C8 does not have masonry panels attached to it, leading to minimal lateral loading and therefore bending stresses. Column C13 resists the load due to the strong axis resisting the lateral loads caused by the masonry panels. Column C6 also resists the lateral load of the masonry with the strong axis however it is only $465mm$ wide as apposed

600mm in C13. This small length leads to a weaker section which then yields in compression. Therefore, in order to avoid yielding in compression, it is important to orientate the cross-section to resist the lateral load induced by the masonry panels. It is also important for column to be large enough to reduce the stresses. The failure of the majority of the column would lead to partial or total collapse of the structure.

6.1.2 Tensile Stress in the Columns

The majority of the columns fail in tension stress. The exception is Column C8 which has no tensile stress as it does not have induced lateral loads from the masonry. The other columns which fail in tension is caused by bending of the column. The results shown does not include the ductility of the steel reinforcement which could result in all the sections avoiding collapse. However, it should be noted that even if the columns do not collapse, there will be significant damage to the reinforcement which would lead to the structure being unsafe. The simplest solution is to increase the tension reinforcement and cross-sectional size of the column. As all columns except the three central ones, i.e. C7, C8 and C9 fail, this would lead to collapse of the structure.

6.1.3 Shear Stress in the Columns

All columns fail in shear stress. This is a the major concern in this structure as this failure will lead to global failure. The simplest solution would be to add a shear wall on all four sides of the structure which then could be designed to resist the shear loading. If a shear wall is not an option, the cross-sectional area of the column must be increased to reduce shear stress.

6.2 Conclusions on the Results with Regard to SANS 10160-4

SANS (2011) regards this building as moment-resisting frame system that is not detailed according to the code. As such, it has a behaviour factor of $q = 2$, which means that the ductility of the system will allow the stresses to be half that of an elastic analysis. With this in mind, it can be calculated that

Columns C8 and C13 would not exceed the yield stresses. The other columns however would all fail in shear which would at least lead to a partial collapse of the structure.

The other aspect which needs to be considered is that the structure is considered as a post-disaster facility in the Stellenbosch region and as such, it should not sustain any damage during an earthquake. If this was the case, then a ductility factor of $q = 1$ would be a more reasonable value.

6.3 Conclusions on the Modeling of Masonry Infill

The modelling of masonry infill panels is a challenging exercise with great problems with calibration. The issues arise from the fact that masonry infill is in fact composed of two materials, namely the mortar and the brick. To model these two materials as a homogeneous material with a single elastic modulus proved challenging, though in all likelihood it would result be the easiest method. It was felt that although the method of modelling masonry in this thesis was not perfect, it resulted in meaningful results.

6.4 Conclusions on the Results

The results of this study show the need for the application of a seismic code in the designing of a reinforced concrete frame. The study also shows the effect that masonry infill panels have on the lateral stiffness of structures and that it cannot be ignored during the design process. Furthermore, it can be deduced that reinforced concrete framed structures in the Cape Town region are susceptible to seismic loading which would result in damage or collapse. It is imperative that retrofitting methods be employed to protect these structures.

6.5 Conclusions on the Results in Context of Reality

A major concern of Wium (2010) is that seismic design is ignored as seismic activity does not occur regularly enough to be a concern. The fact that the

current seismic station system has only been active since 1971 means that there is only 43 years of reliable information available. The issue with this is that the design earthquake is a one in 475 year event. This means that there is less than 10% of the required data of the return period. It can be seen that from earthquake that occurred in Tulbagh in 1969, which claimed twelve lives, that buildings have collapsed due to seismic activity.

Chapter 7

Suggestions for Future Projects

7.1 Introduction

Throughout this thesis assumptions were made that simplified the modelling process. In order for a better understanding of reinforced concrete framed structures with masonry infill panels, further research must be conducted in the following areas. This would reduce the number of assumptions required and therefore the results would be more accurate.

7.1.1 Masonry in South Africa

The properties of the masonry infill panels in this thesis was based on the properties of masonry in the United States. The materials used to produce masonry in South Africa is different as well as the mortar used to join the bricks. The techniques used to construct the panels will also differ from those used in the United States. As such, a study into the properties and the construction techniques used in masonry infill panels in South Africa is required. This study should include research into the lateral stiffness added to a frame when a masonry infill panel is included.

7.1.2 Soil Conditions in South Africa

The soil conditions around the foundation of the structure is important as it transfers the earthquake loading to the structure. This thesis assumed that there would be a perfect transfer of energy to the foundation which is not realistic. The reality is that there will be a loss of energy due to the interaction

between the soil and the foundation. In order to obtain more accurate results, this interaction must be studied and included into any modelling process. Another aspect of the soil conditions not considered is liquefaction. This occurs when the water table is high and when excited by an earthquake, the soil particles lose contact with each other. This results in a diminished capacity of the soil which supports the foundation (Rydelek, 2004). This is of particular concern as the area around Cape Town has a high water table and liquefaction is a possibility. Further more, the results of this study will aid in updating the response spectrums in SANS (2011).

7.1.3 Retrofitting Structures

The conclusion of this thesis is that reinforced concrete framed structures are at risk of damage or collapse when subjected to seismic loading. With this in mind, techniques to retrofit structures such that collapse does not occur must be investigated. This presents a challenge as there are many different situations and each will require a different solution. It is also imperative that buildings such as the one modelled in this thesis are able to resist earthquakes and are fully functional as they are post-disaster centers. Other such buildings are hospitals and fire stations.

7.1.4 Ductility of Reinforced Concrete Framed Structures in South Africa

One assumption made in this thesis is that the structure modelled remained elastic. The reality is that the material yield and becomes plastic during an earthquake and therefore dissipate the energy in the elements. A study into the properties of the materials once yielded in South African buildings would lead to insight into the ductility of the reinforced concrete framed structures with masonry infill panels and from that, it would be possible to update the behaviour factors in SANS (2011).

List of References

- Al-Chaar, G., Mehrabi, A., of Engineers, U.S.A.C., Research, E., (U.S.), D.C. and (U.S.), C.E.R.L. (2008). *Constitutive Models for Nonlinear Finite Element Analysis of Masonry Prisms and Infill Walls*. ERDC/CERL TR. [US Army Corps of Engineers], Engineer Research and Development Center, Construction Engineering Research Laboratory.
- Al-Chaar, G., of Engineers, U.S.A.C., Research, E., (U.S.), D.C. and Laboratory, C.E.R. (2002). *Evaluating Strength and Stiffness of Unreinforced Masonry Infill Structures*. ERDC/CERL TR. US Army Corps of Engineers, Engineer Research and Development Center, Construction Engineering Research Laboratory.
- American Concrete Institute (2008). *Building Code Requirements for Structural Concrete (ACI 318-08) and Commentary*. American Concrete Institute. ISBN 9780870312649.
Available at: <http://books.google.co.za/books?id=c6yQszMV2-EC>
- ASTM (2003). *ASTM A615 / A615M - 13: Standard Specification for Deformed and Plain Carbon-Steel Bars for Concrete Reinforcement*. ASTM International, West Conshohocken, PA.
- Brandt, M., Bejaichund, M., Kgaswane, E., Hattingh, E. and Roblin, D. (2005). *Seismic History of Southern Africa*. Seismological Series. Council for Geoscience.
- Buchholdt, H. and Nejad, S. (2011). *Structural Dynamics for Engineers*. Inst of Civil Engineers Pub. ISBN 9780727741769.
- Chopra, A. (2007). *Dynamics Of Structures, 3/E*. Prentice-Hall international series in civil engineering and engineering mechanics. Pearson Education. ISBN 9788131713297.
- Craig, R.R. (2000). *Mechanics of Materials*. Wiley. ISBN 9780471331766.

- Crisafulli, F., Carr, A. and Park, R. (2000). Analytical modelling of infilled frame structures: A general review. *Bulletin of the New Zealand National Society for Earthquake Engineering*, vol. 33, no. 1, pp. 30–47.
- Daknakhni, W., Hamid, A. and Elgaaly, M. (2004). Strength and stiffness prediction of masonry infill panels. , no. 3089.
- Dassault Systemes (2013). *ABAQUS 6.10 Documentation*. Dassault Systemes Abaqus.
- Dazio, A. (2013). *Elastic and Inelastic Response Spectra*. Proceedings of the Seismic Design of Building Structures.
- Donea, J., Jones, P. and of the European Communities. Joint Research Centre. Ispra Establishment, C. (1991). *Experimental and Numerical Methods in Earthquake Engineering*. Eurocourses: Reliability & Risk Analysis. Springer. ISBN 9780792314349.
- Guevara-Perez, L.T. (2012). Soft story and weak story in earthquake resistant design: A multidisciplinary approach.
- Harrison, L. (2012). *Determining the Frequency of Seismic Activity in South Africa*. Final Project.
- Liauw, T. and Kwan, K. (1984). *Nonlinear behaviour of Non-Integral Infilled Frames*, vol. 8. Computers and Structures.
- Mainstone, R. (1971). *On the Stiffness and Strengths of Infilled Frames*, vol. Supplement IV. Proceedings of the American Society of Civil Engineering.
- McSaveney, E. (2012). *Earthquakes - What causes earthquakes?* Te Ara - The Encyclopedia of New Zealand.
- Mehrabi, A.B. (1994). *Performance of masonry-infilled R/C frames under in-plane lateral loads*.
- Pacific Earthquake Engineering Research Center (2013). *PEER Ground Motion Database*. Pacific Earthquake Engineering Research Center.
- Paulay, T. and Priestley, J. (1992). *Seismic Design of Reinforced Concrete and Masonry Buildings*. Wiley-interscience publication. John Wiley & Sons. ISBN 9780471549154.
- Polyakov, S. (1963). *Masonry in Framed Buildings*.

- Retief, J. and Dunaiski, P. (2009). *Background to SANS 10160: Basis of Structural Design and Actions for Building and Industrial Structures*. SANS standard. SUN Press. ISBN 9781920338107.
- Rydelek, Paul A. Tuttle, M. (2004). Explosive craters and soil liquefaction. *Nature*, vol. 427, no. 6970, p. 115. ISSN 00280836.
- SABS (1989). *Code of Practice for the General Procedures and Loadings to be Adopted in the Design of Buildings*. South African standard: Code of practice. South African Bureau of Standards. ISBN 9780626084622.
- SANS (2011). *Basis of Structural Design and Actions for Buildings and Industrial Structures Part 4: Seismic Actions and General Requirements for Buildings*. South African Bureau of Standards. ISBN 978062626431.
- SANS 10100-1 (2000). *The Structural Use of Concrete Part 1: Design*. South African Bureau of Standards. ISBN 0626124972.
- Simpson, J., Weiner, E. and Press, O.U. (1989). *The Oxford English dictionary*. The Oxford English dictionary: B.B.C. -Chalypsography. Clarendon Press. ISBN 9780198612148.
- Smithsonian (2014). Seismic waves.
Available at: <http://www.mnh.si.edu/earth>
- South African Reinforced Concrete Engineers' Association (2013). *Tensile Properties*. South African Reinforced Concrete Engineers' Association.
- Stafford-Smith, B. (1962). *Lateral Stiffness of Infilled Frames*, vol. 88. Proceedings of the American Society of Civil Engineering, Journal of Structural Division.
- Stavridis, A., Koutromanos, I. and Shing, P.B. (2012). Shake-table tests of a three-story reinforced concrete frame with masonry infill walls. *Earthquake Engineering and Structural Dynamics*, vol. 41, no. 6, pp. 1089–1108. ISSN 1096-9845.
- Sung, Y., Lin, T., Hsiao, C. and Lai, M. (2013). Pushover analysis of reinforced concrete frames considering shear failure at beam-column joints. *Earthquake Engineering and Engineering Vibration*, vol. 12, no. 3, pp. 373–383. ISSN 1671-3664.
- The Concrete Society of the United Kingdom (2013). *Densities*. The Concrete Society of the United Kingdom.
Available at: <http://www.concrete.org.uk/>

- USDE (2012). *Induced Seismicity*. U.S. Department of Energy.
Available at: <http://esd.lbl.gov/research/projects/>
- USGS (2012). *Earthquake Facts*. U.S. Geological Survey.
Available at: <http://earthquake.usgs.gov/learn/facts.php>
- USNBS, N.B.o.S. (1978). *Tentative provisions for the development of seismic regulations for buildings: a cooperative effort with the design professions, building code interests, and the research community*. ATC publication. U.S. Dept. of Commerce, National Bureau of Standards.
- Wium, J. and van Zijl, G. (2005). *The South African Loading Code Revision of Provisions for Seismic Loading*. African Concrete Code Symposium.
- Wium, J.A. (2010 04). *Background to Draft SANS 10160 (2009): Part 4 Seismic Loading*, vol. 52. Journal of the South African Institution of Civil Engineering.

Appendix A

Applied Earthquakes

A.1 The Seismographs of the Earthquakes Applied to the Full Structure

The five earthquakes that the representative structure was tested with were all 5.5-6.5 magnitude earthquakes with a peak ground acceleration between $1.0g$ and $1.5g$. These values are representative of values that could be found for earthquakes found in the Western Cape.

The first earthquake used was the Coalinga earthquake which occurred on the 02/05/1983. It had a magnitude of 6.4 and a peak ground acceleration of $0.104g$. Figure A.1(a) shows the ground motion in the North-South direction and (b) shows the ground motion in the East-West direction as measured at the Parkfield-Cholame Station.

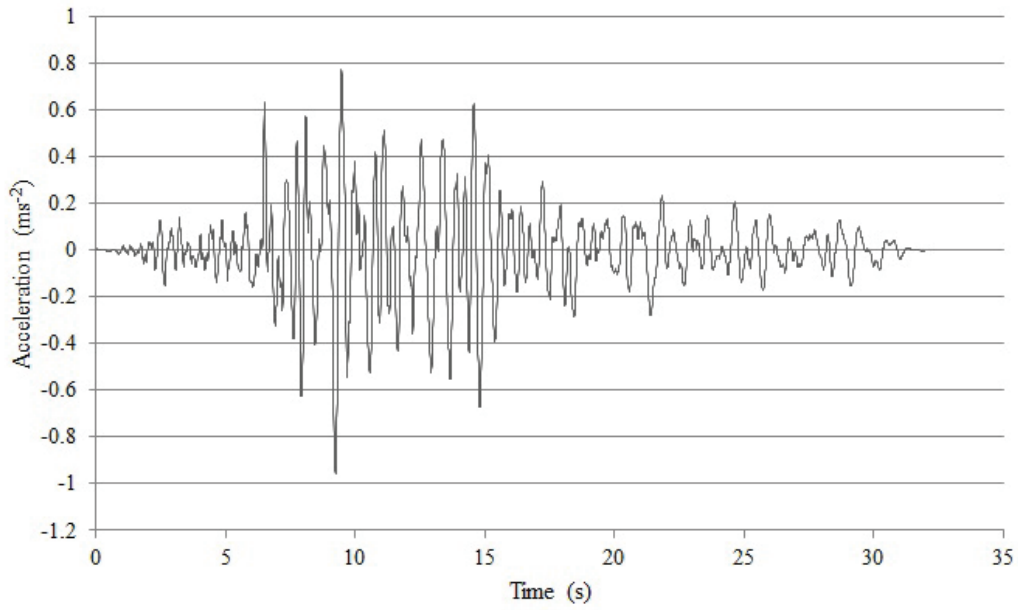
The second earthquake used was the Coyota Lake earthquake which occurred on the 06/08/1979. It had a magnitude of 5.7 and a peak ground acceleration of $0.109g$. Figure A.2(a) shows the ground motion in the North-South direction and (b) shows the ground motion in the East-West direction as measured at the San Juan Bautista Station.

The third earthquake used was the Morgan Hill earthquake which occurred on the 24/04/1984. It had a magnitude of 6.2 and a peak ground acceleration of $0.099g$. Figure A.3(a) shows the ground motion in the North-South direction and (b) shows the ground motion in the East-West direction as measured at the Gilroy Array #1 Station.

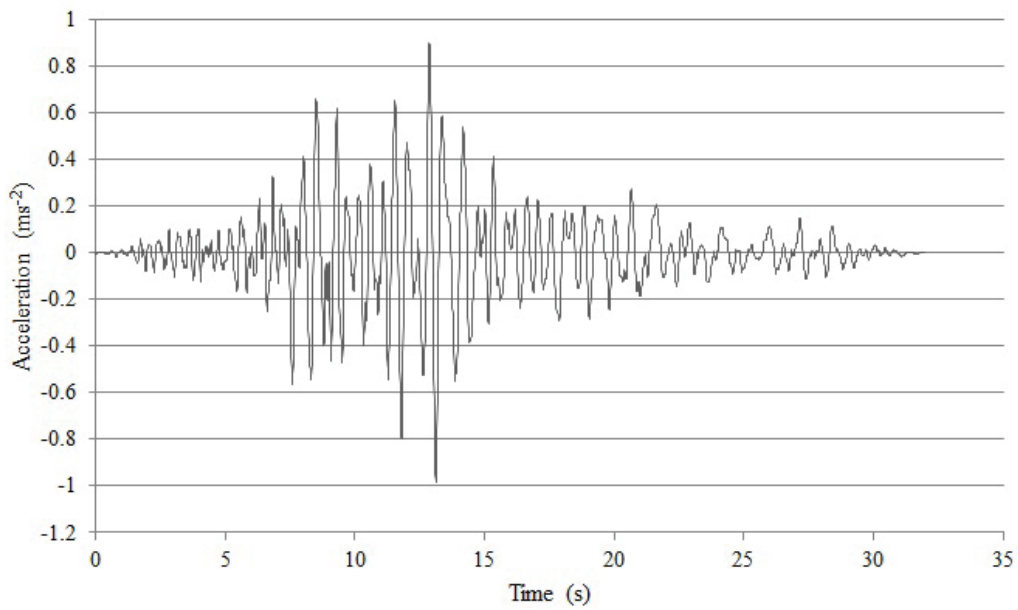
The fourth earthquake used was the Palm Springs earthquake which oc-

curred on the 08/07/1986. It had a magnitude of 6.0 and a peak ground acceleration of $0.111g$. Figure A.4(a) shows the ground motion in the North-South direction and (b) shows the ground motion in the East-West direction as measured at the Anza-Tule Canyon Station.

The final earthquake used was the Whittier Narrows earthquake which occurred on the 01/10/1987. It had a magnitude of 6.0 and a peak ground acceleration of $0.124g$. Figure A.5(a) shows the ground motion in the North-South direction and (b) shows the ground motion in the East-West direction as measured at the Canyon Country Station.

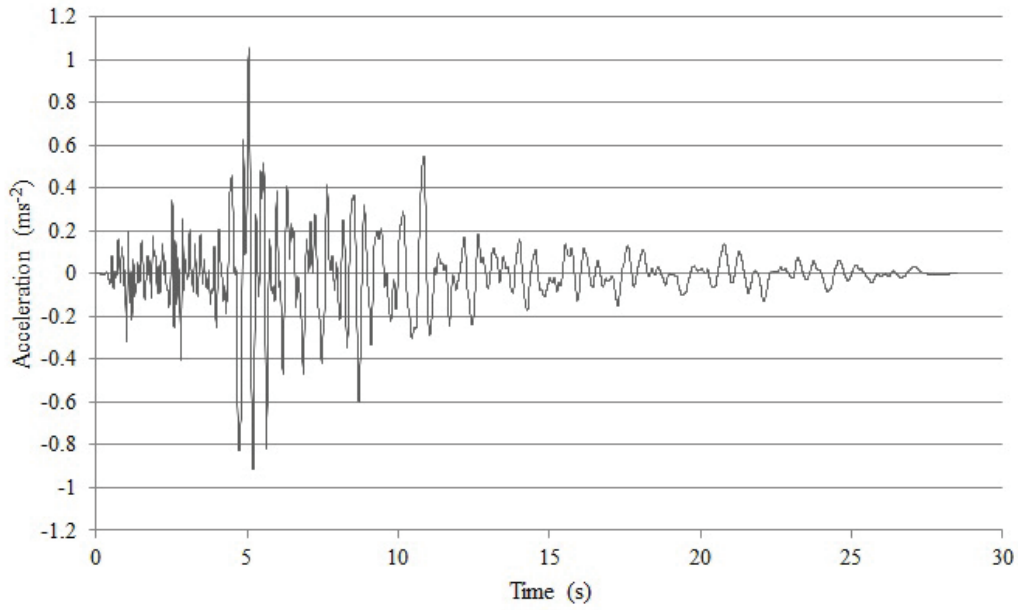


(a) The Ground Acceleration in the North-South Direction

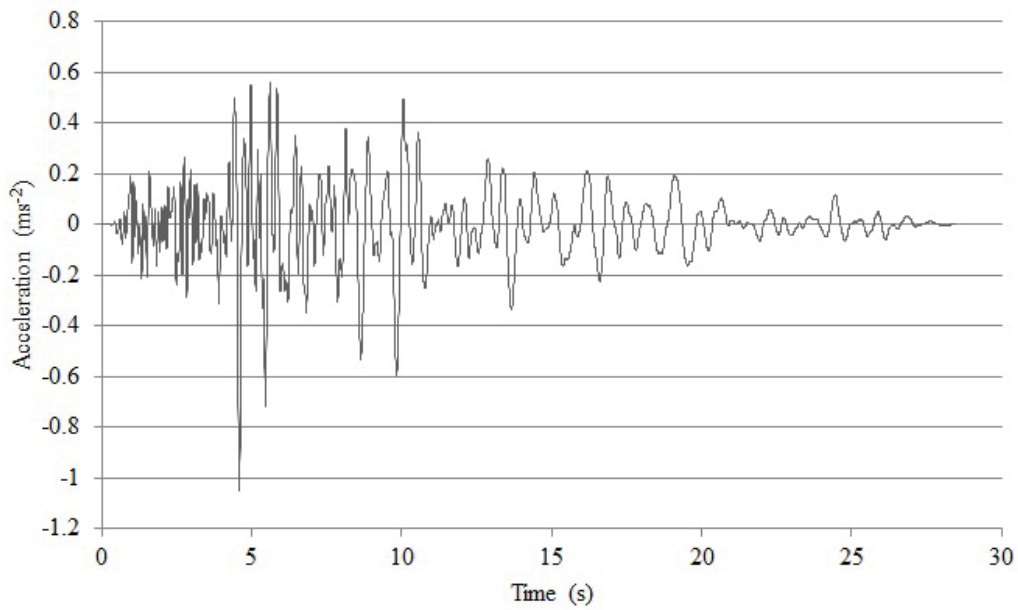


(b) The Ground Acceleration in the East-West Direction

Figure A.1: The Ground Acceleration of the Coalinga Earthquake
(Pacific Earthquake Engineering Research Center, 2013)

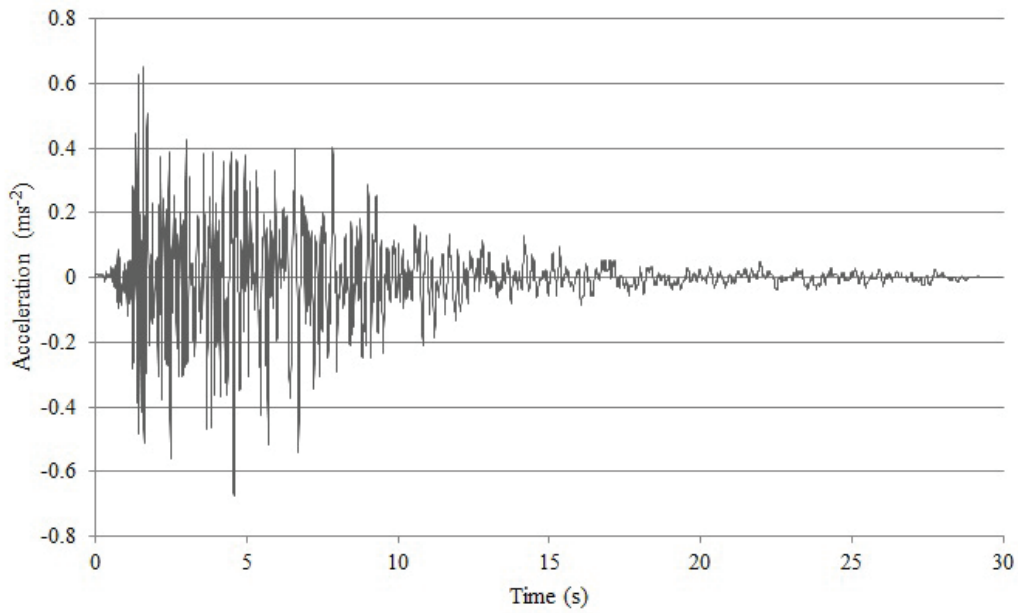


(a) The Ground Acceleration in the North-South Direction

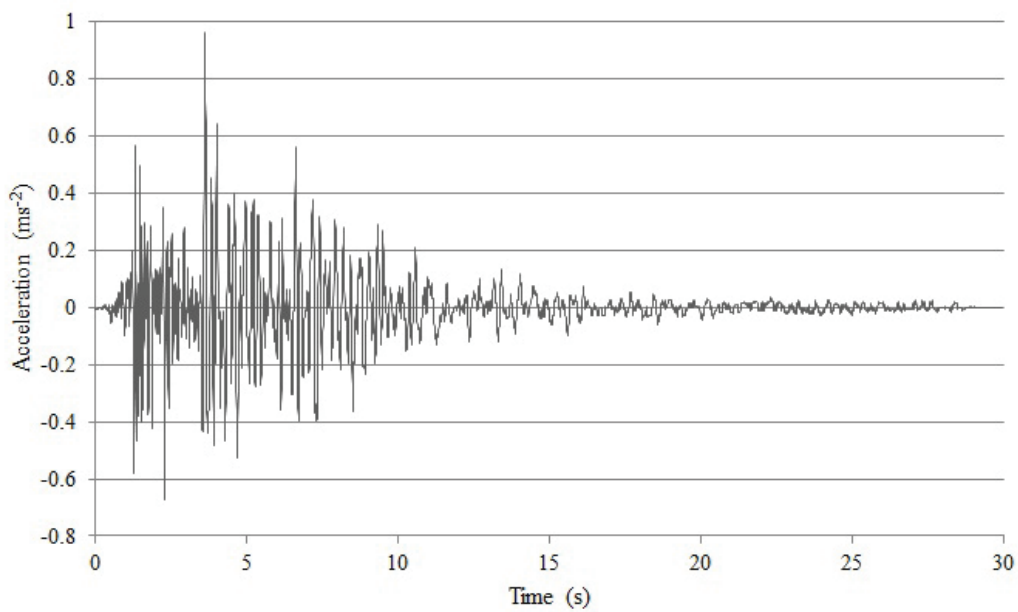


(b) The Ground Acceleration in the East-West Direction

Figure A.2: The Ground Acceleration of the Coyota Lake Earthquake
(Pacific Earthquake Engineering Research Center, 2013)

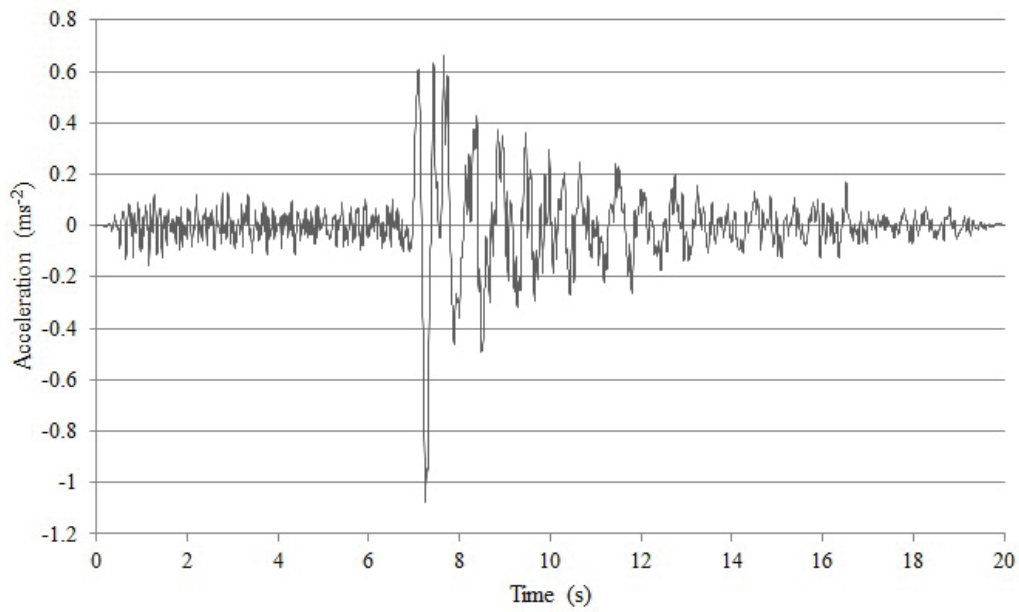


(a) The Ground Acceleration in the North-South Direction

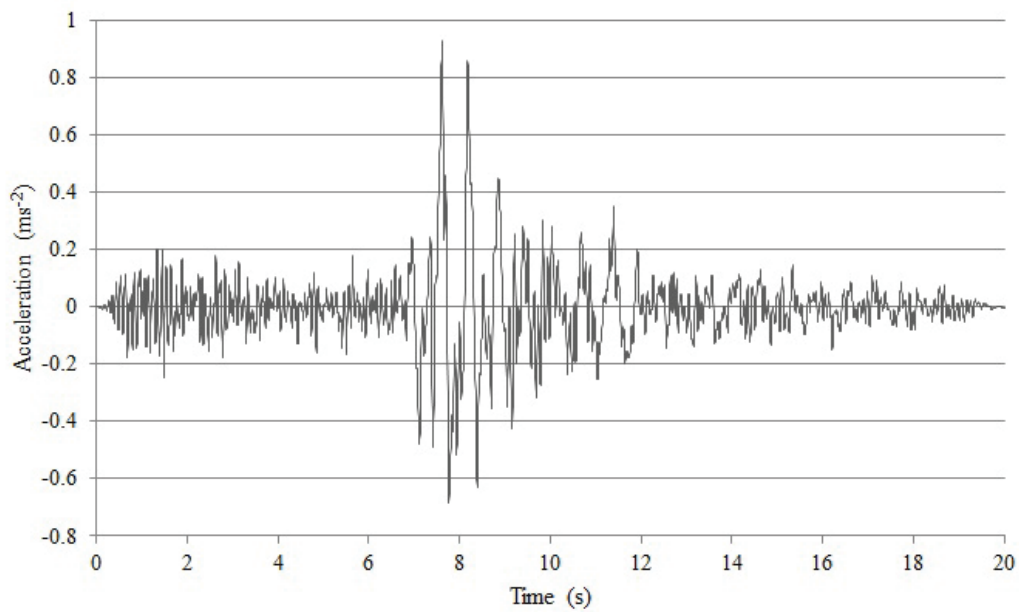


(b) The Ground Acceleration in the East-West Direction

Figure A.3: The Ground Acceleration of the Morgan Hill Earthquake
(Pacific Earthquake Engineering Research Center, 2013)

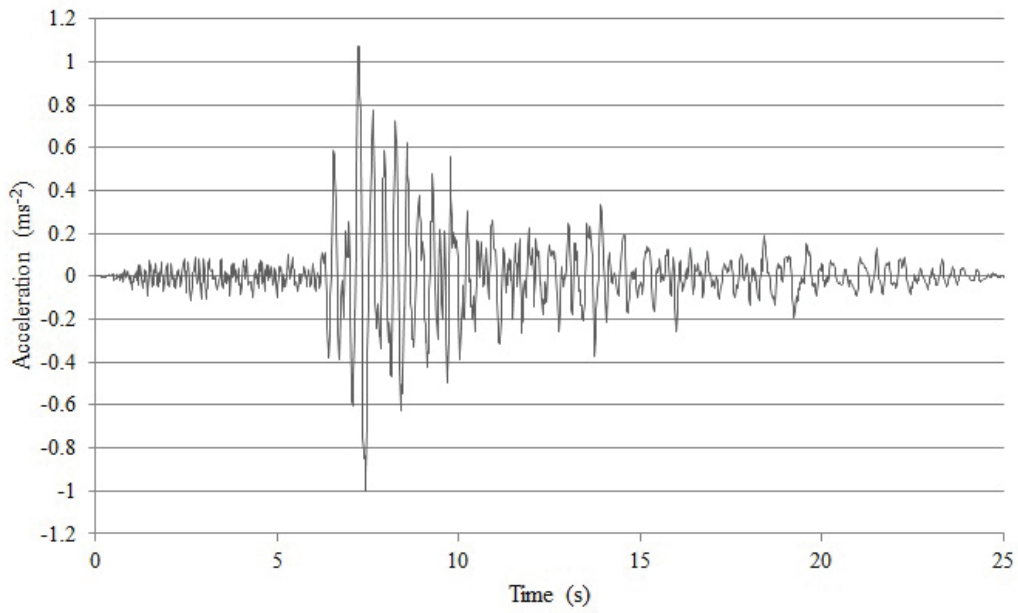


(a) The Ground Acceleration in the North-South Direction

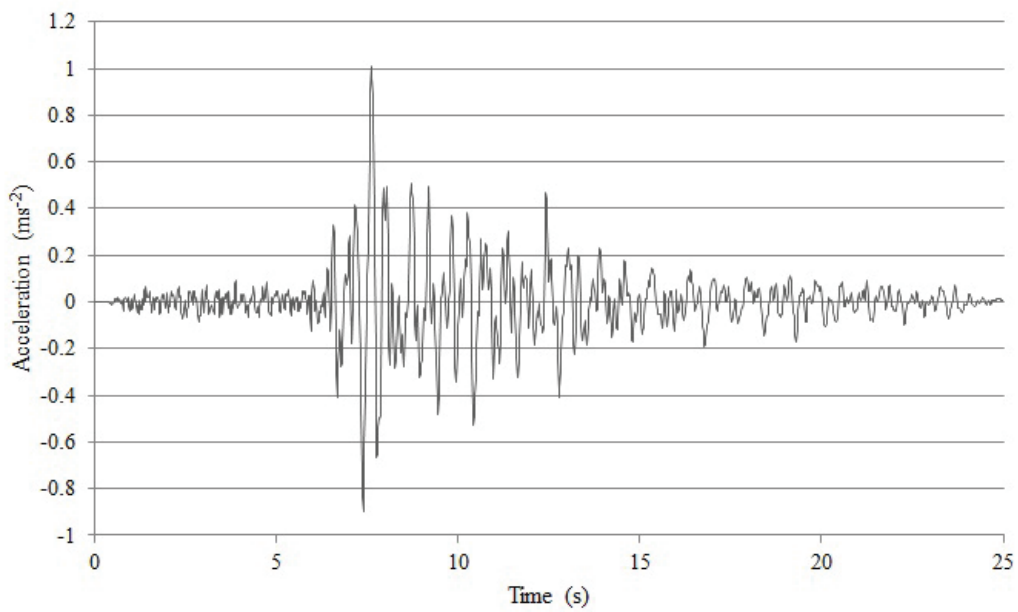


(b) The Ground Acceleration in the East-West Direction

Figure A.4: The Ground Acceleration of the Palm Springs Earthquake
(Pacific Earthquake Engineering Research Center, 2013)



(a) The Ground Acceleration in the North-South Direction



(b) The Ground Acceleration in the East-West Direction

Figure A.5: The Ground Acceleration of the Whittier Narrows Earthquake (Pacific Earthquake Engineering Research Center, 2013)

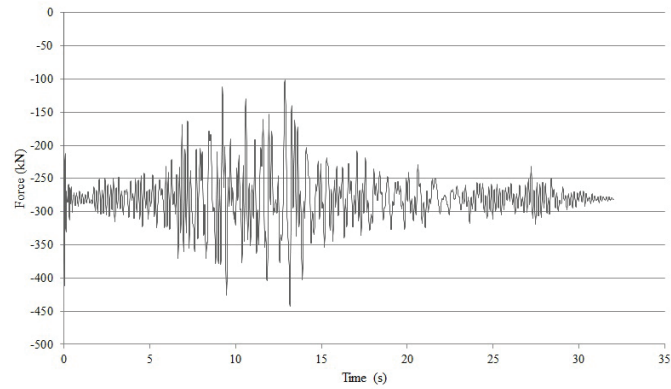
Appendix B

The Forces in the Ground Floor Columns

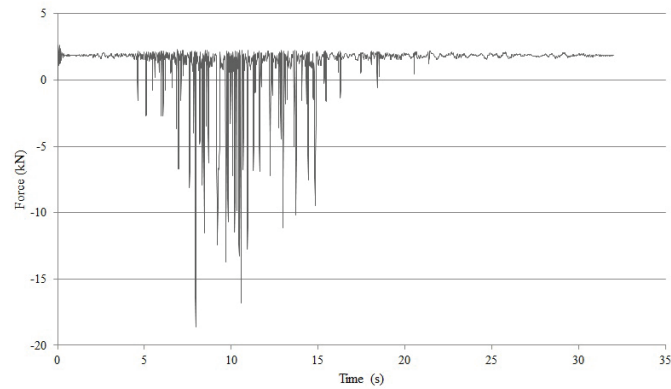
B.1 The Resultant Force Diagrams on the Columns

The results from the 3D beam model on the Columns C1, C3, C6, C8, C11 and C13 are presented in this Appendix. These forces act at the top of the ground floor column. These forces are then applied to the apex of the full three dimensional column.

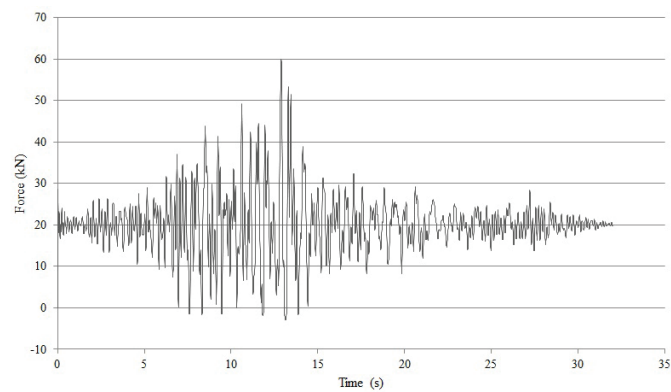
B.1.1 The Resultant Forces During the Coalinga Earthquake



(a) The Axial Force on Column C1

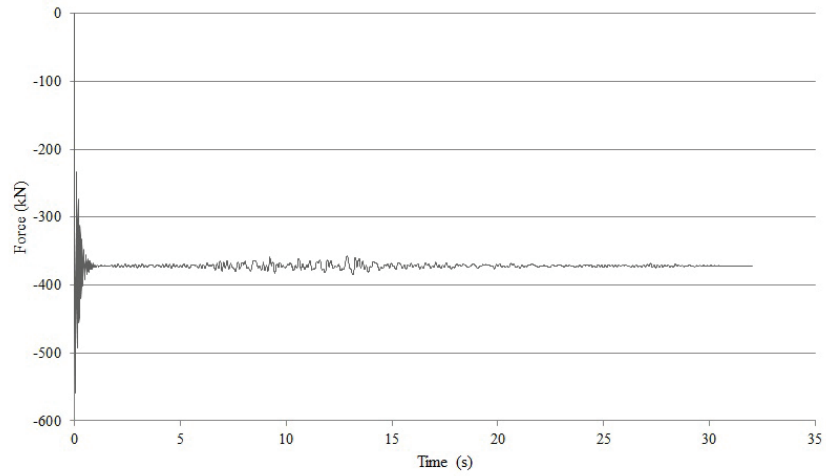


(b) The Shear Force on Column C1 in the Direction of the Long Side

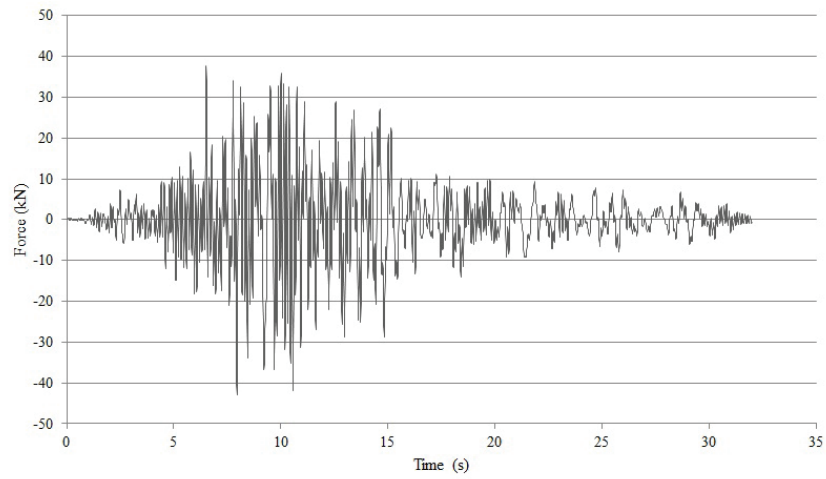


(c) The Shear Force on Column C1 in the Direction of the Short Side

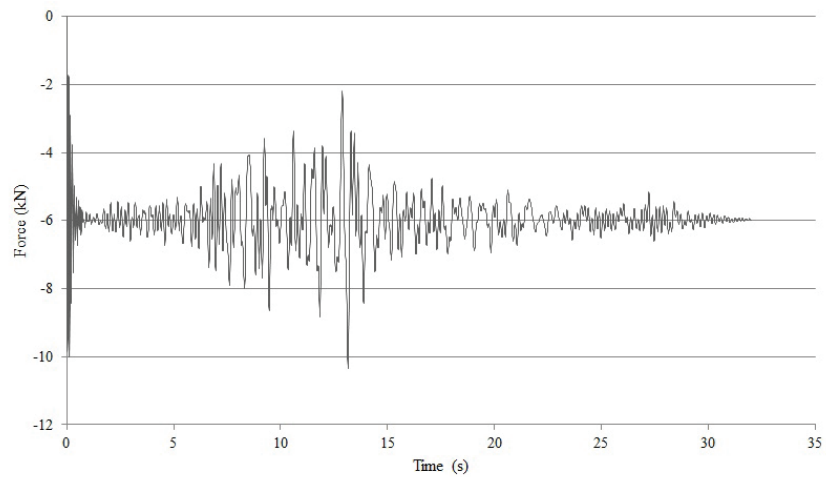
Figure B.1: The Forces in Column C1 when the Coalinga Earthquake is Applied



(a) The Axial Force on Column C3

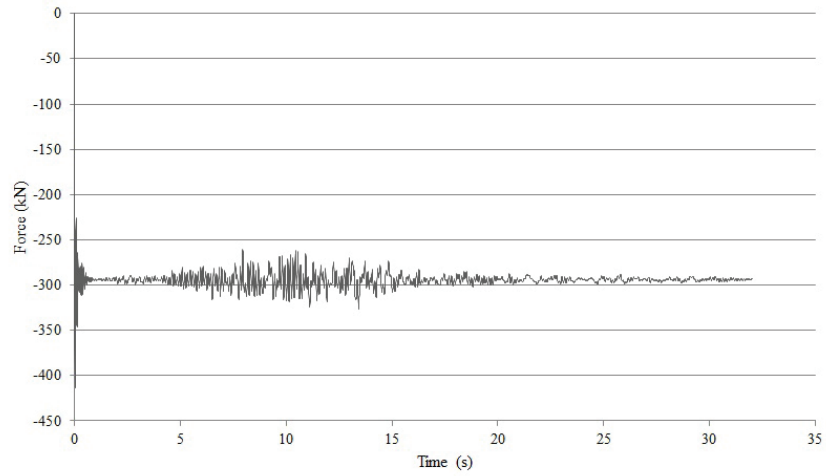


(b) The Shear Force on Column C3 in the Direction of the Long Side

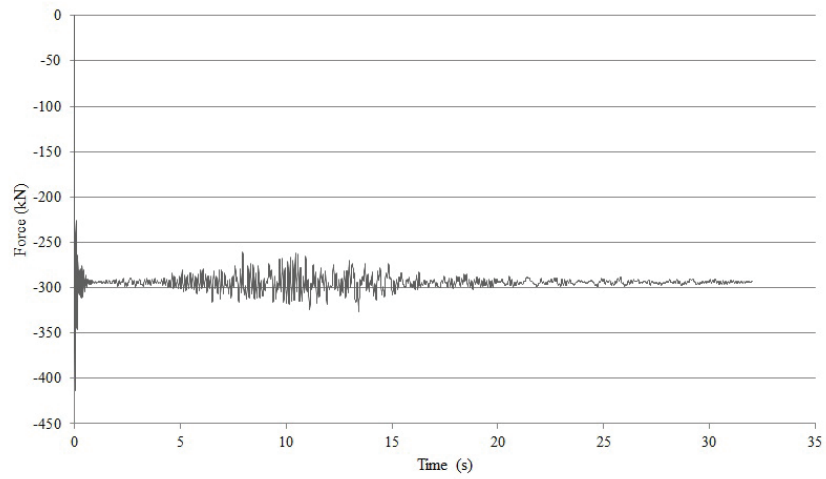


(c) The Shear Force on Column C3 in the Direction of the Short Side

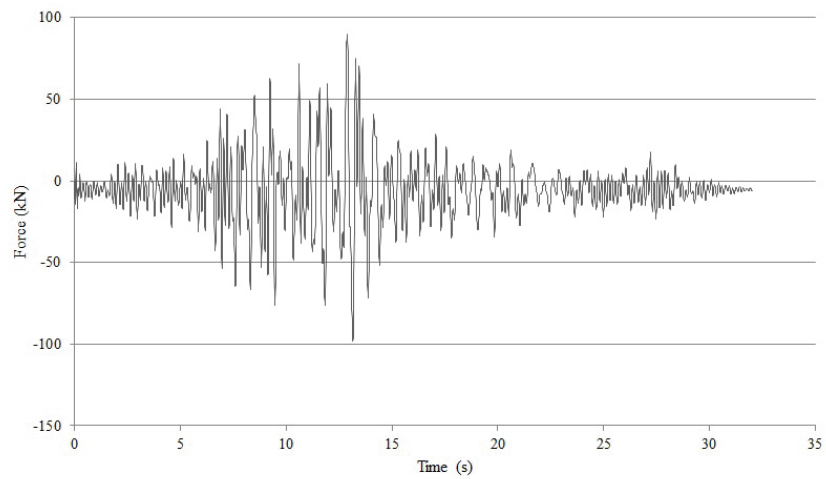
Figure B.2: The Forces in Column C3 when the Coalinga Earthquake is Applied



(a) The Axial Force on Column C6

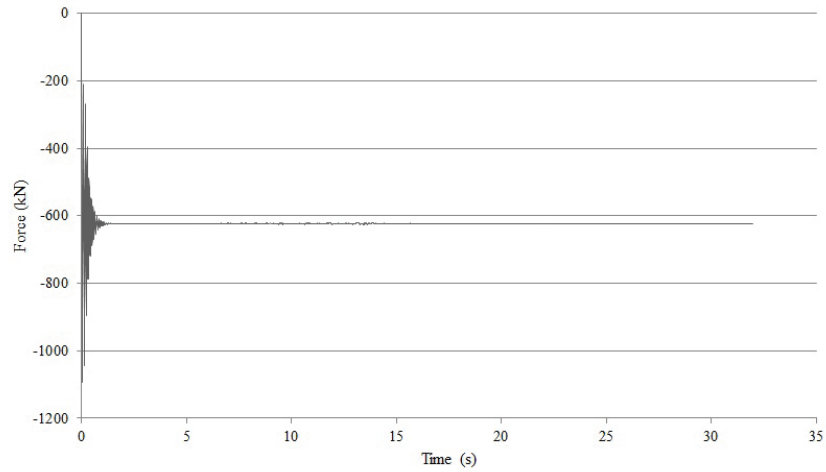


(b) The Shear Force on Column C6 in the Direction of the Long Side

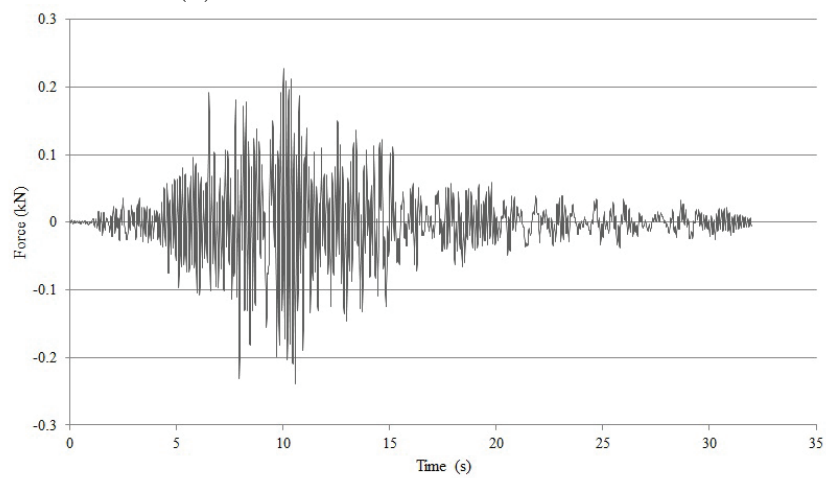


(c) The Shear Force on Column C6 in the Direction of the Short Side

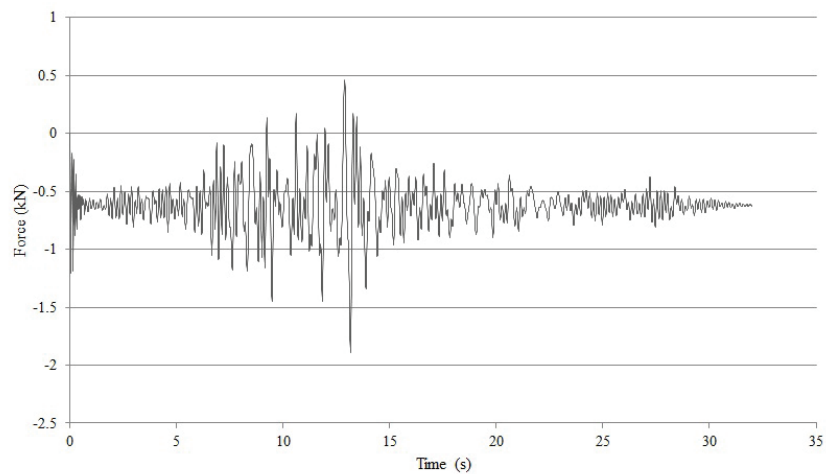
Figure B.3: The Forces in Column C6 when the Coalinga Earthquake is Applied



(a) The Axial Force on Column C8

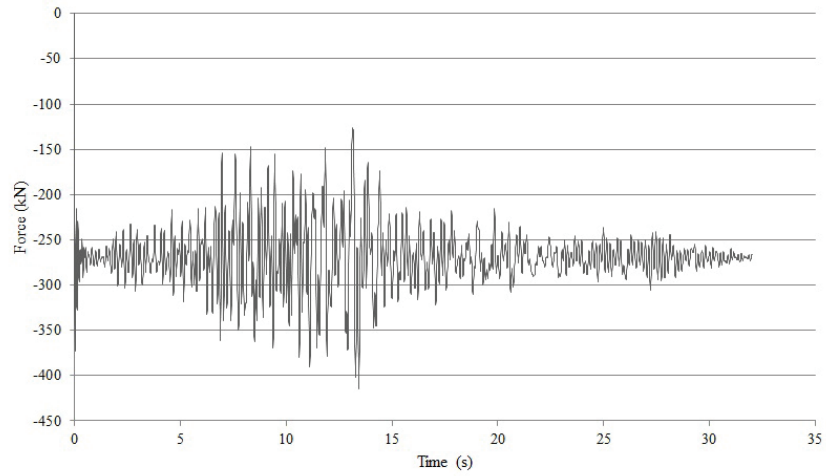


(b) The Shear Force on Column C8 in the Direction of the Long Side

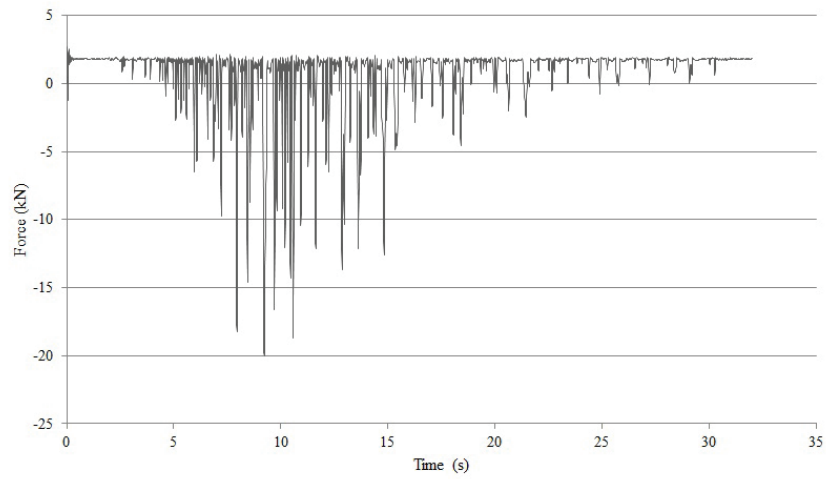


(c) The Shear Force on Column C8 in the Direction of the Short Side

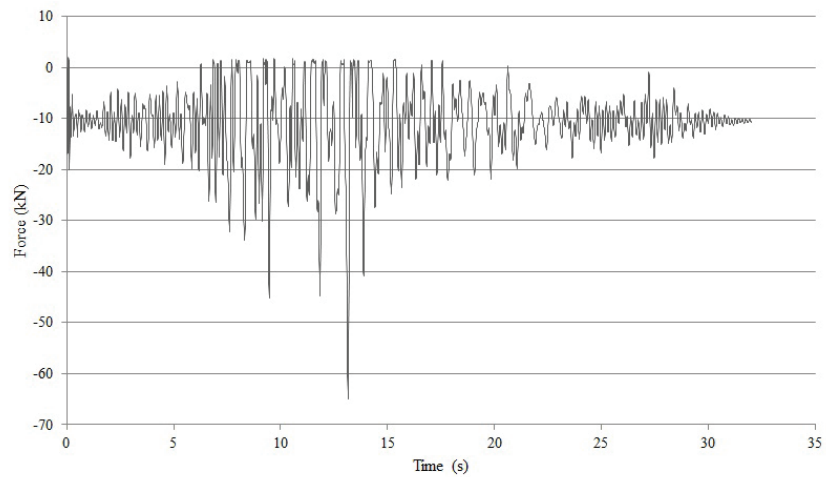
Figure B.4: The Forces in Column C8 when the Coalinga Earthquake is Applied



(a) The Axial Force on Column C11

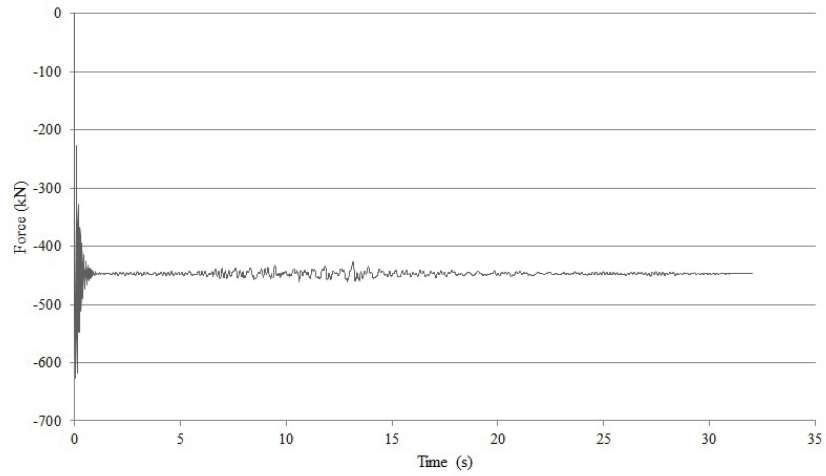


(b) The Shear Force on Column C11 in the Direction of the Long Side

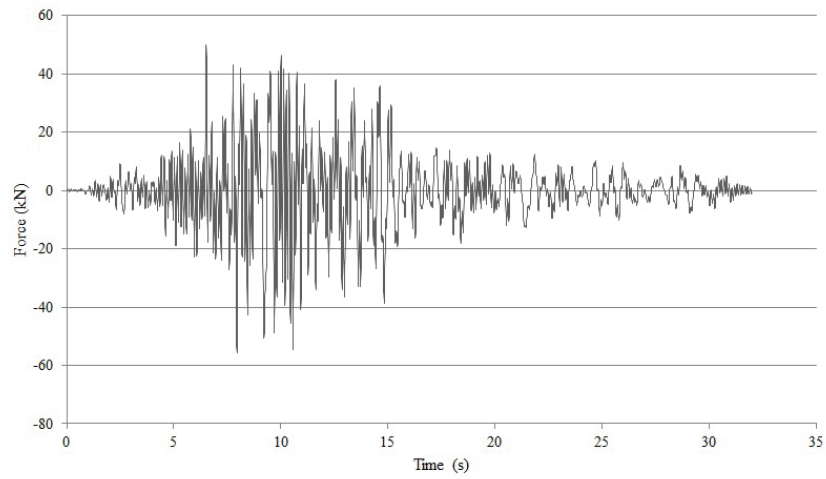


(c) The Shear Force on Column C11 in the Direction of the Short Side

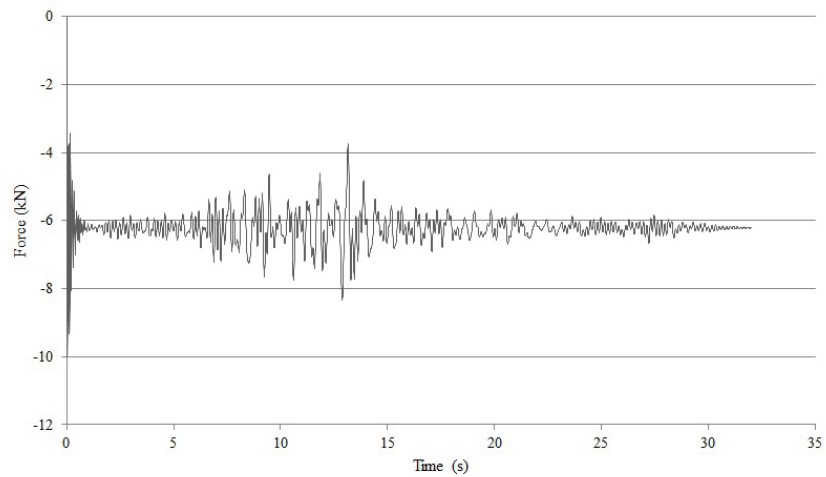
Figure B.5: The Forces in Column C11 when the Coalinga Earthquake is Applied



(a) The Axial Force on Column C13



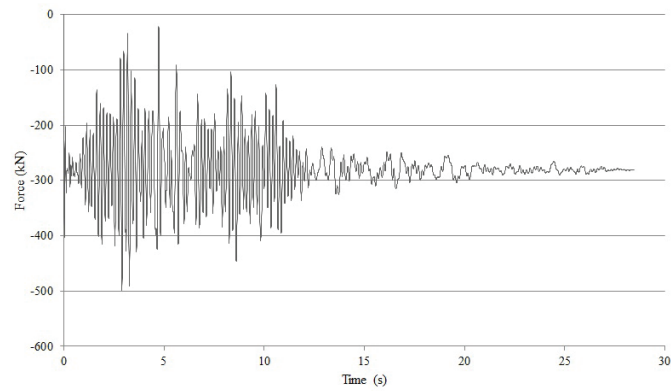
(b) The Shear Force on Column C13 in the Direction of the Long Side



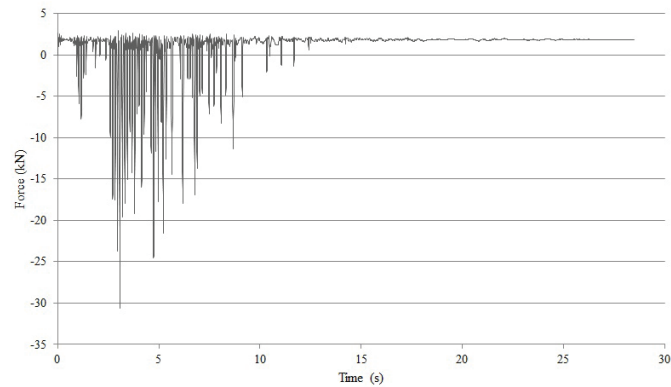
(c) The Shear Force on Column C13 in the Direction of the Short Side

Figure B.6: The Forces in Column C13 when the Coalinga Earthquake is Applied

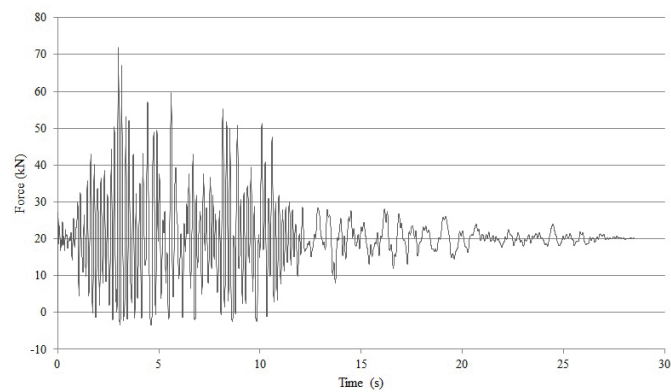
B.1.2 The Resultant Forces During the Coyota Lake Earthquake



(a) The Axial Force on Column C1

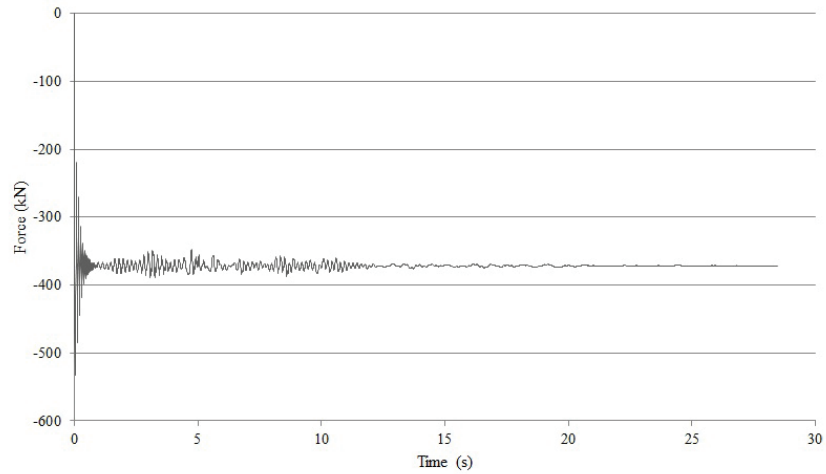


(b) The Shear Force on Column C1 in the Direction of the Long Side

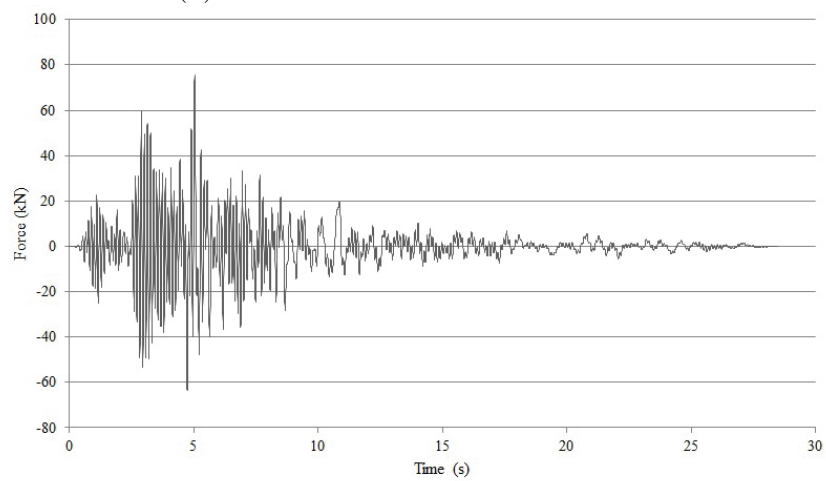


(c) The Shear Force on Column C1 in the Direction of the Short Side

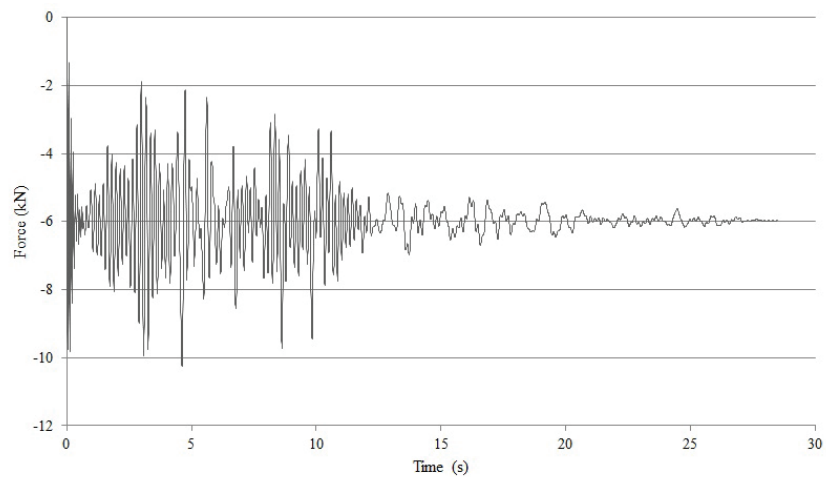
Figure B.7: The Forces in Column C1 when the Coyota Lake Earthquake is Applied



(a) The Axial Force on Column C3

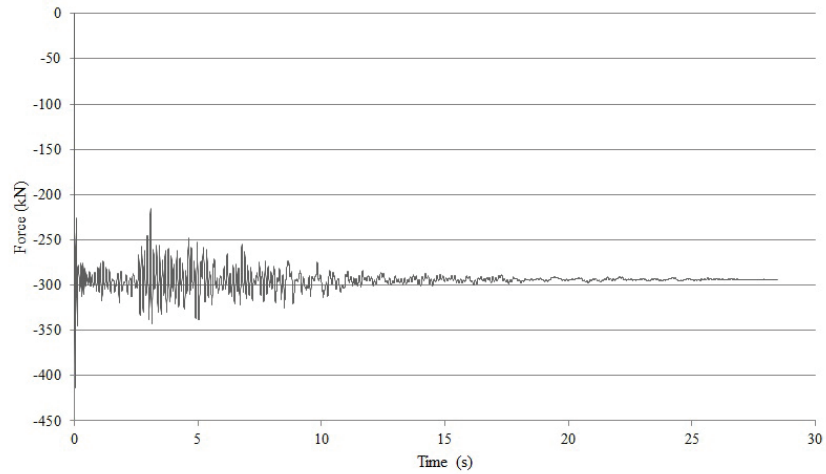


(b) The Shear Force on Column C3 in the Direction of the Long Side

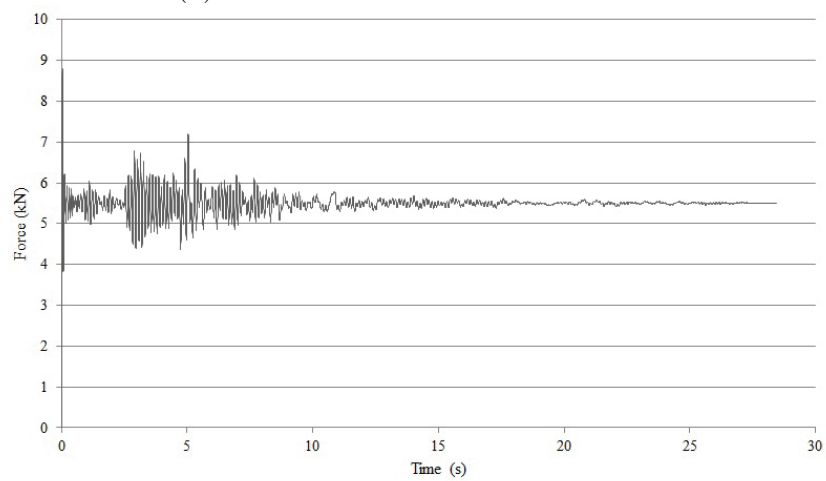


(c) The Shear Force on Column C3 in the Direction of the Short Side

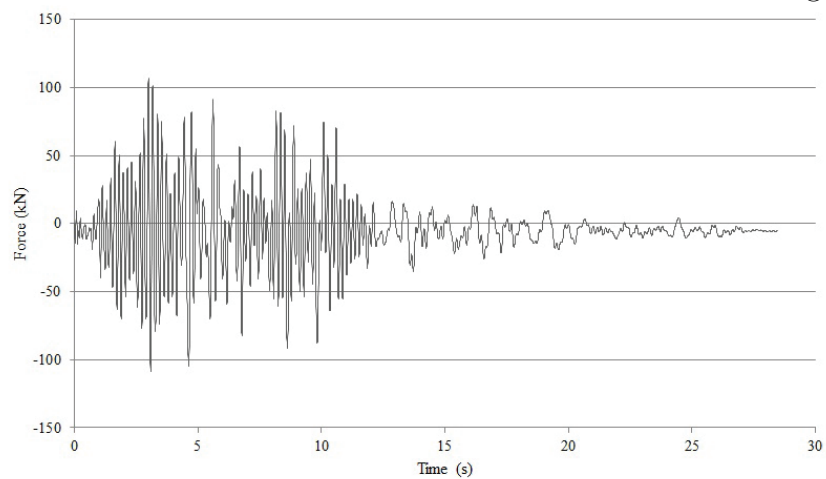
Figure B.8: The Forces in Column C3 when the Coyota Lake Earthquake is Applied



(a) The Axial Force on Column C6

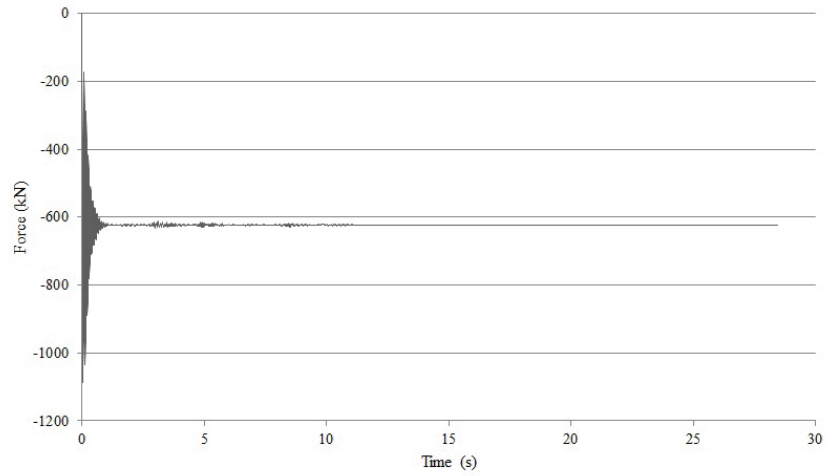


(b) The Shear Force on Column C6 in the Direction of the Long Side

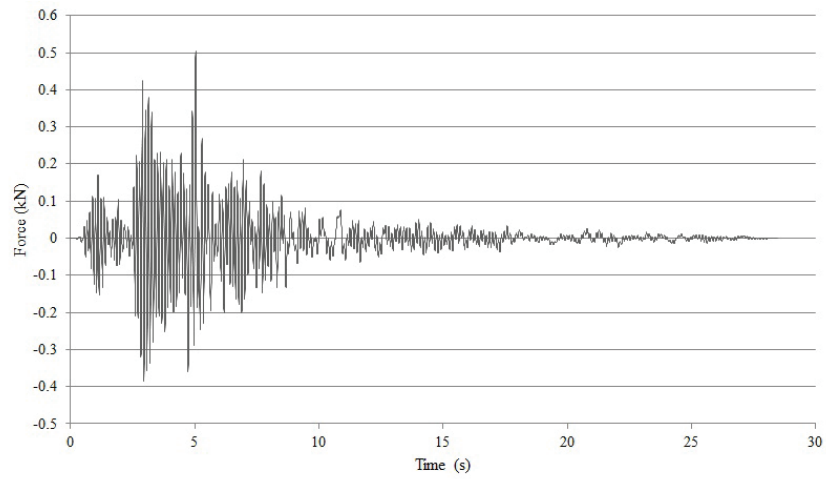


(c) The Shear Force on Column C6 in the Direction of the Short Side

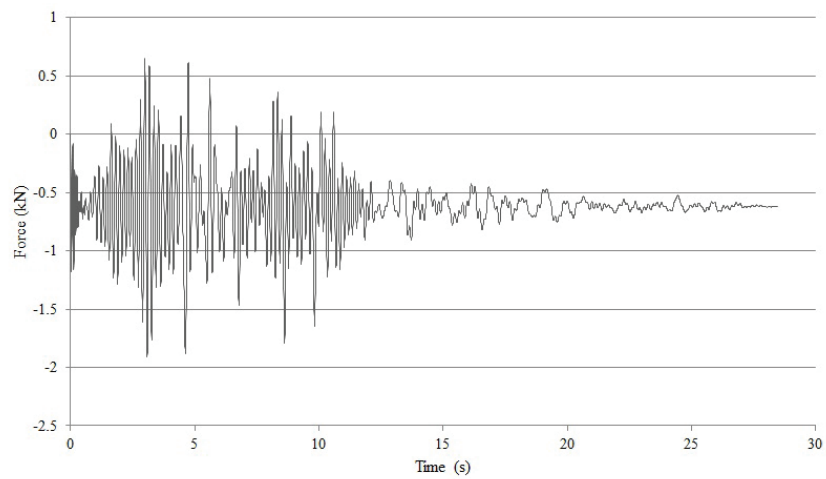
Figure B.9: The Forces in Column C6 when the Coyota Lake Earthquake is Applied



(a) The Axial Force on Column C8

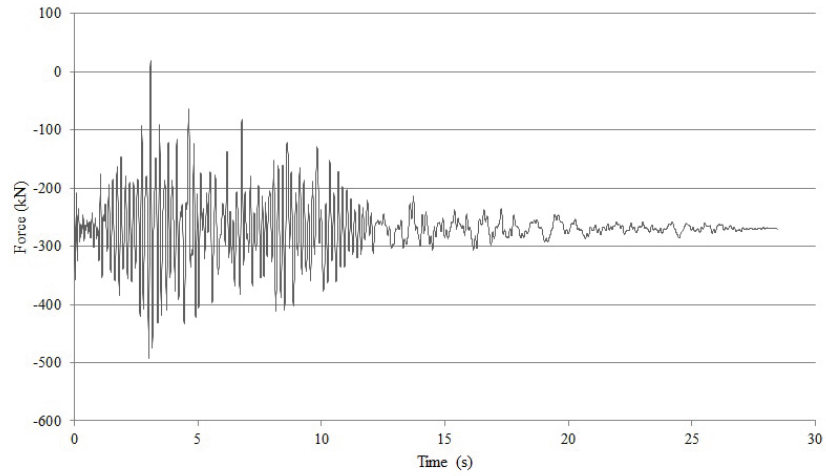


(b) The Shear Force on Column C8 in the Direction of the Long Side

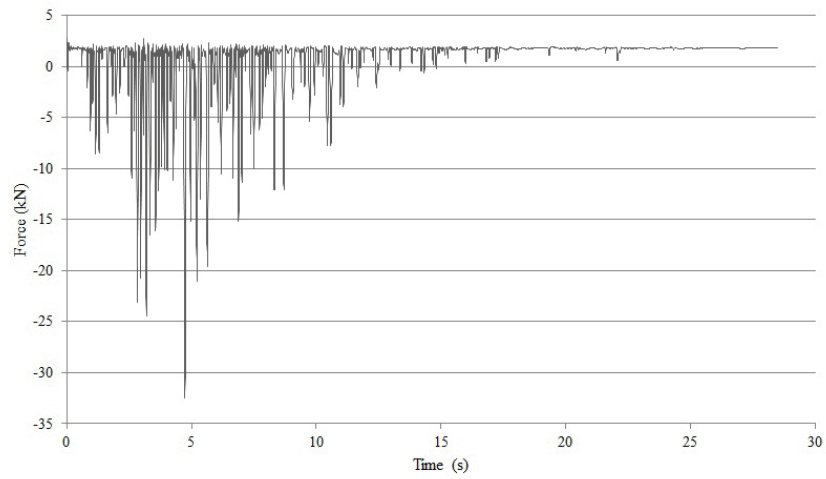


(c) The Shear Force on Column C8 in the Direction of the Short Side

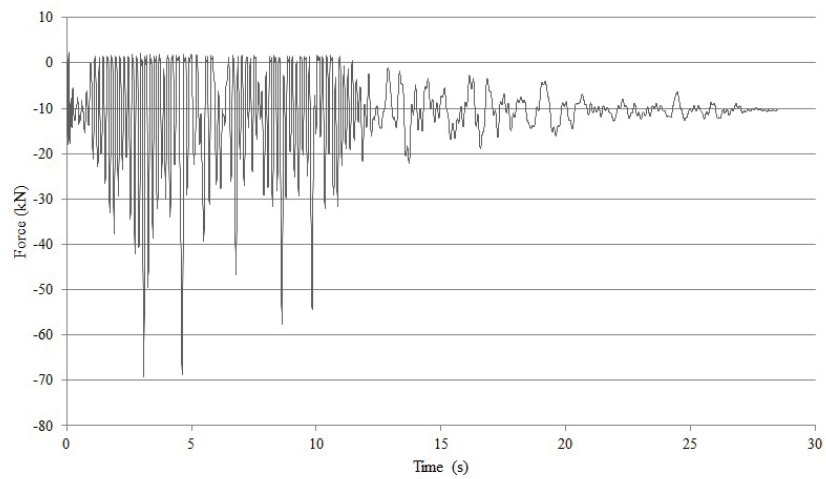
Figure B.10: The Forces in Column C8 when the Coyota Lake Earthquake is Applied



(a) The Axial Force on Column C11

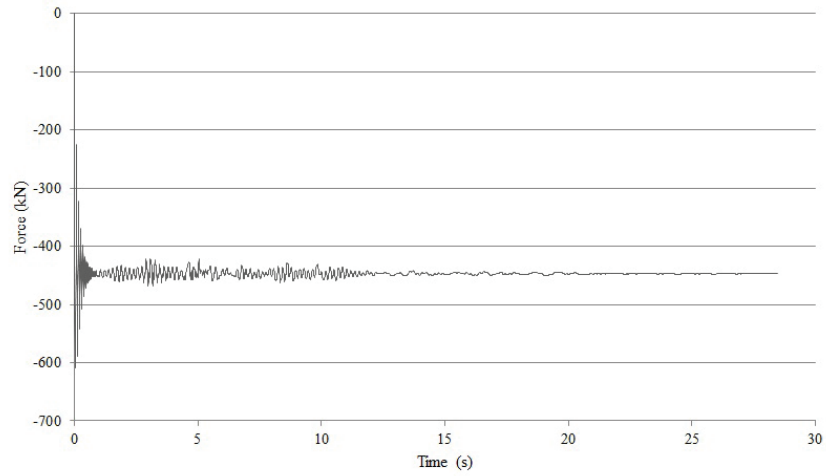


(b) The Shear Force on Column C11 in the Direction of the Long Side

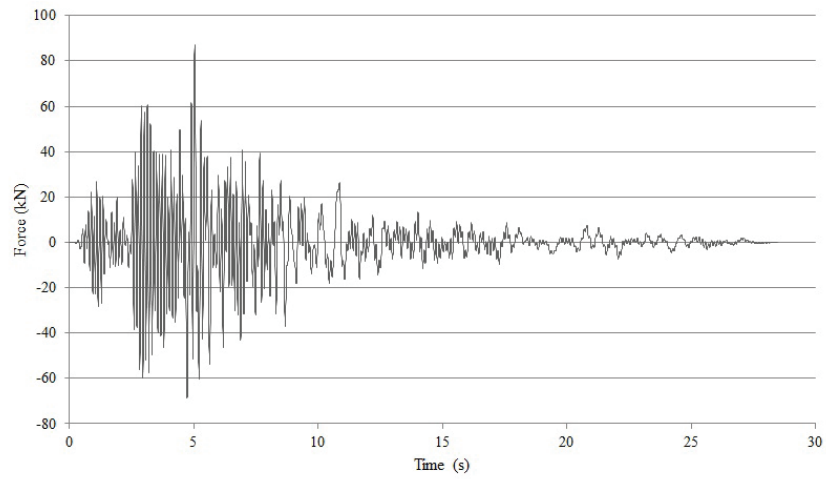


(c) The Shear Force on Column C11 in the Direction of the Short Side

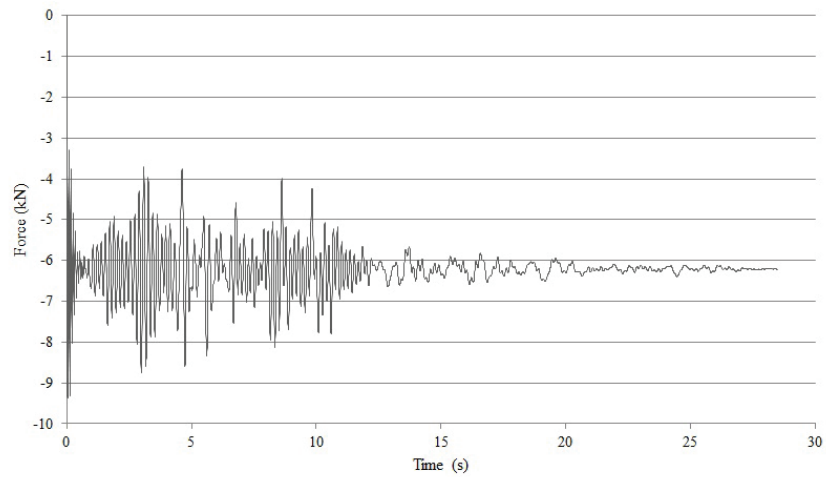
Figure B.11: The Forces in Column C11 when the Coyota Lake Earthquake is Applied



(a) The Axial Force on Column C13



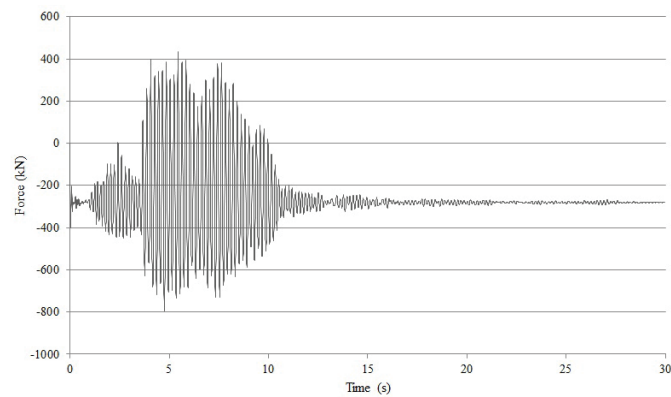
(b) The Shear Force on Column C13 in the Direction of the Long Side



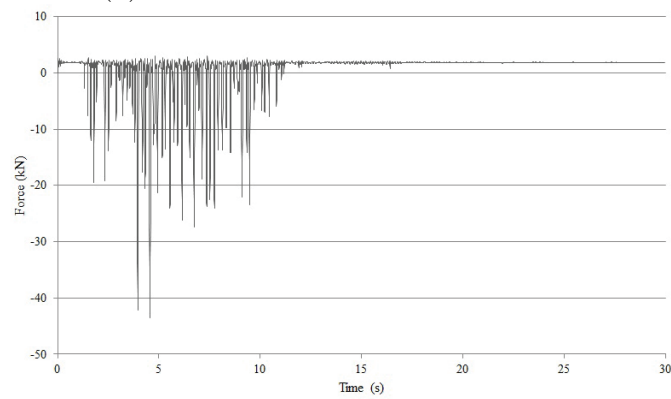
(c) The Shear Force on Column C13 in the Direction of the Short Side

Figure B.12: The Forces in Column C13 when the Coyota Lake Earthquake is Applied

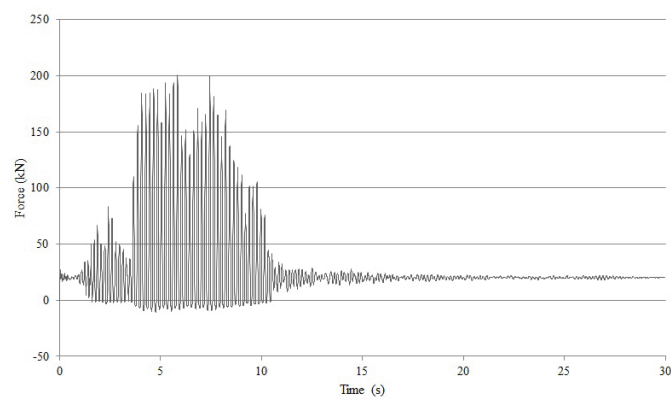
B.1.3 The Resultant Forces During the Morgan Hill Earthquake



(a) The Axial Force on Column C1

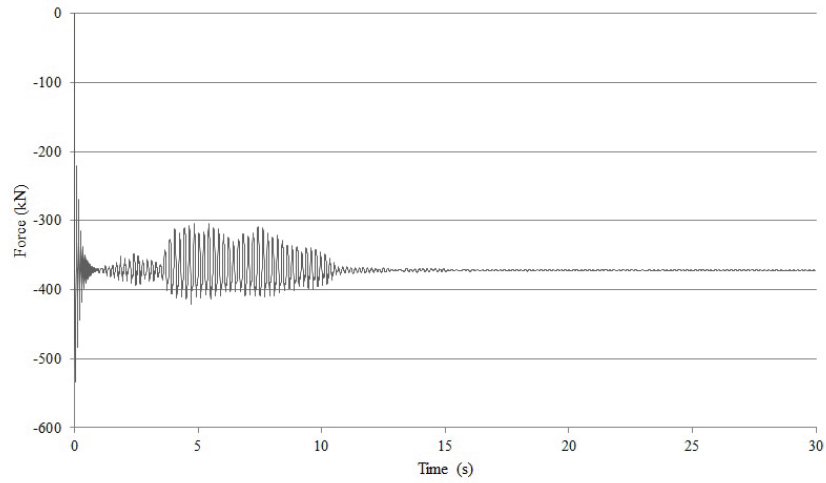


(b) The Shear Force on Column C1 in the Direction of the Long Side

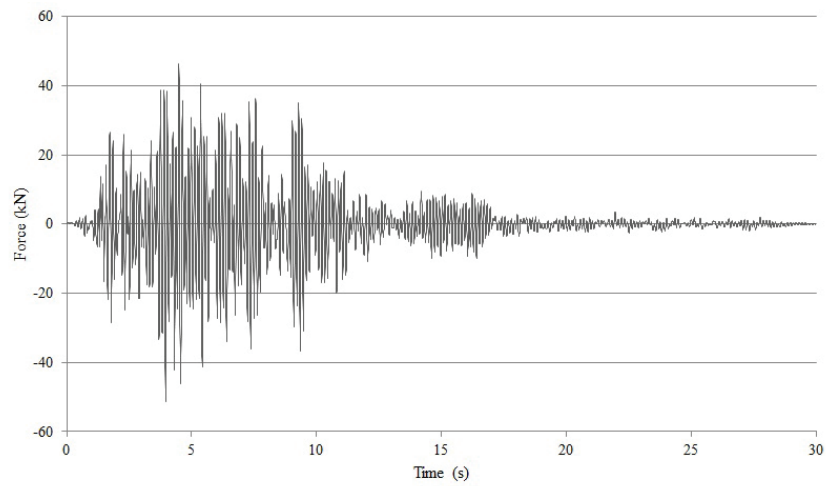


(c) The Shear Force on Column C1 in the Direction of the Short Side

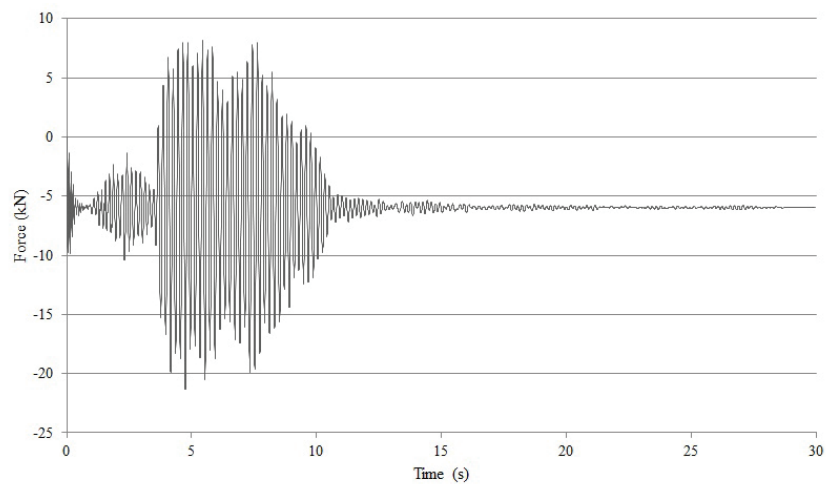
Figure B.13: The Forces in Column C1 when the Morgan Hill Earthquake is Applied



(a) The Axial Force on Column C3

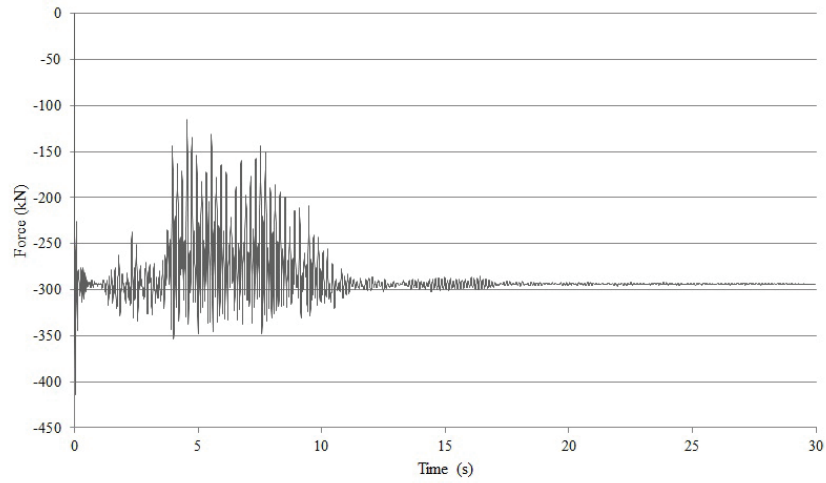


(b) The Shear Force on Column C3 in the Direction of the Long Side

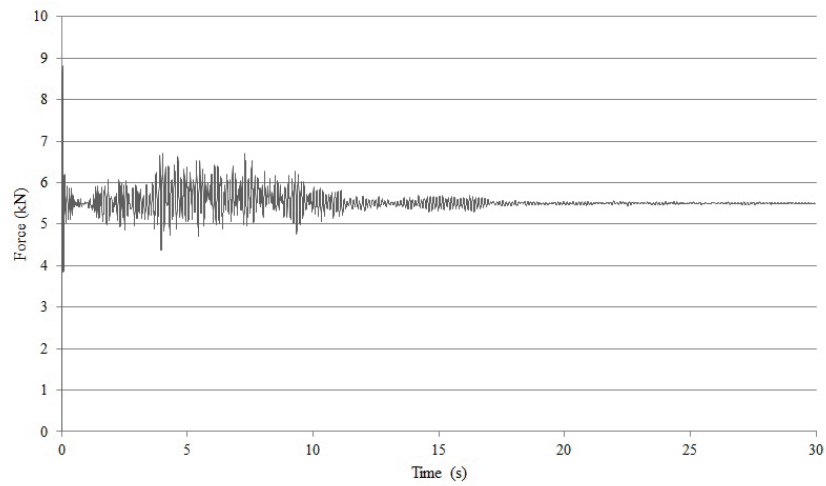


(c) The Shear Force on Column C3 in the Direction of the Short Side

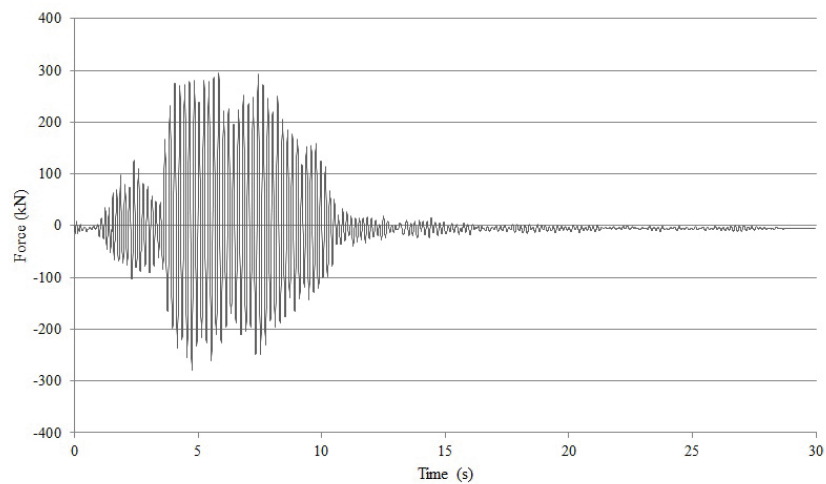
Figure B.14: The Forces in Column C3 when the Morgan Hill Earthquake is Applied



(a) The Axial Force on Column C6

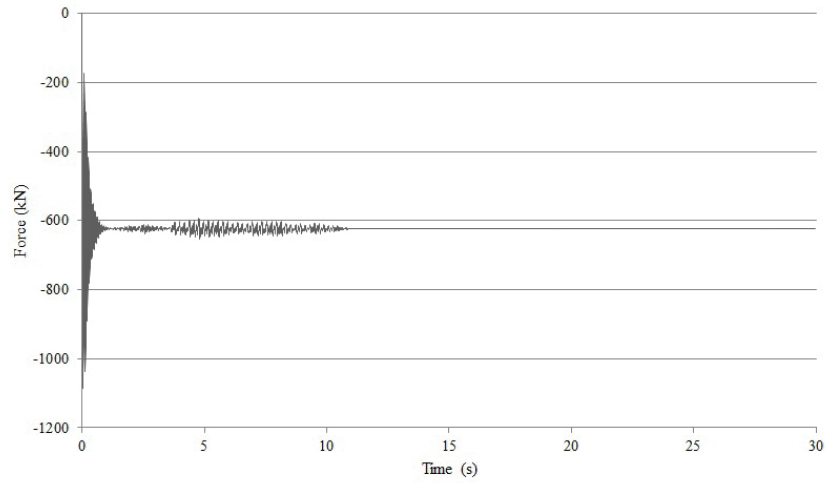


(b) The Shear Force on Column C6 in the Direction of the Long Side

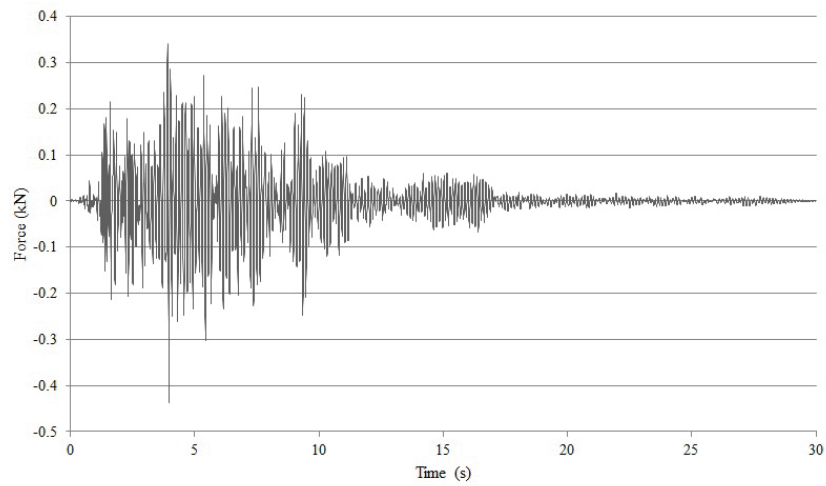


(c) The Shear Force on Column C6 in the Direction of the Short Side

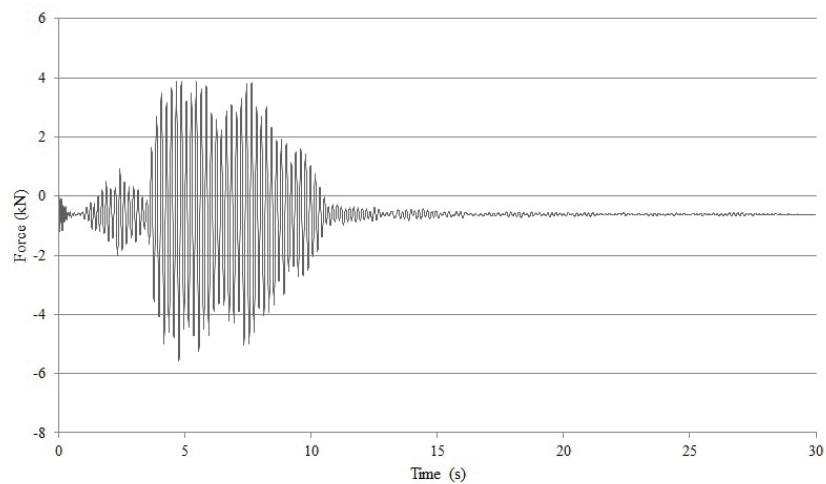
Figure B.15: The Forces in Column C6 when the Morgan Hill Earthquake is Applied



(a) The Axial Force on Column C8

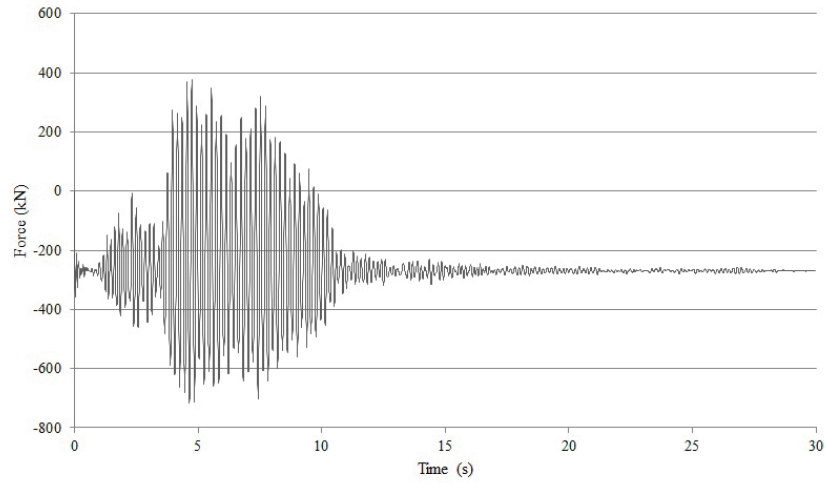


(b) The Shear Force on Column C8 in the Direction of the Long Side

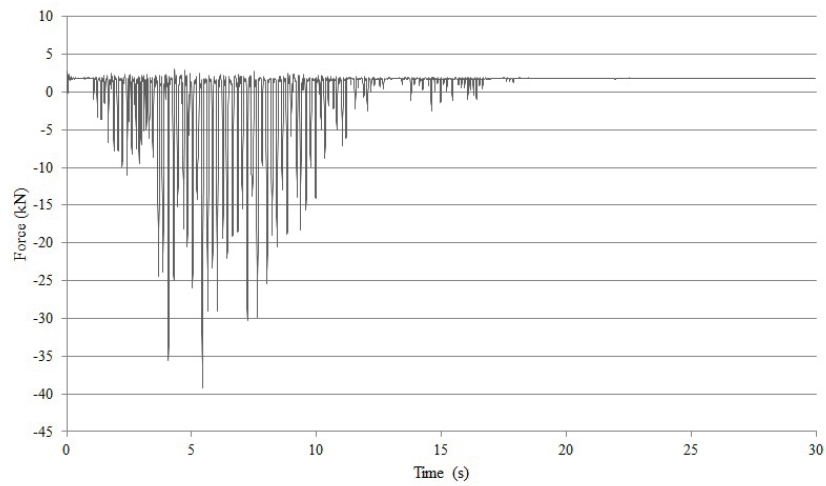


(c) The Shear Force on Column C8 in the Direction of the Short Side

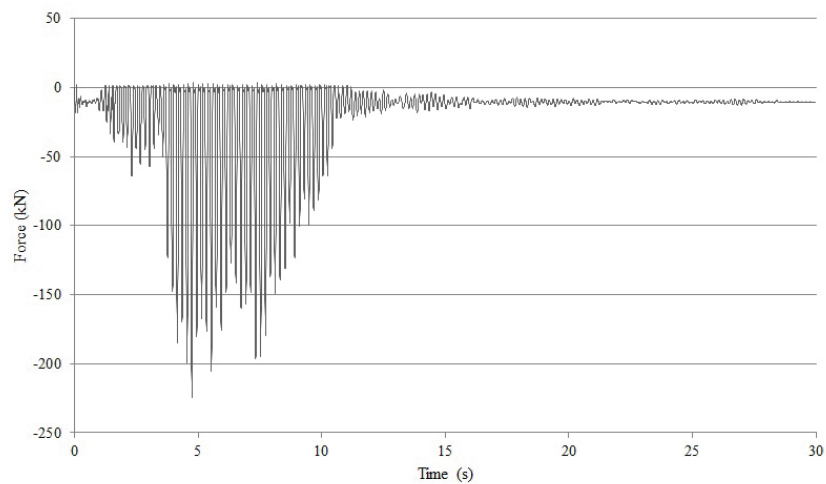
Figure B.16: The Forces in Column C8 when the Morgan Hill Earthquake is Applied



(a) The Axial Force on Column C11

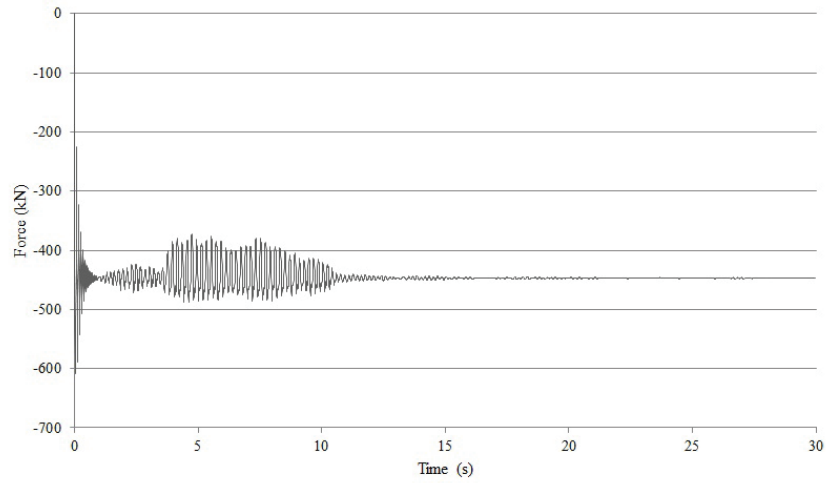


(b) The Shear Force on Column C11 in the Direction of the Long Side

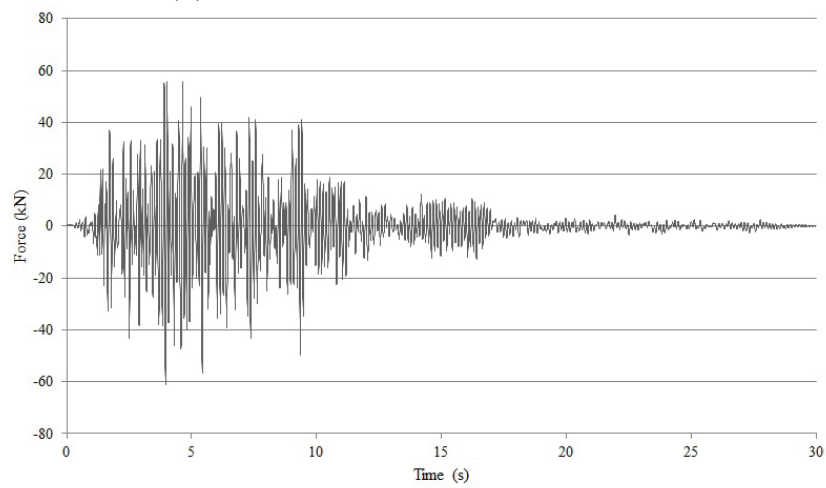


(c) The Shear Force on Column C11 in the Direction of the Short Side

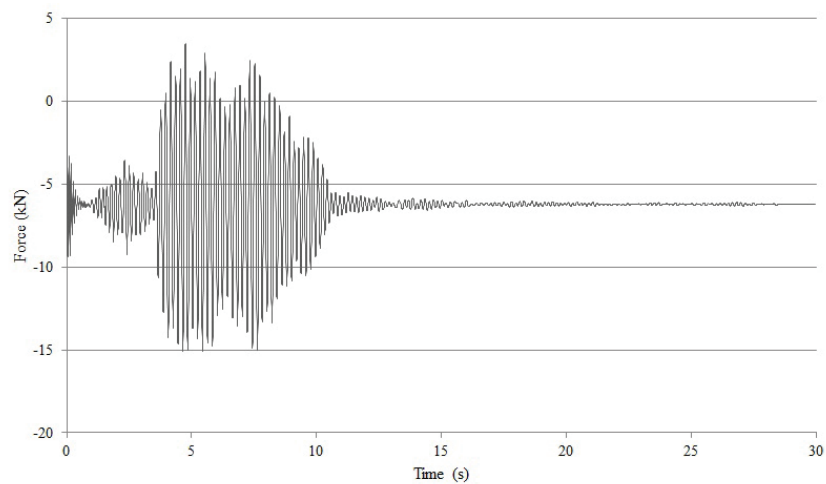
Figure B.17: The Forces in Column C11 when the Morgan Hill Earthquake is Applied



(a) The Axial Force on Column C13



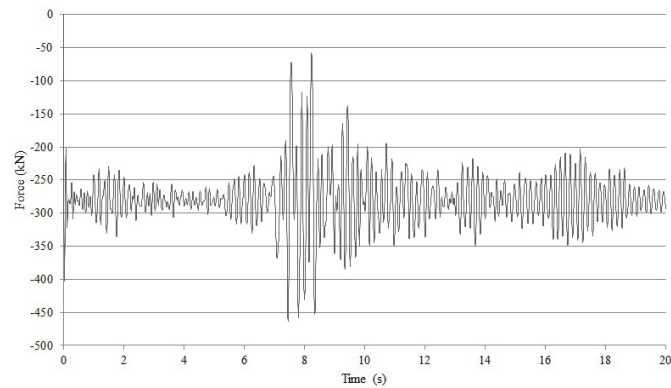
(b) The Shear Force on Column C13 in the Direction of the Long Side



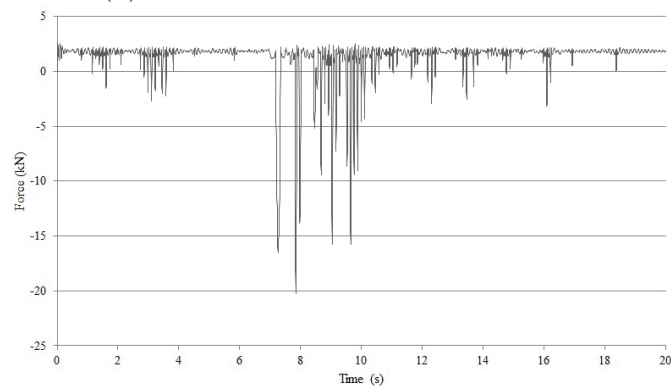
(c) The Shear Force on Column C13 in the Direction of the Short Side

Figure B.18: The Forces in Column C13 when the Morgan Hill Earthquake is Applied

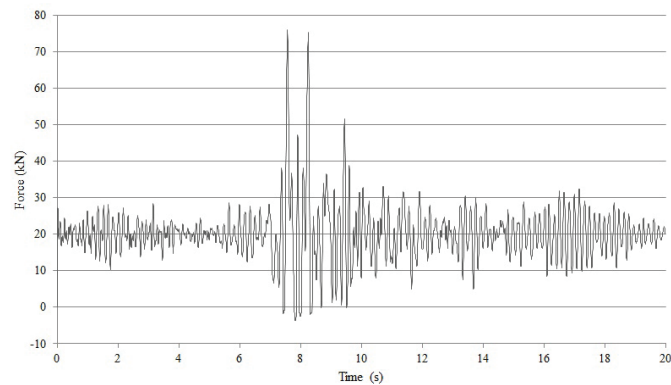
B.1.4 The Resultant Forces During the Palm Springs Earthquake



(a) The Axial Force on Column C1

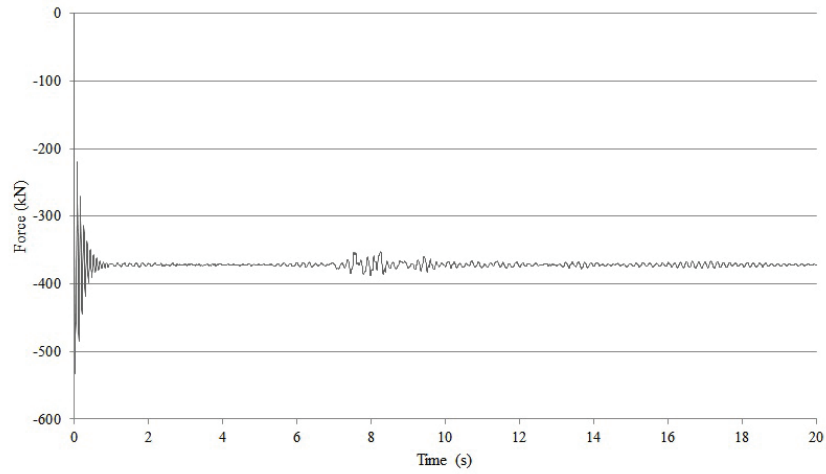


(b) The Shear Force on Column C1 in the Direction of the Long Side

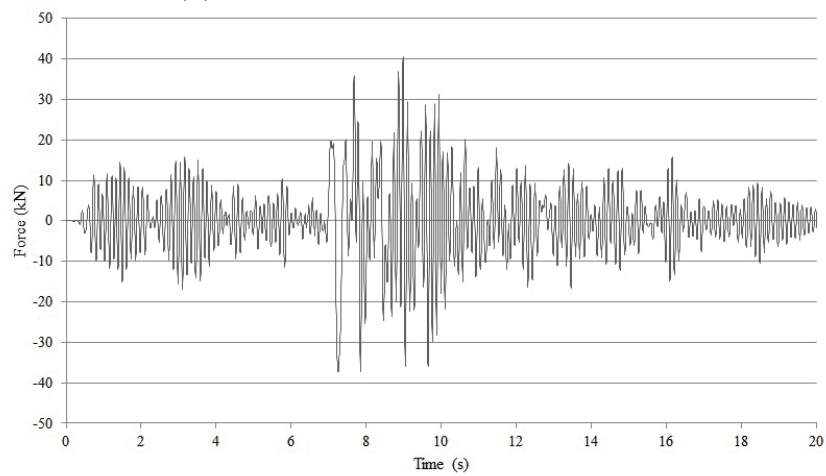


(c) The Shear Force on Column C1 in the Direction of the Short Side

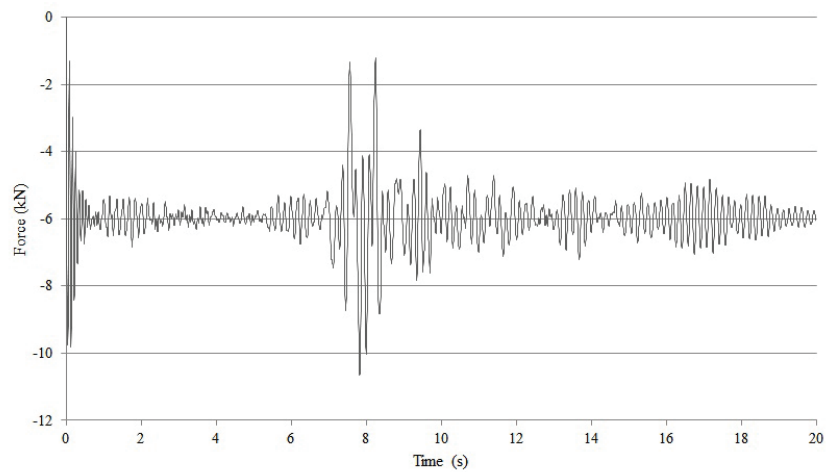
Figure B.19: The Forces in Column C1 when the Palm Springs Earthquake is Applied



(a) The Axial Force on Column C3

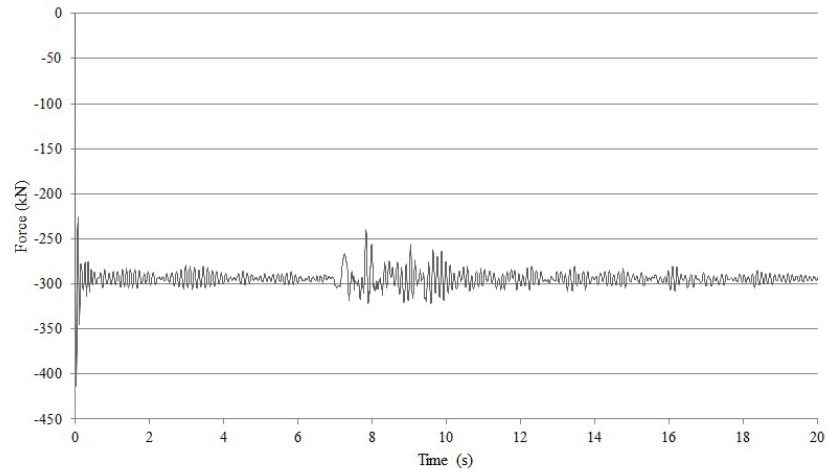


(b) The Shear Force on Column C3 in the Direction of the Long Side

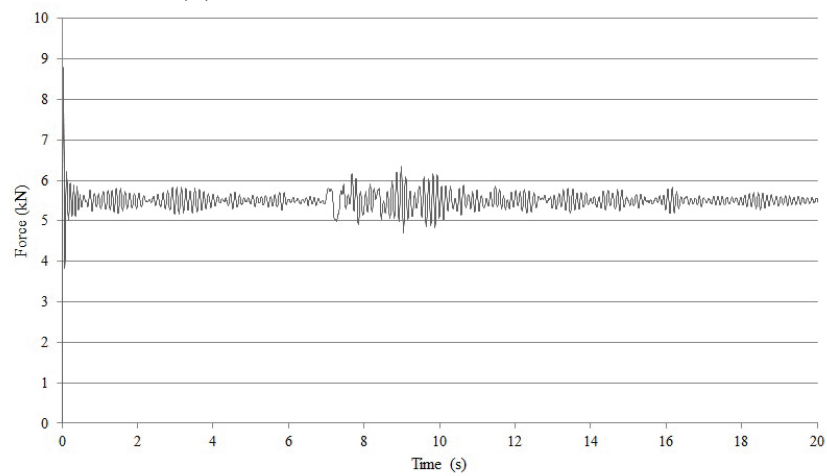


(c) The Shear Force on Column C3 in the Direction of the Short Side

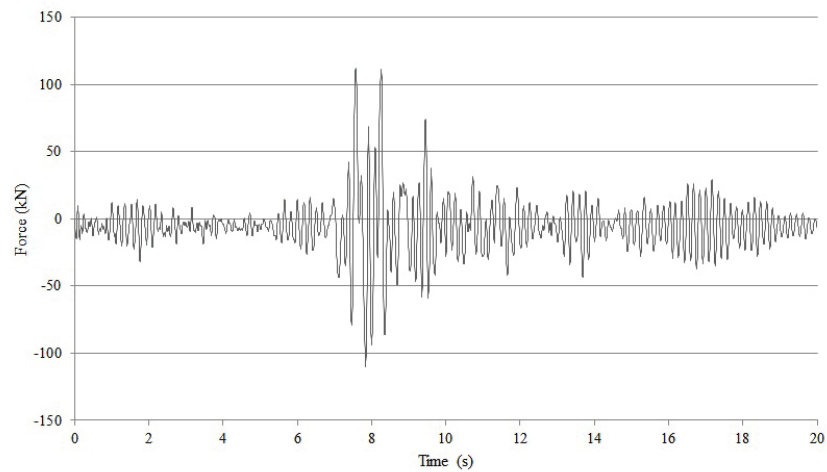
Figure B.20: The Forces in Column C3 when the Palm Springs Earthquake is Applied



(a) The Axial Force on Column C6

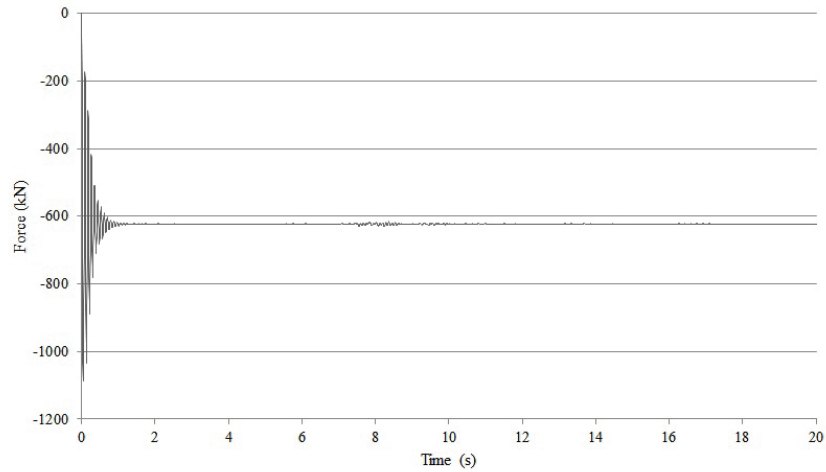


(b) The Shear Force on Column C6 in the Direction of the Long Side

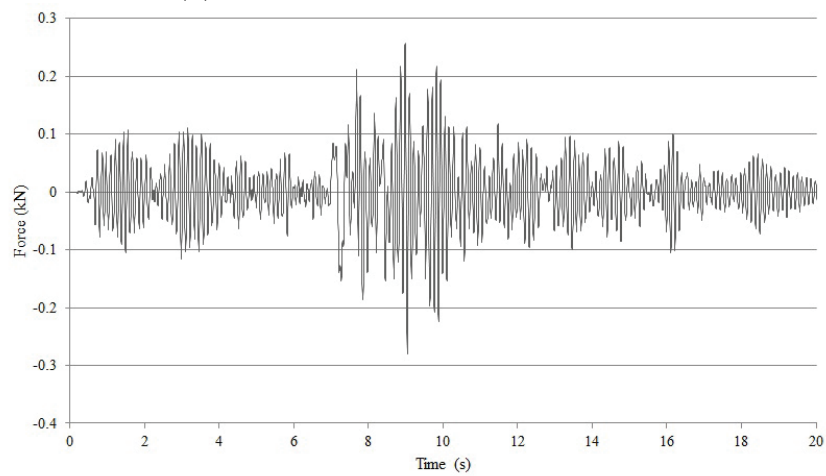


(c) The Shear Force on Column C6 in the Direction of the Short Side

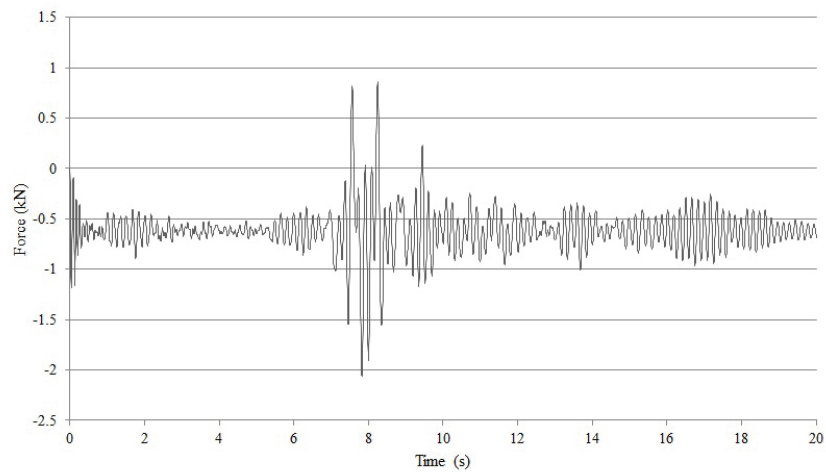
Figure B.21: The Forces in Column C6 when the Palm Springs Earthquake is Applied



(a) The Axial Force on Column C8

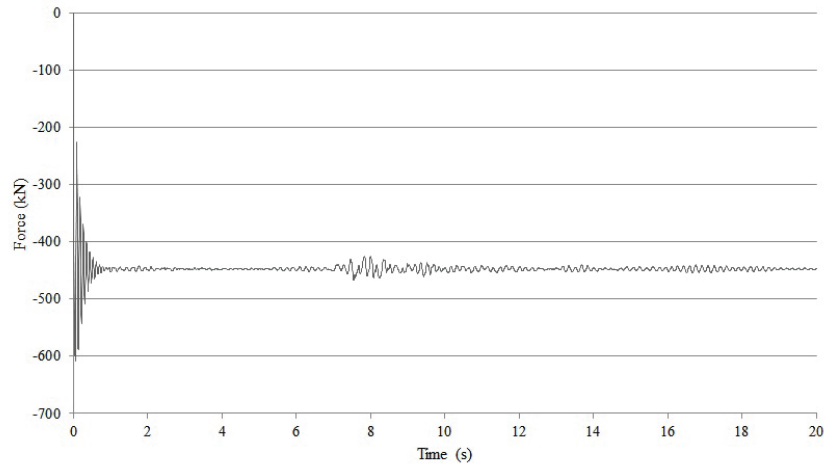


(b) The Shear Force on Column C8 in the Direction of the Long Side

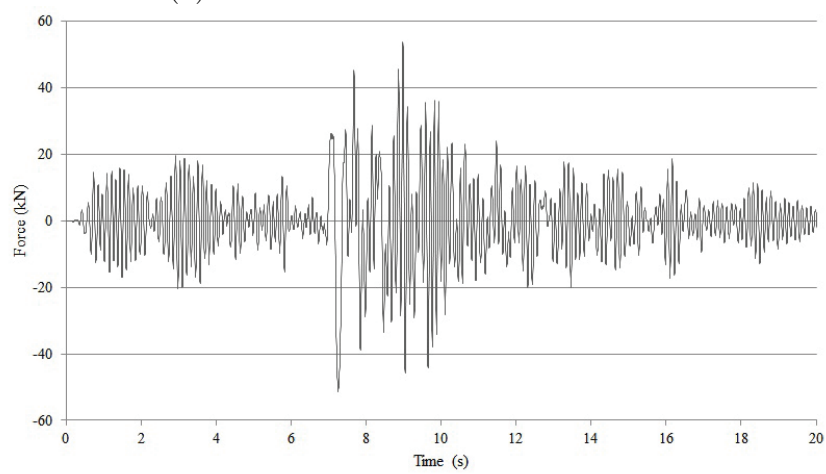


(c) The Shear Force on Column C8 in the Direction of the Short Side

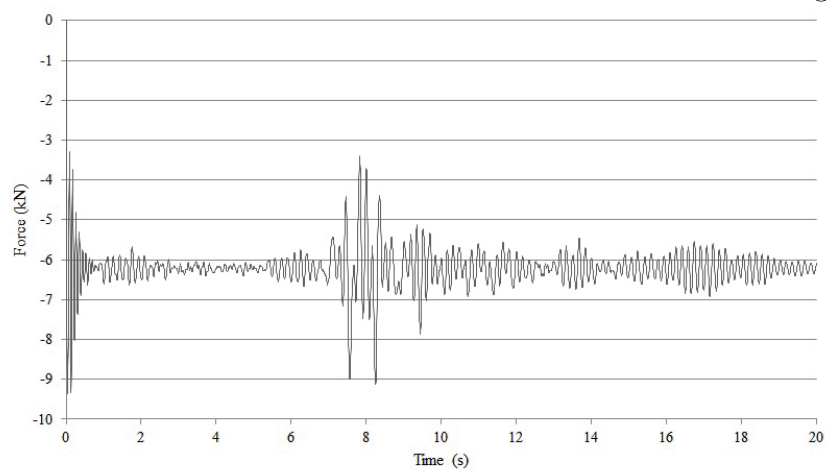
Figure B.22: The Forces in Column C8 when the Palm Springs Earthquake is Applied



(a) The Axial Force on Column C11

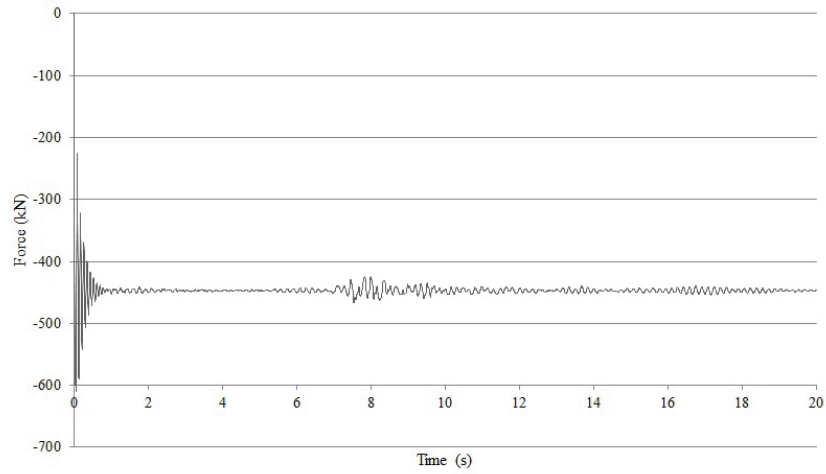


(b) The Shear Force on Column C11 in the Direction of the Long Side

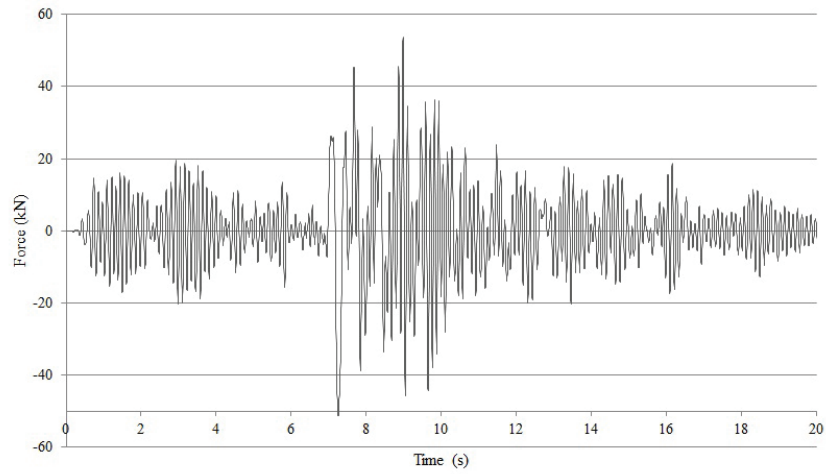


(c) The Shear Force on Column C11 in the Direction of the Short Side

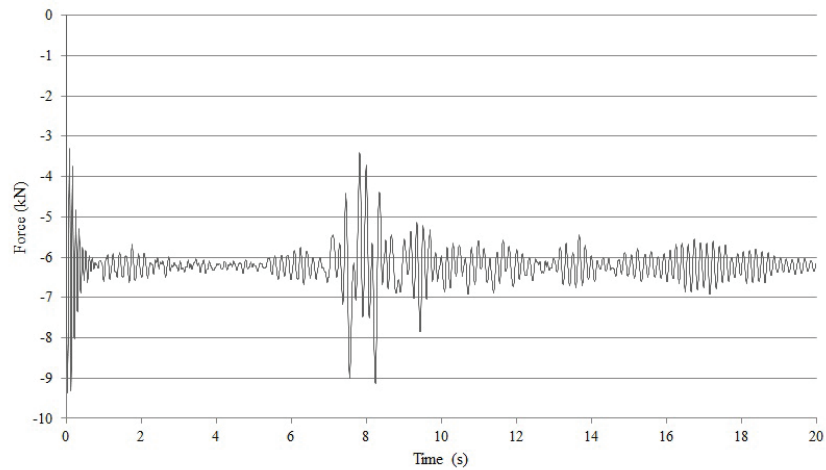
Figure B.23: The Forces in Column C11 when the Palm Springs Earthquake is Applied



(a) The Axial Force on Column C13



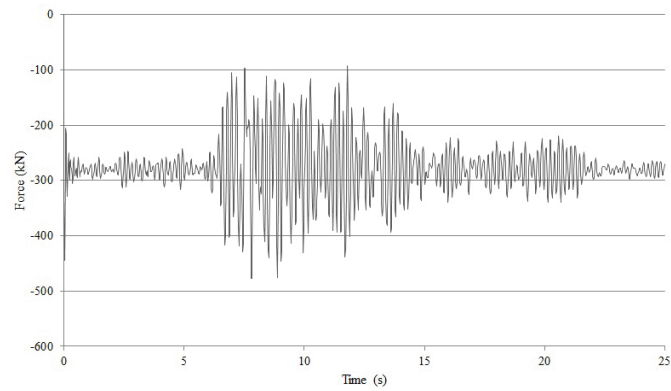
(b) The Shear Force on Column C13 in the Direction of the Long Side



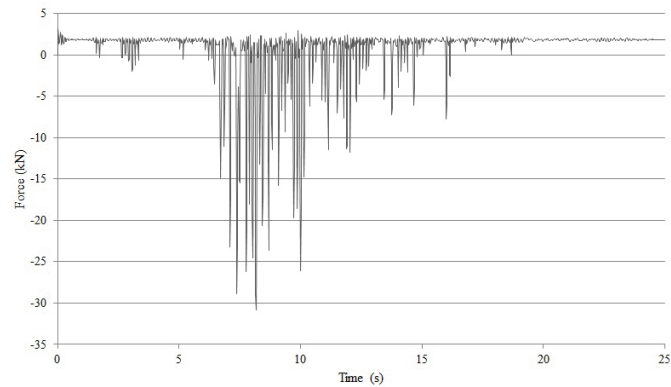
(c) The Shear Force on Column C13 in the Direction of the Short Side

Figure B.24: The Forces in Column C13 when the Palm Springs Earthquake is Applied

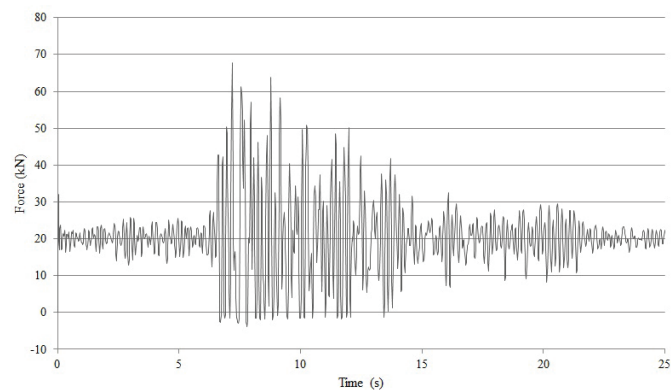
B.1.5 The Resultant Forces During the Whittier Narrows Earthquake



(a) The Axial Force on Column C1

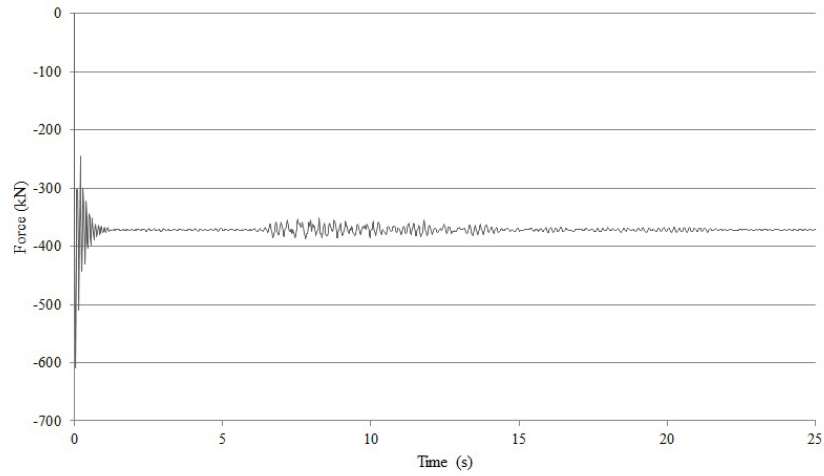


(b) The Shear Force on Column C1 in the Direction of the Long Side

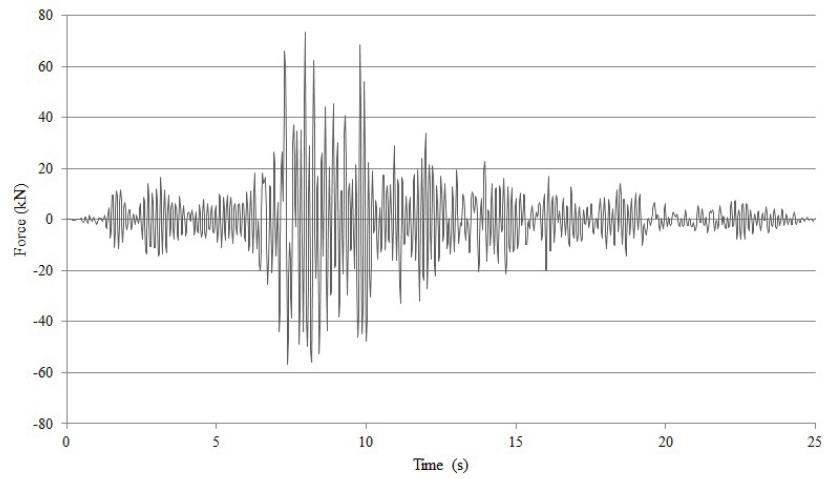


(c) The Shear Force on Column C1 in the Direction of the Short Side

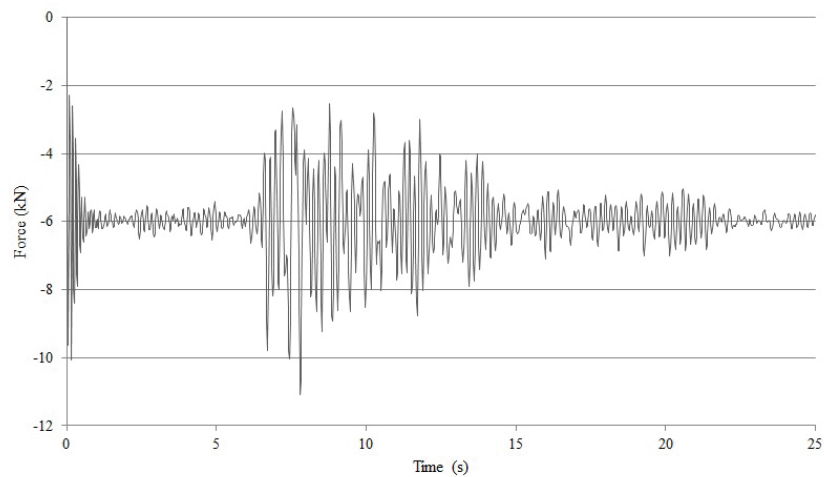
Figure B.25: The Forces in Column C1 when the Whittier Narrows Earthquake is Applied



(a) The Axial Force on Column C3

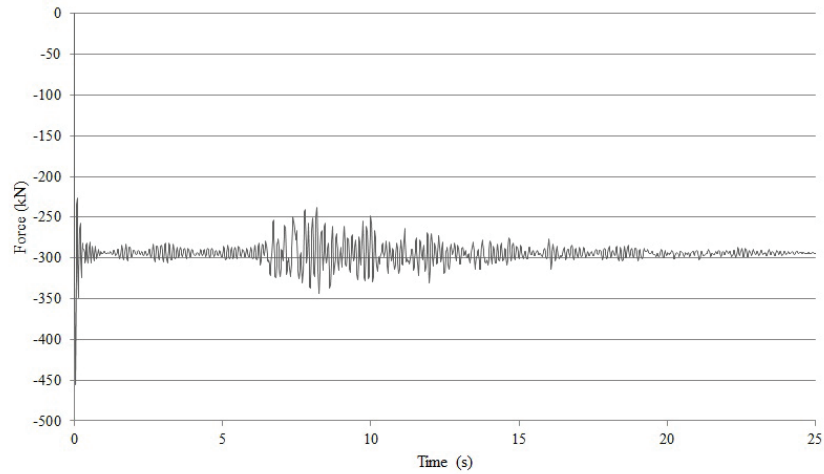


(b) The Shear Force on Column C3 in the Direction of the Long Side

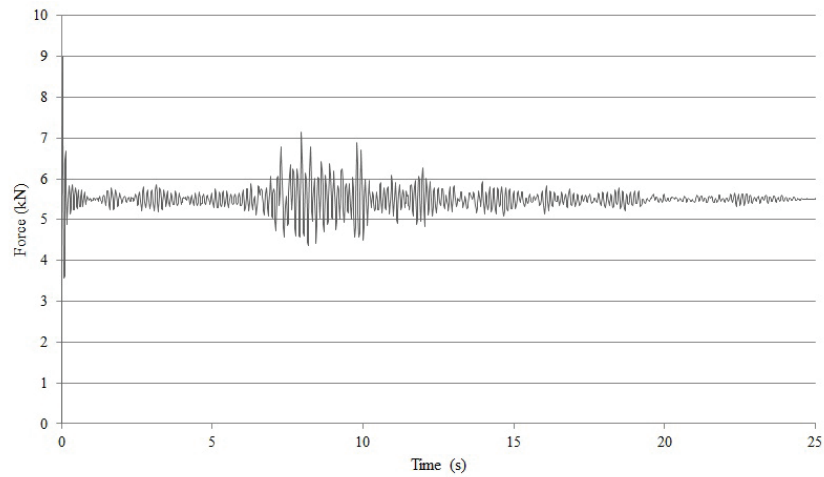


(c) The Shear Force on Column C3 in the Direction of the Short Side

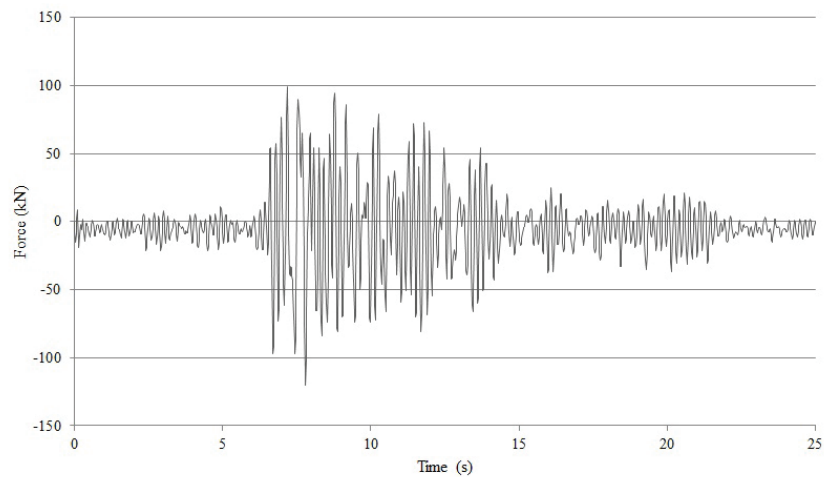
Figure B.26: The Forces in Column C3 when the Whittier Narrows Earthquake is Applied



(a) The Axial Force on Column C6

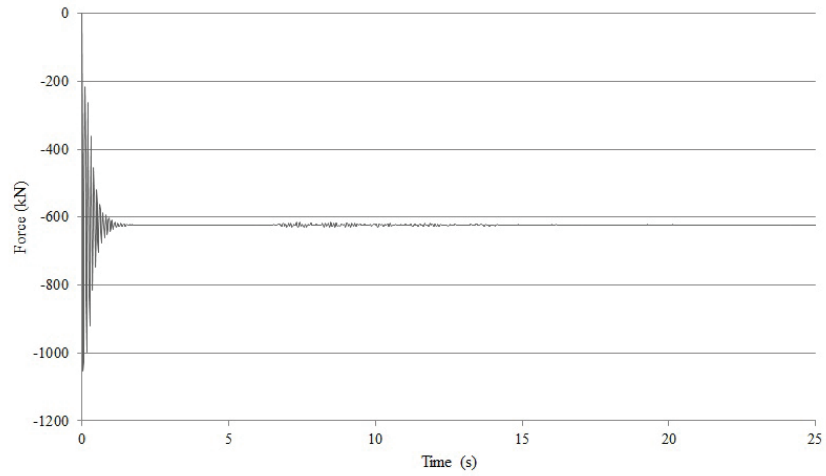


(b) The Shear Force on Column C6 in the Direction of the Long Side

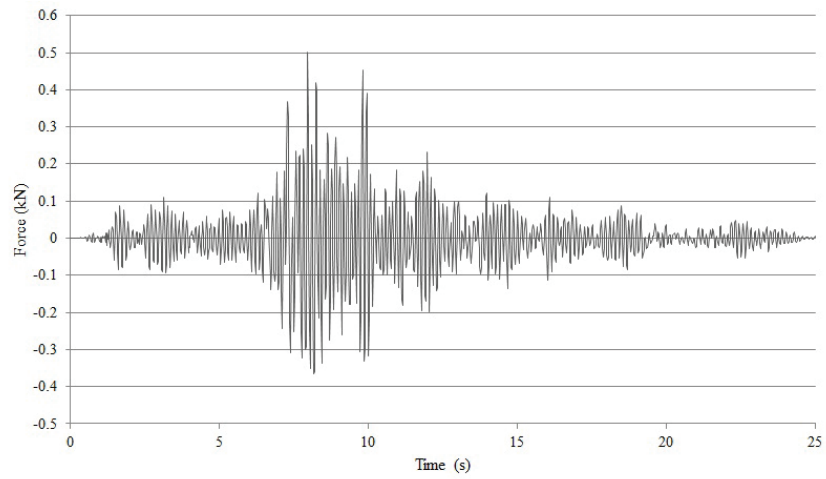


(c) The Shear Force on Column C6 in the Direction of the Short Side

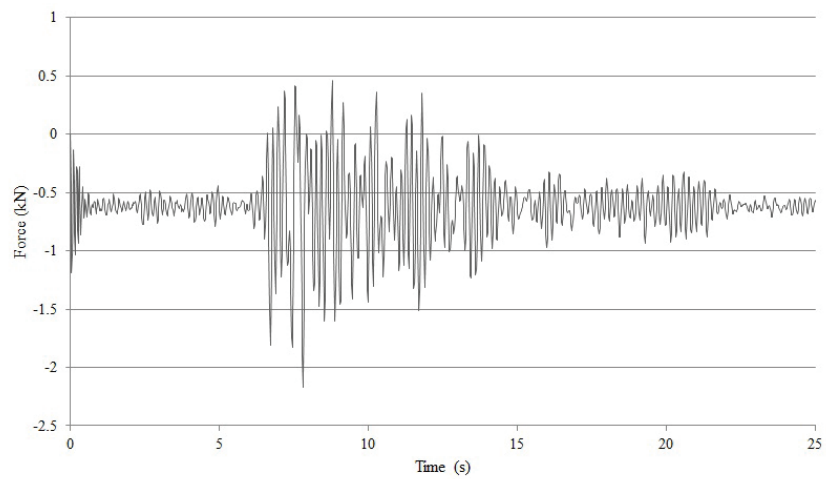
Figure B.27: The Forces in Column C6 when the Whittier Narrows Earthquake is Applied



(a) The Axial Force on Column C8

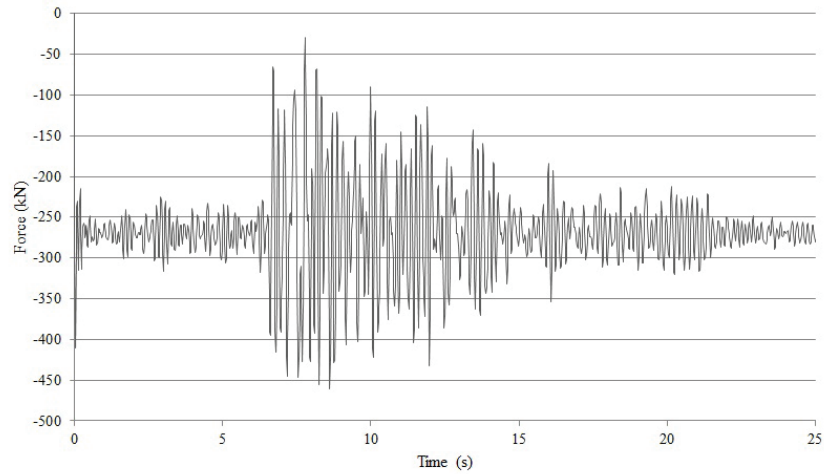


(b) The Shear Force on Column C8 in the Direction of the Long Side

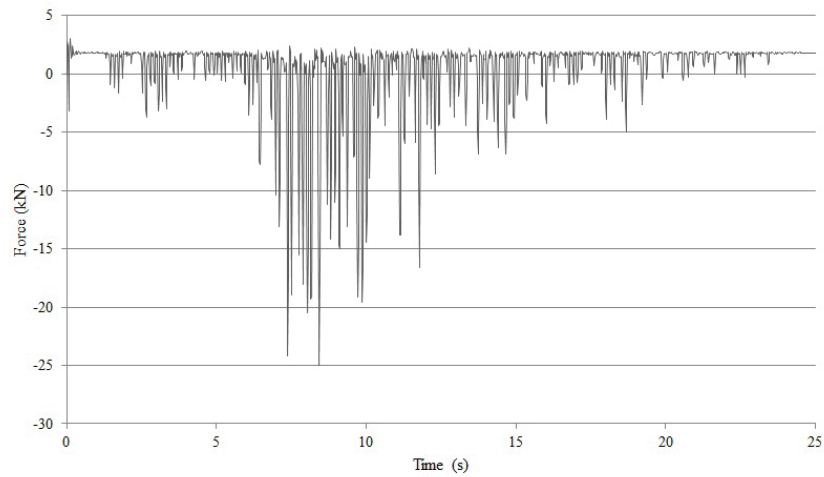


(c) The Shear Force on Column C8 in the Direction of the Short Side

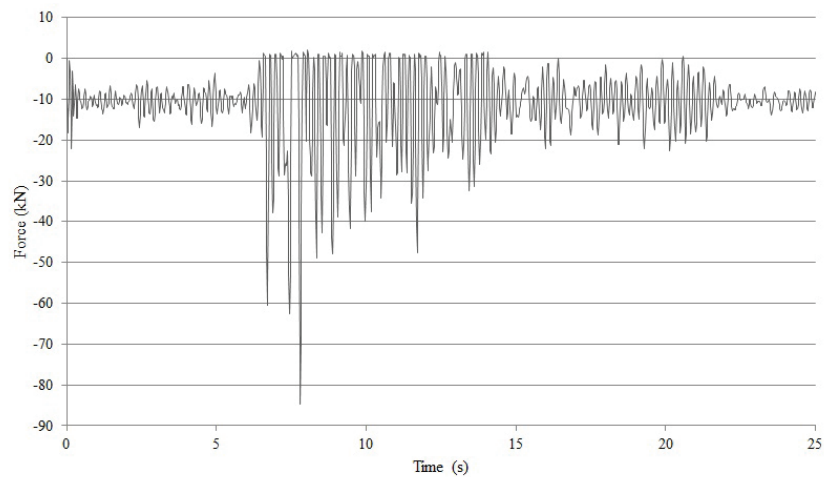
Figure B.28: The Forces in Column C8 when the Whittier Narrows Earthquake is Applied



(a) The Axial Force on Column C11

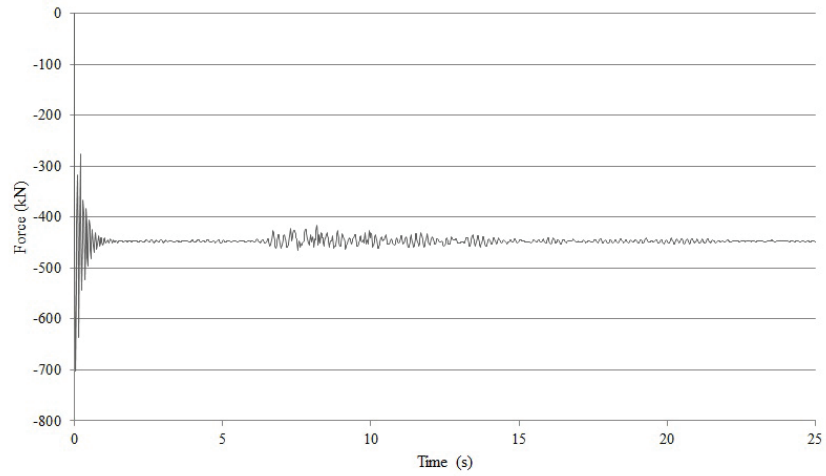


(b) The Shear Force on Column C11 in the Direction of the Long Side

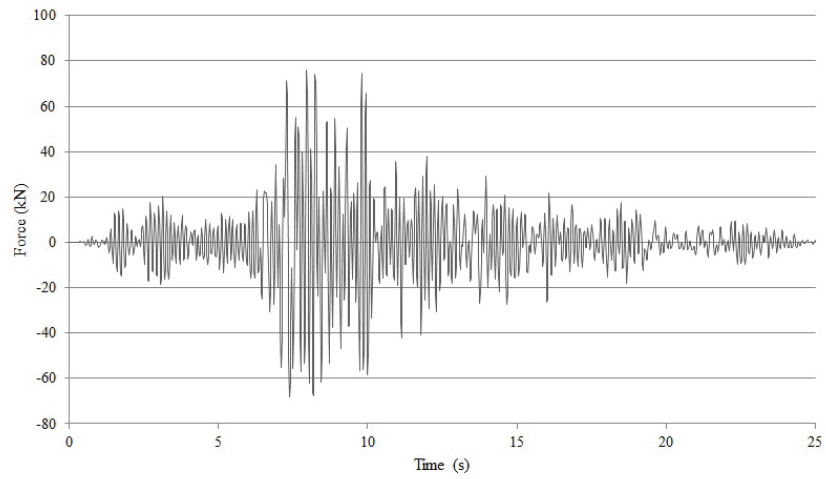


(c) The Shear Force on Column C11 in the Direction of the Short Side

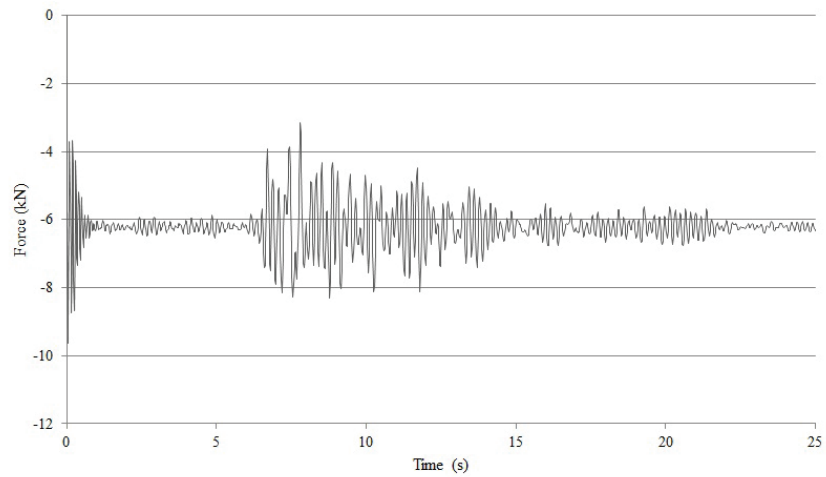
Figure B.29: The Forces in Column C11 when the Whittier Narrows Earthquake is Applied



(a) The Axial Force on Column C13



(b) The Shear Force on Column C13 in the Direction of the Long Side



(c) The Shear Force on Column C13 in the Direction of the Short Side

Figure B.30: The Forces in Column C13 when the Whittier Narrows Earthquake is Applied